2017-08-01

# Performance-Based Liquefaction Triggering Analyses with Two Liquefaction Models Using the Cone Penetration Test

Alex Michael Arndt
*Brigham Young University*

Performance-Based Liquefaction Triggering

Analyses with Two Liquefaction Models

Using the Cone Penetration Test


Alex Michael Arndt


A thesis submitted to the faculty of
Brigham Young University
in partial fulfillment of the requirements for the degree of

Master of Science


Kevin W. Franke, Chair
Kyle M. Rollins
Paul W. Richards


Department of Civil and Environmental Engineering

Brigham Young University

ABSTRACT

Performance-Based Liquefaction Triggering
Analyses with Two Liquefaction Models
Using the Cone Penetration Test

Alex Michael Arndt
Department of Civil and Environmental Engineering, BYU
Master of Science

This study examines the use of performance-based engineering in earthquake liquefaction hazard analysis with Cone Penetration Test data (CPT). This work builds upon previous research involving performance-based liquefaction analysis with the Standard Penetration Test (SPT). Two new performance-based liquefaction triggering models are presented herein. The two models used in this liquefaction analysis are modified from the case-history based probabilistic models proposed by Ku et al. (2012) and Boulanger and Idriss (2014). Using these models, a comparison is made between the performance-based method and the conventional pseudo-probabilistic method. This comparison uses the 2014 USGS probabilistic seismic hazard models for both methods. The comparison reveals that, although in most cases both methods predict similar liquefaction hazard using a factor of safety against liquefaction, by comparing the probability of liquefaction, the performance-based method on average will predict a smaller liquefaction hazard.

Keywords: cone penetration test, CPT, CPTLiquefY, earthquake, liquefaction, performance-based earthquake engineering, PBEE, probabilistic, probability of liquefaction, uncertainty

# ACKNOWLEDGEMENTS

TABLE OF CONTENTS

LIST OF TABLES

LIST OF FIGURES

# 1 INTRODUCTION

Earthquakes are often events that cause great damage and destruction. Earthquake related phenomenon such as liquefaction, lateral spread, and settlement have in the recent past contributed to the destruction of cities and homes, as well as inflicting an irreparable cost to human life. An example of this is the Canterbury earthquake sequence (2010-2012), which occurred near Christchurch, New Zealand. Liquefaction caused by the main earthquake and subsequent aftershocks contributed to billions of dollars in damage and the loss of over one hundred lives (Bannister and Gledhill, 2012). Recently, research into earthquake caused phenomenon such as liquefaction has increased the understanding of how damage to buildings and lifelines can occur during an earthquake event. This research has allowed for the creation of many sophisticated procedures that attempt to predict the likelihood of liquefaction and associated risks occurring at a specified location.

Through the use of procedures like performance-based earthquake engineering (PBEE) developed by the Pacific Earthquake Engineering Research center (PEER), there now exist approaches for earthquake engineering that allow design in terms of the likelihood of an earthquake event rather than the raw possibility of such an event. Also, these approaches allow for the systematic consideration of various forms of uncertainty in the analysis. These advances allow engineers to more effectively asses the risk of damage from an earthquake depending on the significance of the designed structure and other factors.

Prior PBEE liquefaction research has been focused on incorporating soil resistance data collected from Standard Penetration Testing (SPT). In recent years new liquefaction triggering models have been produced using earthquake case histories with Cone Penetrometer Test (CPT) data. The CPT has several unique advantages over the SPT; CPT data is recorded at much smaller depth increments which allows the development of a nearly continuous soil profile, and CPT results have been shown to be much more repeatable than the SPT data, which can vary significantly within a few lateral feet (Robertson and Wride, 1998). These advantages are extremely useful in the analysis of liquefaction potential which should consider the susceptibility of a complete soil profile. Because no PBEE liquefaction triggering procedure incorporating CPT data currently exists, this thesis will present a CPT-based procedure to be used alongside the current SPT-based PBEE procedure.

This thesis develops and presents a new CPT performance-based liquefaction initiation procedure and applies it to two existing probabilistic CPT-based liquefaction models: Ku et al. [probabilistic version of Roberson and Wride] (2012), and Boulanger and Idriss (2014). A comparative study is presented in which 10 cities in the US are analyzed using the CPT performance-based procedure and the conventional pseudo-probabilistic procedure with both triggering models. The comparison of these two procedures will allow researchers to gain a greater understanding of the strengths of the CPT performance-based procedure as well as the inconsistencies and bias associated with the conventional pseudo-probabilistic procedure.

## 2    SEISMIC LOADING

Energy from an earthquake is often defined in terms of magnitude or intensity.  Because of this categorization of earthquakes, the extent to which a soil can liquefy is often analyzed as a function these parameters.  To be able to analyze the potential for seismic effects at a site including liquefaction, engineers must understand all potential sources of seismic loading.  This chapter will discuss the fundamental concepts related to estimating seismic loading for engineering analysis. Although a detailed discussion of the geology of earthquakes is beyond the scope of this thesis, background understanding of this topic clarifies these concepts.

### 2.1    Earthquakes

Earthquakes have the potential to be violent and destructive events.  Over time, scientists have tried to better understand and the sudden movement of faults which are the cause of earthquakes.  To explain the energy released from a fault rupture, ideas such as elastic rebound theory have been developed.  Elastic rebound theory states that rock along a fault store elastic stress until the time they are no longer able to resist; at which time the stored energy is released in the form of an earthquake (Wood 1912).  The seismic moment was developed to help quantify the amount of energy released or "work done" by an earthquake and is given as:

$$M_O = \mu A \bar{D} \tag{2-1}$$

where $\mu$ is the rupture strength of the rock on the fault, A is the fault rupture area, and $\bar{D}$ is the average displacement along the fault.

Another common earthquake magnitude value, related to the seismic moment is the moment magnitude. This value is widely utilized in standard earthquake liquefaction analyses, as is given as:

$$M_W = \frac{\log(M_o)}{1.5} - 10.7 \tag{2-2}$$

The calculation of the amount of energy released from an earthquake can be a complex task, but estimating the amount of that energy felt by a soil at a particular site is often further complicated by phenomenon such as site effects. Examples of site effects are: near source effects, directivity effects, basin effects, and others (Kramer 1996). Some of these effects have been studied and characterized effectively, but most still require a large amount of study to better understand their effects on the parameters of a liquefaction analysis.

With so many variables and so much uncertainty involved in the categorization of seismic loading, researchers have looked to past earthquake events to refine their prediction of future seismic loading. Based on current and past measurements of ground motions, researcher have looked for patterns to help in the calculation of seismic potential.

## 2.2 Ground Motion Parameters (GMPs)

When earthquakes occur, ground motions can be observed by instruments such as seismographs and accelerographs. The data collected during an earthquake event can be compiled into a graphical representation called a time history. These time histories usually

contain orthogonal acceleration, velocity, or displacement data over time at the measurement location during an earthquake event.  This data is extremely useful as it can be used to estimate ground motions for similar future events.  GMPs are often used to categorize amplitude, frequency content, or duration of an event.  Figure 2-1 is a representation of a time history containing acceleration data.
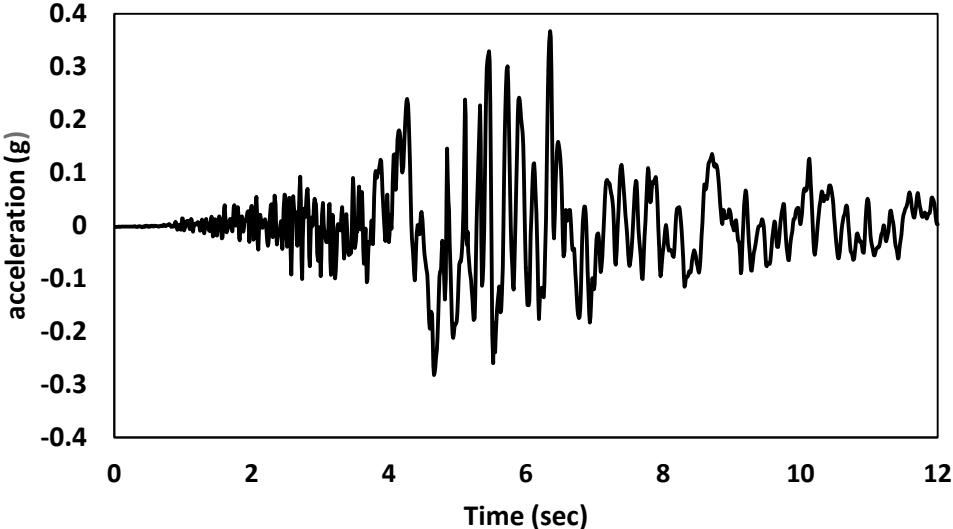


**Figure 2-1: Example time history representing acceleration data from the Loma Prieta Earthquake.**

Earthquake amplitude is a key parameter that can be described by several GMP's such as peak ground acceleration or peak acceleration (PGA or $a_{max}$), peak ground velocity or peak velocity (PGV or $V_{max}$), and peak ground displacement (PGD).  Each of these parameters are useful for the analysis of certain structures, but PGA and $a_{max}$ are the most commonly used parameters in engineering analysis.  Potential limitations exist with the use of amplitude GMPs because earthquakes time histories with a similar amplitude can represent earthquakes that

release very different amounts of energy depending on other factors. Figure 2-2 illustrates an example of this limitation in amplitude time history data.



Figure 3.12   Accelerograms from (a) the N29W Melendy Ranch record of the 1972 Stone Canyon ($M = 4.6$) earthquake and (b) the longitudinal record from the 1967 Koyna ($M = 6.5$) earthquake. The time and acceleration scales are identical for both records. Peak accelerations are very close, illustrating the limitations of using peak amplitude as a sole measure of strong ground motion. (After Hudson, 1979; used by permission of EERI.)

**Figure 2-2: Time histories with different durations (after Kramer, 1996).**

Other GMPs describe frequency content. Frequency content describes how the energy of a ground motion is distributed across a range of frequencies or periods. A Fourier spectrum is a common way that these frequencies are interpreted. Another way to interpret frequency content is a response spectrum, which plots the maximum response of a series of single degree of freedom oscillators with varying natural periods as a function of natural period or frequency. In many cases, structural response is synonymous with a value termed spectral acceleration (SA) at the structures natural period.

Engineers also consider the duration of an earthquake with duration GMPs. The consideration of duration is useful as damage can accumulate as the length of time that a

structure is exposed to strong ground motions increases. The most common duration GMP is bracketed duration, which is the length of time between the first and last exceedance of a given threshold acceleration. A common threshold used in practice is 0.05g. Another useful duration GMP is the equivalent number of cycles, which is a function of earthquake magnitude. This GMP attempts to quantify the number of stress cycles an earthquake is likely to impart based on the magnitude of the event.

Several GMPs exist that consider amplitude, frequency content, and duration simultaneously. Examples of these GMPs are Arias intensity ($I_a$) and cumulative absolute velocity (CAV). In practice, some engineers prefer to use these parameters as they contain more information than commonly used values such as PGA or $a_{max}$. However, because of the complicated relationship between amplitude, frequency content and duration, common practice involves looking at a variety of GMPs independently to obtain a more detailed understanding of the ground motions. Unfortunately, many of the popular liquefaction analysis methods are based solely on $a_{max}$ and $M_W$. Other methods do exist based on $I_a$ but these methods are limited. The methods discussed in this thesis are derived from the simplified method developed by Seed and Idriss (1971) which uses $a_{max}$ and $M_W$ as GMPs.

## 2.3    Ground Motion Prediction Equations (GMPEs)

The many earthquake ground motions recorded in the last few decades have allowed for the creation of a large database of earthquake time histories. From this database, researchers have created a series of empirical ground motion parameter relationships based on inputs that can be reasonably estimated a priori, such as source-to-site distance and moment magnitude ($M_W$). These relationships are called attenuation relationships or ground motion prediction equations

(GMPEs). Engineers use GMPEs to predict ground motion parameters that could occur at their site of interest from a given earthquake event.

As with most empirical relationships, GMPEs tend to have significant data scatter. Because of this, the equations are most applicable in locations of high seismicity (i.e. Japan, California, etc.) where more recorded ground motion data exists. Significant limitations to the use of GMPE's exist in locations without a large amount of recorded ground motions. The Ergodic assumption, which assumes that two ground motions in two different geographical locations should be similar if other variables are held constant (e.g., magnitude, source-to-site distance), is often used to allow these relationships to be applied in regions where less earthquakes have been recorded. Without use of the Ergodic assumption, GMPEs would require a site-specific correlation which would either not be possible or be cost-prohibitive for most applications.

Early attenuation relationships were solely based on magnitude and distance parameters. Figure 2-3 shows what one of these early relationships may have looked like. Over time, these relationships have become more complex as more ground motion data has become available. Late in the decade of the 2000's the Pacific Earthquake Engineering research center (PEER) began an initiative to develop a universal, vetted ground motion database comprised of all currently available crustal earthquake data. Following the completion of the database, five research teams were chosen by PEER to develop new GMPEs called New Generation Attenuation (NGA) relationships (Abrahamson and Silva, 2008; Boore and Atkinson, 2008; Chiou and Youngs, 2008; Campbell and Bozorgnia, 2008; and Idriss, 2008). These equations allow the correlation of values such as PGA, PGV, and SA based on measurable earthquake parameters. After the success of NGA-West, another update, NGA-West2 was completed in

2013. This new update focused on addressing issues including directivity and directionality, along with the treatment of epistemic (model) uncertainty. Ground motion data recorded from between 2008 and 2013 was also included in this update.
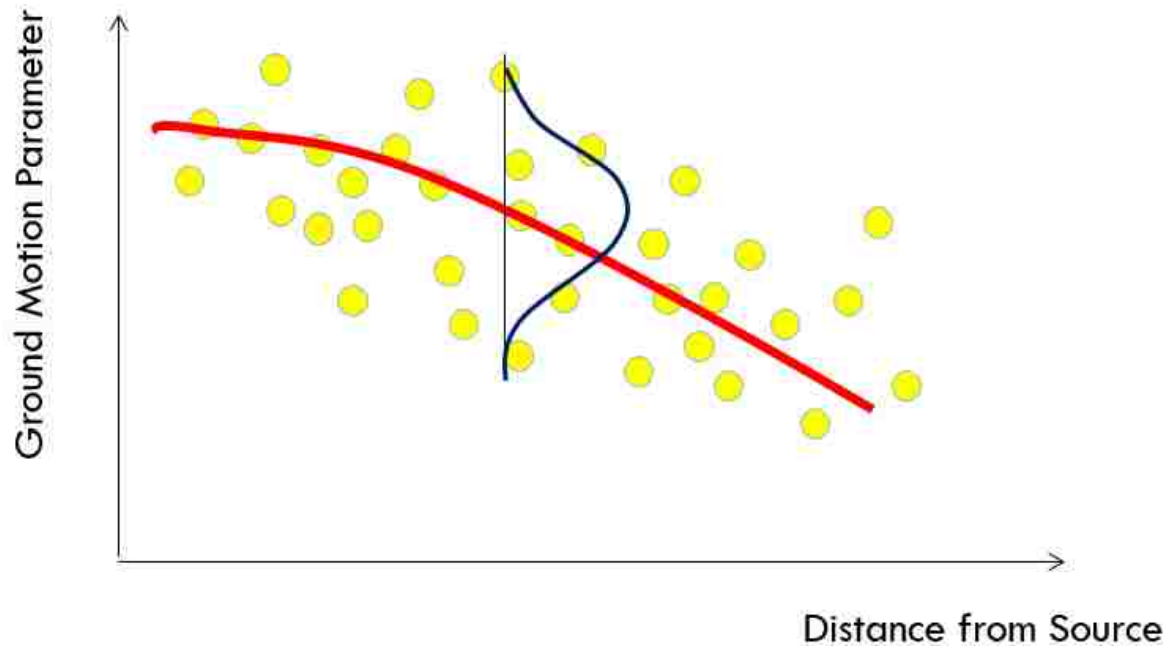


**Figure 2-3: Graphical representation of a basic attenuation relationship.**

NGA-West and NGA-West2 have provided an update for attenuation relationships in the western US and areas of high seismicity from crustal sources, but solutions are still needed for regions with low seismicity (i.e. Central and Eastern US). NGA East is a program that has set out to update the attenuation relationship for continental tectonic regions. These relationships are especially focused on the regions in the central and eastern US, where large earthquakes are possible but not common. Also, ground motions near subduction zones sources, which have a unique earthquake "fingerprint", were not included in the original NGA relationships, but are currently being evaluated in a separate study by PEER.

**2.4    Modification Factors Based on Local Site Effects**

Prior to NGA-West2, ground motions developed using GMPEs did not consider several effects that have been observed and have been known to cause significant changes in measured ground motions.    If these effects are not properly considered in the GMPEs, they must be accounted for by engineering judgement, and local experience.    The effects that are often not considered include near source and directivity effects, basin effects, soil amplification, and topographical effects.

**2.4.1    Near Source, Basin, and Topographical Effects**

Near source, basin and topographic effects are known to change the measured ground motions at sites.    Near source and directivity effects are caused by a pulse initiated as a fault rupture travels in one direction down the fault (Abrahamson 1997).    The reach of near source and directivity effects are often within 10-15 km of a fault; this distance depends significantly on the soil type and geologic setting of the site (Kramer 1996).    A key to directivity effects is based on if the earthquake occurs "towards" or "away" from the site as well as if the site is located in a fault normal or fault parallel orientation.    Directivity effects can greatly increase the amount of damage that would occur from the earthquake as the energy tends to arrive in one large pulse rather than arrive over a longer duration.

Basin effects occur in lower lying regions surrounded by mountain ranges.    These effects have been known to amplify and dampen ground motions significantly depending on location. Basin effects are caused by the reflection of earthquake waves off the exposed bedrock where the basin sediments meet mountain ranges.    The interaction of seismic waves that occurs at the edges of the basins is complex and causes different frequency patterns and interference.    The complex

nature of these interactions makes it very difficult to fully predict ground motions in basin regions like the mountain west region of the United States.
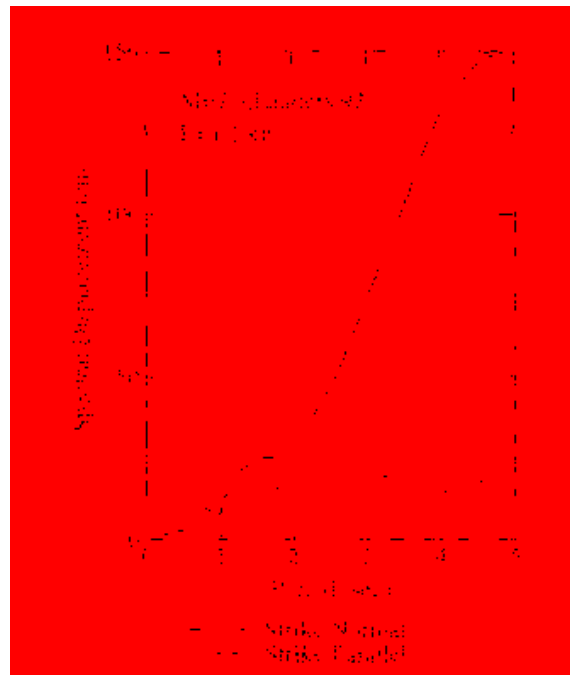


**Figure 2-4: Comparison of directivity effects on spectral displacement during the Landers 1992 earthquake (after Kramer, 1996).**

Topographic effects are another complex factor which can also influence the ground motions that will result from an earthquake. These effects are caused by constructive interference of earthquake waves as they are pushed up to higher elevations. Some of the strongest ground motions ever recorded have been attributed to topographic effects, such as the 1.78g acceleration felt on a hill in Tarzana, CA during the Northridge 1994 earthquake (Spudich et al., 1996). These effects have been observed to cause significant changes locally to displacements or accelerations, but usually do not cause large scale regional ground amplifications.

11

### 2.4.2   Site Amplification Effects

Site amplification effects will influence most all possible surface ground motions.  Site amplification is caused by the modification of earthquake waves as they travel through soil that has a much lower stiffness compared to bedrock.  Values of PGA are commonly representative of accelerations in bedrock, while $a_{max}$ commonly represents a measure of peak acceleration at the ground surface.  Several methods have been developed to account for site amplification in a liquefaction analysis.  Stewart et. al. took a statistical approach to quantify site amplification.  Stewart et. al. (2003) presented a relationship based on the geologic age of a soil.

$$F_{PGA} = \frac{a_{max}}{PGA} = \exp\left[a + b * \ln(PGA\right] + \varepsilon \qquad\qquad (2\text{-}3)$$

$$\varepsilon = \sigma * n \qquad\qquad (2\text{-}4)$$

In this equation $F_{PGA}$ is a site amplification factor, $a_{max}$ is the peak acceleration at the ground surface, PGA is the peak ground acceleration at bedrock, and $a$ and $b$ are regression coefficients correlated from data trends for different site categories (i.e. site class, depositional environment).  An optional error term $\varepsilon$ is also included which is the based on the standard deviation $\sigma$ of the selected geologic environment multiplied by $n$, the number of standard deviations considered, either below or above the mean (ex. -1,1,2).  The Quaternary age values should generally be used for analysis of soils within a few meters of the surface.  Most liquefiable soils will also fall within the Quaternary age group.  Stewart et. al. also presents regression values correlating to NEHERP site class A through D for use in analysis.

**Table 2-1: Example values from Stewart et. al. (2003)**

| Holocene lacustrine/marine | | | Quaternary alluvium | | |
|---|---|---|---|---|---|
| a | b | $\sigma$ | a | b | $\sigma$ |
| -0.59 | -0.39 | 0.47 | -0.15 | -0.13 | 0.52 |
| Holocene colluvium | | | Holocene mixed sediments | | |
| a | b | $\sigma$ | a | b | $\sigma$ |
| -0.11 | -0.1 | 0.52 | -0.5 | -0.33 | 0.51 |

A more complex solution to approximate $a_{max}$ from PGA is a numerical site response analysis. These types of analysis are more site-specific than using Stewart et al. or other relationships, but can be prohibitively expensive in some cases because of they require the classification of the soil profile and its dynamic properties at various depths through significant in-situ and lab testing. Numerical modeling such as finite-element and finite-difference can be used in both equivalent linear or non-linear site-response analyses (Kramer 1996).

Linear analysis is the simplest of these analyses. Transfer functions have been defined which can modify the frequency/period of earthquake time histories. This analysis is relatively simple to run, but relies on broad assumptions. For example, in this analysis shear velocity ($v_s$), soil shear modulus (G), and soil damping ratio ($\xi$) do not change with soil strain, and thus cannot accurately model the natural non-linearity of soil.

To more accurately model the effect of the non-linearity of soil, non-linear approaches are available to model site response. The equivalent linear procedure is one of these models which uses a single shear modulus and equivalent damping ratio for each layer of a soil profile. After these values are assumed a linear site response is run to calculate effective strain values. With new effective strains values, G and $\xi$ are recalculated, after which the entire process is

repeated iteratively until a prescribed tolerance in the computed shear strain is met (Kramer 1996). Problems associated with equivalent linear analysis is that "spurious resonances" can occur and the iterative procedure can give non-unique results (Kramer 1996). Alternatively, effective stress non-linear analysis involves the breaking up of site response into a series of small time steps. Forward-difference approximation (finite difference method) is often used to model this complex behavior. Because of the complex nature of this calculation, a large amount of computing power is required to model each time step. This method is much less prone to spurious resonances but does require a good constitutive model to base the soil behavior on. Unfortunately, a universal constitutive model does not exist to model the behavior of all soil types, limiting the usefulness of non-linear analyses to cases where multiple constitutive models can be incorporated, vetted, and calibrated.

Linear and non-linear analyses are useful to engineers in such cases where a greater amount of confidence is desired in the site response. These analyses can serve as a more accurate model of site-specific site response rather than the empirically regressed or codified site amplification values, which are based on a statistical fit to a large sample of data, but do not necessarily represent the specific dynamic behavior at the site of interest. These complex approaches can also help model other effects such as pore pressure generation over time.

Overall, the simplest and most commonly used of these approaches are the correlations developed by Stewart, Liu et al. (2003). Although straightforward, this method requires an estimate of PGA, which can be computed from a seismic hazard analysis. The Stewart approach, along with a seismic hazard analysis will be used in this study to account for site response effects on bedrock earthquake ground motions.

## 2.5 Seismic Hazard Analysis

Seismic Hazard Analysis is a procedure used to predict strong ground motions at a given site. Two basic methods have been developed called deterministic seismic hazard analysis (DSHA) and probabilistic hazard analysis (PSHA). Each of these methods are used in engineering practice when strong ground motion parameters are to be estimated.

## 2.5.1 Deterministic Seismic Hazard Analysis

Deterministic seismic hazard analysis is the original method used by engineers to quantify earthquake hazard at a location. This method represents and single scenario in which an earthquake occurs and produces ground motions. This process begins by identifying and characterizing all potential seismic sources that could produce significant motions at the site of interest (Kramer, 1996). Each source is then assigned a value called site-to-source distance, which is commonly the shortest distance from the site to the source. Next, known characteristics of the sources are then compiled (size, rupture length, fault orientation, etc.). Later, using these characteristics and distances attenuation relationships such as NGA are used to approximate GMPs. From this data, the controlling earthquake is found and used to define design ground motions to be used at the site of interest.

DSHA contains certain disadvantages that have troubled researchers. DSHA focuses on one potential scenario which causes it to ignore the results of other possible scenarios which may be more likely to occur. Although DSHA generally tries to design for a conservative earthquake, it can sometimes give unrealistic results because there is no systematic way to deal with the uncertainty that exists within the attenuation relationships.

### 2.5.2    Probabilistic Seismic Hazard Analysis

Probabilistic seismic hazard analysis (PSHA) is a more recent addition to earthquake engineering. Beginning in the 1960's, PSHA was developed to better account for the uncertainty in many of the inputs in a seismic hazard analysis (Cornell 1968). PSHA also aims to overcome another issue of DSHA in that it attempts to consider not a single scenario but all possible scenarios and their corresponding likelihood of occurrence. The development of PSHA is a significant step in earthquake engineering research, as outputs from this analysis can be considered as existing in the realm of probability or likelihood of an earthquake occurring, rather than simply giving overdesigned values for the largest possible "super quake" that could occur at a site. In order to better understand the individual parts of a PSHA, each of the uncertainties involved are discussed below.

*Spatial Uncertainty*

Spatial uncertainty is associated with the actual location of an earthquake. It is currently impossible to predict exactly at what part of a seismic source an earthquake will occur. Spatial uncertainty tries to account for this by dividing potential sources (i.e. faults, etc.) into small segments which can be assigned likelihoods to generate the ground motions. Generally, a uniform probability density function (PDF) is used to model this uncertainty unless there is sufficient evidence to prove that another PDF more accurately represents the spatial uncertainty.

*Size Uncertainty*

The size uncertainty of future ground motions such as $M_W$ or PGA are also unknown. Seismic sources can cause earthquakes that vary in size and duration. As the size of the earthquake heavily affects the value of GMPs, it is vital to have a good idea of what size an

earthquake will be before it occurs. This uncertainty has been categorized by recurrence laws. Recurrence laws attempt to create a relationship between the return period of an earthquake and the annual rate of exceedance of a specified earthquake magnitude. Several different types of recurrence laws exist including slip-dependent recurrence laws (Slemmons 1982), bounded Gutenberg-Richter recurrence laws (Guttenburg and Richter 1944), and Characteristic Earthquake recurrence laws (Youngs and Coppersmith 1985, Wells and Coppersmith 1994). Each of these laws involve different considerations but in general they are used to determine a mean annual rate of exceedance ($\lambda_m$) which is the inverse of the return period ($T_R$) of a certain earthquake magnitude as shown in the following expression.

$$\lambda_m = \frac{1}{T_R} \hspace{8cm} \text{(2-5)}$$

Overall, these laws attempt to quantify the uncertainty in the size of an earthquake event by defining the likelihood of an earthquake exceeding a minimum magnitude (generally 4.0) to occur in any given year. This annual rate of exceedance essentially consolidates size uncertainty into the next topic, temporal uncertainty.

*Temporal Uncertainty*

Temporal uncertainty is associated with the fact that it is not known when an earthquake will actually occur. Because of the uncertain nature of the exact time of earthquake occurrence, researchers have treated earthquakes as random events. This classification seems to work well as the distribution of earthquake occurrence is often over thousands of years and is difficult to accurately model. Considering these events as random has allowed for use of the Poisson probability model which assigns all times an equal probability of occurrence. Using the Poisson

model the following expression has been developed to predict the probability of at least one exceedance of a certain level of ground shaking in a selected amount of years.

$$P[N \geq 1] = 1 - e^{-\lambda_m t} \tag{2-6}$$

This probability is calculated where $\lambda_m$ is the average annual rate of exceedance of the ground motion, and $t$ is the number of years considered.

Other researches have attempted to develop time dependent models (Wong 2012). These models take into account that earthquakes are not fully independent events. Currently these models are not widely used as there is a significant lack of earthquake data which is required to make a strong relationship. The primary constraint for developing these relationships is the fact that the return period of earthquakes is generally far larger than the timeframe of historical earthquake data collection.

*Attenuation Model Uncertainty*

Attenuation uncertainty is a product of the data spread in attenuation models used to predict ground motions in a PSHA. As discussed in section 2.3, the attenuation models are not perfect, but each have their benefits. Common practice has been to use a weighted average of the results from several attenuation models to minimize this uncertainty. Although using average results from multiple attenuation relationships is a straightforward way to resolve this uncertainty, this practice has led to some concerns with relatively low median estimates of ground motions from large magnitude earthquakes. NGA-west2 has attempted to capture this uncertainty more effectively for use in engineering practice. PEER has published reports that give regressed uncertainty values to use for each attention model. Currently, the most common way to deal with attenuation uncertainty is to minimize it using the average of multiple models.

As more sophisticated relationships are developed such as those from NGA-west2, this uncertainty will be able to be more accurately accounted for.

*PSHA process*

The PSHA process begins with identifying and characterizing all possible seismic sources. This step has been greatly aided by the development of seismic source models like those developed USGS and others (Petersen, Frankel et al. 2008). These models produce seismic source deaggregations which contain information about potential seismic sources (ie. distance from site, expected magnitude). These databases also contain probabilistic data like uncertainty in size, distance, time, among others. This information is contained in a property called contribution to hazard, and is statistically distributed depending on the uncertainty in the collected data. The example deaggregation plot in Figure 2-5 shows that there is some spatial uncertainty in the earthquakes expected to have a potential magnitude from 6.0 to 7.0. This can be seen as the contribution percentage is spread over a large number of distance values in the deaggregation. All these sites considered together contribute to the total probabilistic seismic hazard at the site.
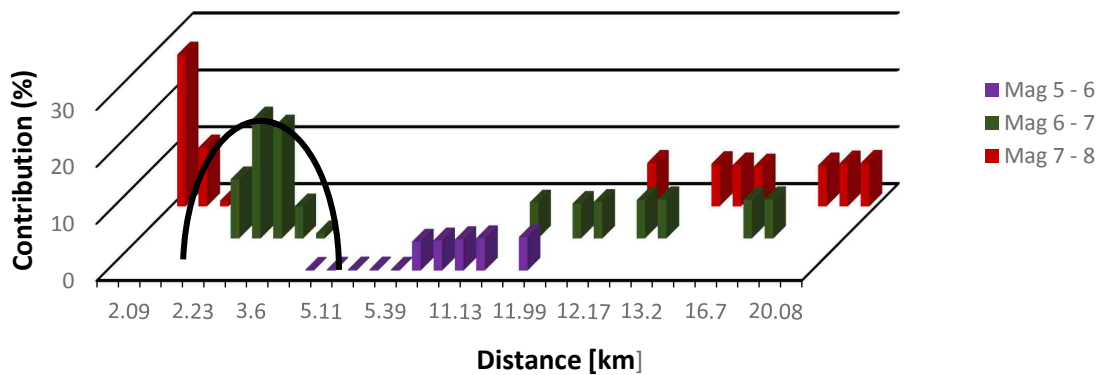
**Figure 2-5: Deaggregation plot for Salt Lake City at a 2475-year return period.**

The second step to run a PSHA is to develop a recurrence relationship that will give an average rate of occurrence for each earthquake magnitude. Next, GMPs are estimated for each potential seismic source using GMPEs and probability density functions. With each potential source of uncertainty in the calculations considered, it is then possible to calculate the probability that the estimated GMPs will be exceeded during a specified design period.

## 2.6 Seismic Hazard Curves and the Total Probability Theorem

By use of the total probability theorem, it is possible to use the conditional probabilities of each seismic source to exceed a GMP to find the overall total probability that the ground motion will be exceeded in the given timeframe. The consideration of all hazards from each seismic source is done by use of the equation:

$$\lambda_{y*} = \sum_{i=1}^{N_S} v_i \sum_{j=1}^{N_m} \sum_{k=1}^{N_R} P\left[Y > y* \mid m_j, r_k\right] P\left[M = m_j\right] P\left[R = r_k\right] \quad (2\text{-}7)$$

Where $\lambda_{y*}$ is the mean annual rate of exceedance of a threshold GMP ($y*$) and $P\left[Y > y* \mid m_j, r_k\right]$ is the probability of a GMP of interest $Y$ exceeding the given threshold GMP with a certain magnitude $m_j$, site to source distance $r_k$, and an average rate of threshold magnitude exceedance $v_i$. $P\left[M = m_j\right]$ and $P\left[R = r_k\right]$ are the probabilities that the magnitude and site to source distance will be equal to the considered $m_j$ and $r_k$ values. This summation equation essentially adds all the conditional probabilities of each source one by one to get the total seismic hazard at a site. When used over a range of different threshold GMP values, a useful plot called a seismic hazard curve is created. Figure 2-6 shows an example of a hazard curve created using the PSHA procedure in the form of data from the USGS deaggregations for a location in Salt Lake City,

20

Utah (Latitude 40.7 N, Longitude 111.89 W).  This curve provides a relationship between a

GMP on the x-axis and the mean annual rate of exceedance of that GMP on the y-axis.  These

curves are useful to engineers as they can be used to find the return period of other design

parameters such as structural damage and monetary cost, as well as predict ground motions at a

wide range of return periods.
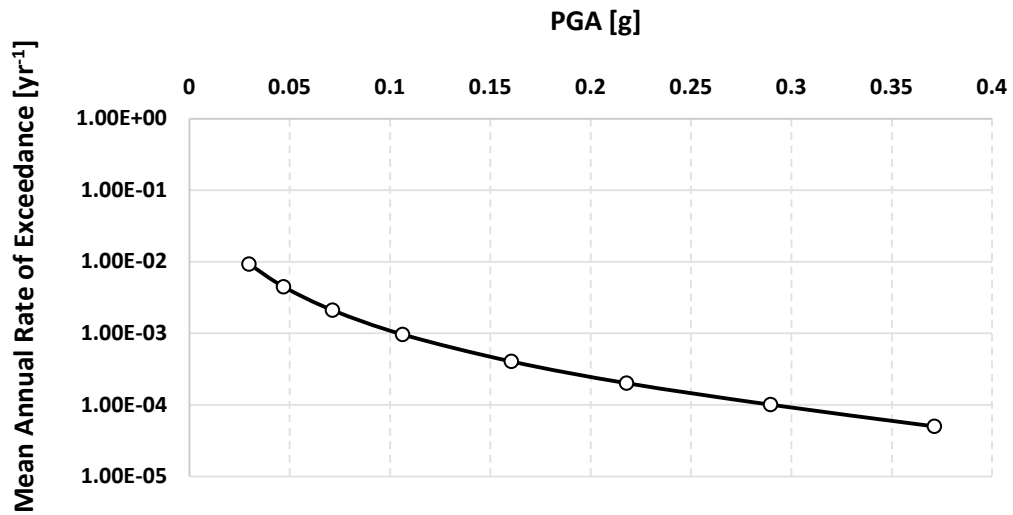


**Figure 2-6: Example seismic hazard curve for site in Salt Lake City, UT.**

# 3    EARTHQUAKE LIQUEFACTION

Earthquake liquefaction is a recently discovered natural phenomenon. Although evidence of liquefaction can now be identified from many historic and pre-historic earthquake events, it was not until the 1960's that researchers began to recognize the phenomenon. Two large earthquakes that occurred during that decade, one in Alaska and another in Niigata, Japan provided key case histories allowing researchers to observe the power of liquefaction. From these first observations, earthquake liquefaction began to be defined as the transformation of a granular material from a solid to a liquefied state as a consequence of increased pore-water pressure and reduced effective stress (Marcuson 1978)

Since that time, researchers have become more and more interested in the occurrence or even non-occurrence of liquefaction and related hazards. As more observations have been made after other major earthquakes the understanding of liquefaction has begun to be improved. From these observations, earthquake liquefaction related phenomenon have been divided into categories such as: lateral spread, settlement, flow failure and others. These effects are often easy to identify after an earthquake and provide an indication that liquefaction has occurred.

By analyzing the potential liquefaction hazard at a site, it is theoretically possible to mitigate or at least minimize the danger from liquefaction hazards. Because of this, researchers have attempted to predict liquefaction occurrence and mitigate risk from future events. Methods currently exist that allow engineers in design to account for the risk of such occurrences.

To gain a deeper understanding of the risk a site may have involving earthquake liquefaction, a system has been developed which supplies criteria to determine if liquefaction hazards may be a concern. Factors that should be systematically considered in a liquefaction analysis are: susceptibility, initiation, and effects (Kramer 1996).

## 3.1 Liquefaction Susceptibility

The determination of the ability of a soil to liquefy is a major part of a liquefaction analysis. If the soil at a potential building site is not considered to be liquefiable then liquefaction and associated settlements and lateral spreads are much less likely to need to be addressed. Criteria have been defined by which to judge if a soil is likely to be susceptible to liquefaction. Examples of susceptibility criteria are: historical, geological, compositional, and state criteria (Kramer 1996).

### 3.1.1 Historical Criteria

The historical criteria relates to whether liquefaction has occurred at a site in the past. This is primarily based on historical records or physical evidence that liquefaction or its effects have previously occurred. Assessment of the history of the site can be very helpful in deciding what effect may be problematic at the site. If a soil has been known to have liquefied sometime in the past it can be defined as likely being susceptible to liquefaction. For example, Youd and Wieczorek (1984) noted the reoccurrence of liquefaction (sand boils) at certain locations in the Imperial Valley of southern California from earthquake events in 1930, 1950, 1957, and 1979. These observations helped classify the soil at these locations as being susceptible to liquefaction. Although the criteria is limited relating to the non-occurrence of liquefaction in the past, which

does not a guarantee that liquefaction will not occur at a site in the future, the historical criteria does serve as a good initial test for a site-specific liquefaction analysis.
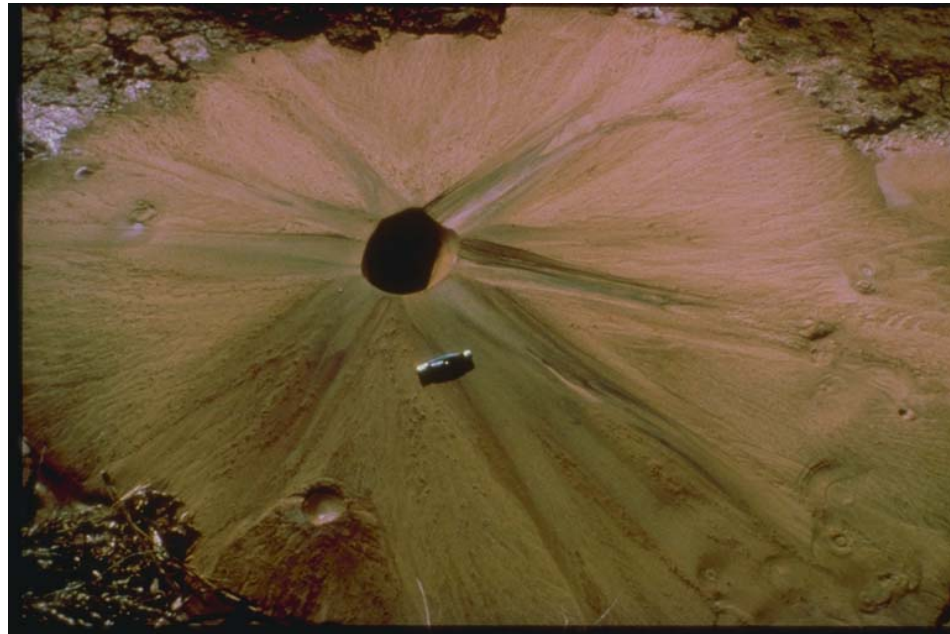


**Figure 3-1: A sand boil (evidence of liquefaction) near El Centro, CA (after NOAA/NGDC, University of Colorado at Boulder).**

### 3.1.2 Geological Criteria

The geologic history of a soil has been shown to serve as a useful tool to approximate liquefaction potential. In general, an increased geologic age has been seen to reduce the risk of a soil being liquefiable. Holocene fluvial, deltaic and Aeolian deposits have shown to have the highest susceptibilities to liquefaction (Youd and Hoose 1977). Poorly compacted artificial fills have been shown to be particularly prone to liquefaction as seen in the San Francisco during the Loma Prieta earthquake in 1989 (Ferritto, 1992). Lower susceptibilities are found in Holocene alluvial and Pleistocene sand deposits. Glacial tills, and clay-rich or pre-Pleistocene deposits are often considered immune to liquefaction (Youd and Hoose 1977). Other studies have also

compared the susceptibility of different geologic deposits as summarized in (Andrus and Hayati 2009).
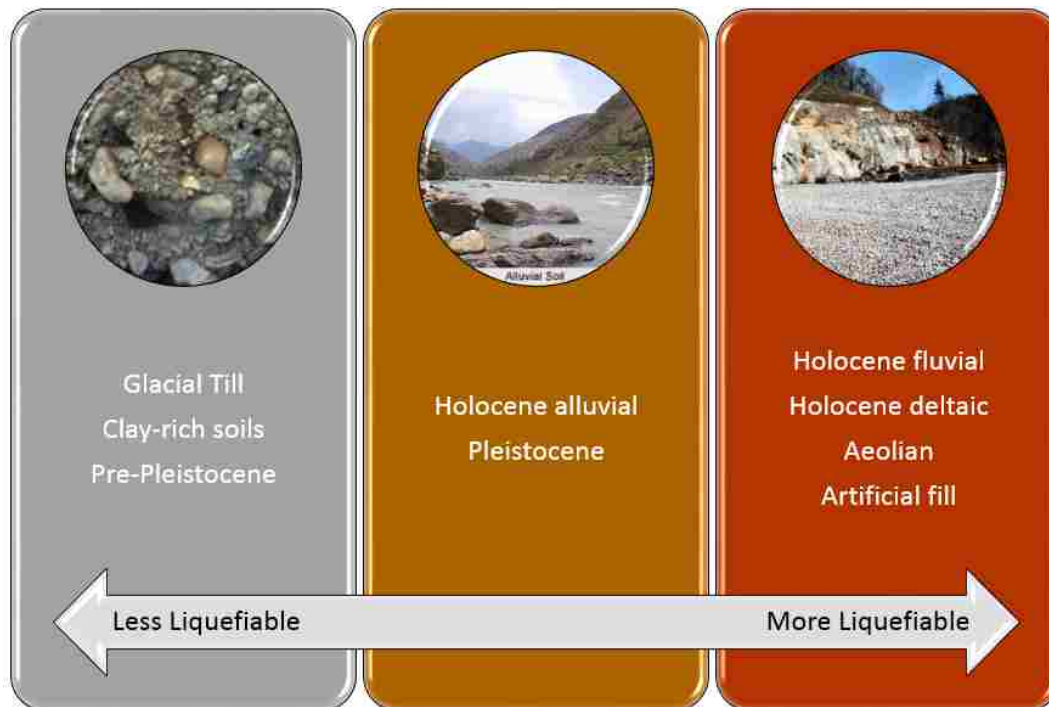


**Figure 3-2: Geologic criteria as based on Youd and Hoose (1977).**

The depth at which a soil is found in a profile can also have a significant impact on its liquefaction potential.  Soils deep beneath the surface often tend to be less susceptible than soils near the surface.  Because of this, shallow sediments, usually less than 15 meters below the surface should be the main focus of any liquefaction analysis.  Particle size uniformity can also have a smaller effect on liquefaction potential, with soils with uniform-sized particles being the most susceptible.

The saturation of a soil is also a key component to its liquefaction susceptibility.  It has been assumed for many years that if a soil is above the water table then it would not be susceptible to liquefaction. At the time, it was believed that the required pore-water pressure

would not build up in an unsaturated soil layer during an earthquake event which occurs relatively quickly. There has been some research conducted to contest this belief, such as (Unno, Kazama et. al 2008), but the current standard remains that soil that lies above the water table should be considered non-liquefiable.

### 3.1.3   Compositional Criteria

The composition of a soil at a site is another critical step in a liquefaction analysis. From experience, it has been observed that soils with a high fines content will be much less likely to liquefy than soils primarily composed of sands or gravels. The Chinese criteria (Wang 1979) have been widely used since the early 1980's as a means for evaluating the liquefaction susceptibility of silts and clays (Boulanger and Idriss 2006). The Chinese criteria is governed by the following:

Fraction finer than 0.005mm ≤ 15%

Liquid Limit, LL ≤ 35%

Natural Water Content $w_c$, $0.9LL \leq w_c$

Liquidity Index $\leq 0.75$

However, recent events such as the Kocaeli earthquake in 1999 have caused researchers to reexamine the liquefaction potential of fine grained soils. Bray and Sancio (2006) along with Boulanger and Idriss (2006) have established their own updated criteria for liquefaction susceptibility of these soils. When taking into account recent field data these criteria are seen as a more accurate judgment of the susceptibility of clays and silts.

Bray and Sancio published the following criteria which focuses more on soil plasticity. They state that a fine-grained soil may liquefy if:

Plastic Index (PI) < 12

Water content ($w_c$)/LL > 0.85

Figure 3-3 shows the new criteria in graphical form.  These plots also show that the new criteria appears to provide a good match for the liquefaction case histories used in the Bray and Sancio study as well as other previous studies.
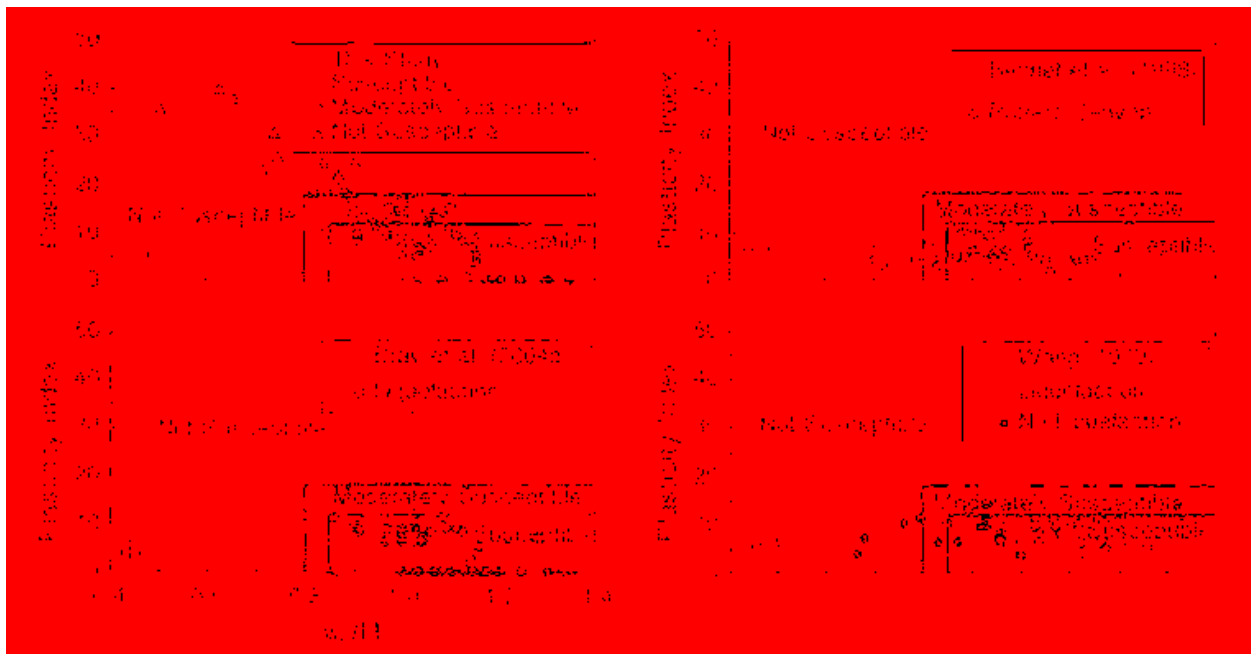


**Figure 3-3: Graphical representation of Bray and Sancio criteria with data from other studies.**

Boulanger and Idriss (2006) presented their observations on the susceptibility of fine-grained soils to liquefaction.  From experimentation with monotonic and cyclic loading triaxial tests they observed a region on the plasticity chart where a transition occurs from more sand-like

behavior to more clay-like behavior occurs when considering liquefaction potential. Figure 3-4 shows the results of their findings which are: Soils with a PI > 7 will almost always exhibit clay-like behavior and will generally not be susceptible to liquefaction; if a soil is classified as CL-ML the PI cutoff should be lowered to 4 as these soils exhibited clay-like behavior.
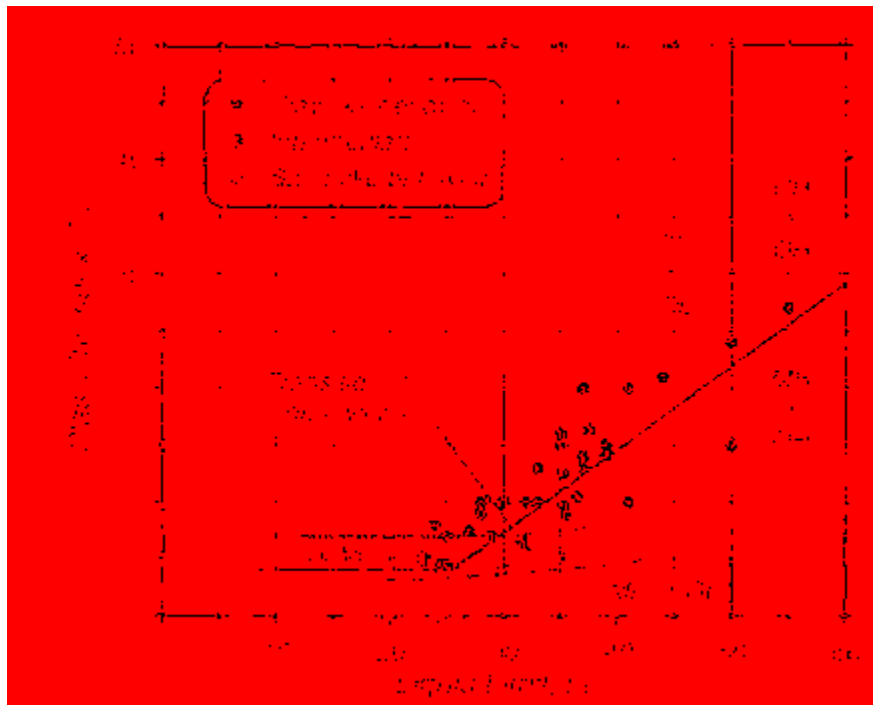


**Figure 3-4: Results from Boulanger and Idriss 2006 plotted on plasticity chart (after, Boulanger and Idriss 2006).**

Other criteria have also been suggested for assessing the susceptibility of soils to liquefy based on their soil particle composition.

### 3.1.4   State Criteria

Another way to look at the liquefaction susceptibility is found through the branch of geotechnical engineering called state mechanics. State criteria can help classify a soil's liquefaction potential by observing its initial stress state. The stress state of a soil is a function of

28

the effective stress felt by the soil ($\sigma'$) and the soil's void ratio ($e$) which relates to the density

of the soil. Research in this field began with many drained strain-controlled triaxial tests done

by Arthur Casagrande in the 1920s. From these tests, Casagrande began to observe that

regardless of initial state (dense or loose), soils with the same confining stress when sheared

appeared to converge to an intermediate void ratio (density). In other words, initially loose

samples contracted as they were sheared, while initially dense specimens dilated to a less dense

state. Casagrande then predicted that all soils when sheared would eventually converge to a

critical void ratio $e_c$. For a range of different values of confining stress $\sigma'_{3c}$, correlating critical

void ratios can be plotted to represent the critical void ratio (CVR) line (Figure 3-5). The CVR

line came to define the boundary between contractive and dilative soils (Casagrande 1936).
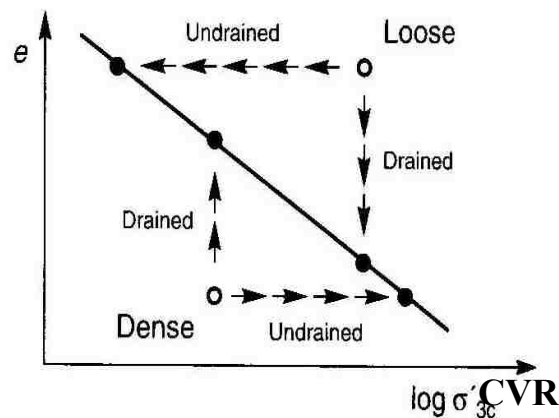


**Figure 3-5: Casagrande CVR Line (after Kramer, 1996).**

Although undrained tests were not widely available at the time of Casagrande's research,

he assumed that his work done with drained test could translate into that realm as well. Because

of this he assumed that soils that plotted above the CVR would develop positive excess pore

pressures and thus be susceptible to liquefaction, while soils below the CVR would develop

negative pore pressures which would not allow the soil to be susceptible to liquefaction, but

actually strengthen these soils in undrained loading. For several years, the CVR line was considered an acceptable division of susceptible and non-susceptible soils.

In 1938, Casagrande's ideas were brought into doubt. In that year, the Fort Peck Dam in Montana failed from flow liquefaction. When investigating the failure of this dam it was found that the initial states of some of the soils that failed in the dam had plotted beneath the CVR line and thus should not have been susceptible to liquefaction. Because of this contradiction to the findings of Casagrande, one of his PhD students named Castro began to do more testing to determine if something was missing from the CVR theory. Castro's research came to find that Casagrande had oversimplified the separation of contractive and dilative soils.

By the time Castro began his research, undrained shear tests were now more widely available. Using these tests, Castro was able to more accurately define the behavior of soils by considering the influence of induced pore pressures. Figure 3-6 shows the 3-dimensional results of these tests, split between three 2 dimensional plots. Line A in Figure 3-6 represents loose soil samples which were seen to contract under monotonic loading and exhibit liquefaction. Line B represents dense samples which were observed to only briefly contract, and then dilate never reaching a liquefied state. Line C represents soil of a density between loose and dense. These samples did enter a short phase of strain-softening behavior before dilating and gaining strength. Castro named this strange behavior "limited liquefaction".

After completing this research, Castro defined a steady state deformation (Castro and Poulus 1977). This was defined as a state of soil where a deformation occurs under constant shear and confining stress but without a change in volume. In this state, the soil is given a strength called the steady state strength ($S_{Su}$). Essentially the steady state line is the true

boundary between contractive and dilative behavior in undrained conditions that Casagrande had

been attempting to find years before.  Figure 3-7 shows the difference between the SSL and CVR

in $e$ - $\log(\sigma')$ space.  As seen below the SSL is approximately parallel to the CVR but plots

below it.  The distance between the two lines depends on the soil being considered.  Fortunately,

the SSL has found to be a much more accurate evaluator of liquefaction potential.  From Castro's

results, it was seen that if a soil in its initial state plots below the SSL then the soil will not be

susceptible to flow liquefaction.  If a soil in its initial state plots above the SSL it may be

susceptible to flow liquefaction if its steady state strength ($S_{Su}$) is exceeded during shear

loading.
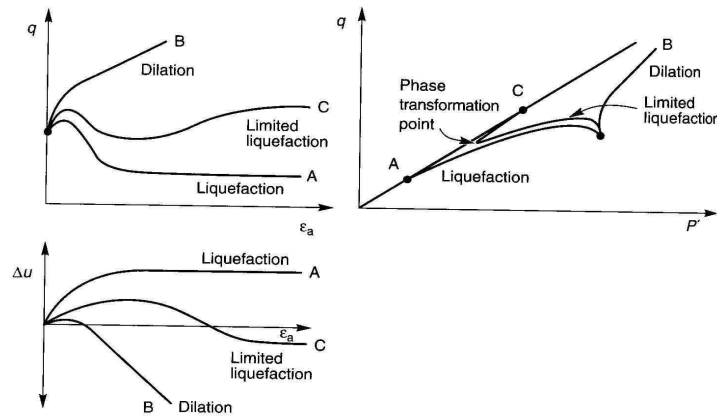
**Figure 3-6: Observations from Castro's undrained triaxial tests (after Kramer, 1996).**
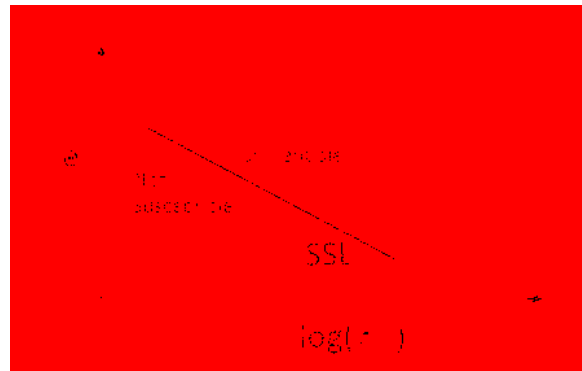
**Figure 3-7: Representation of Castro's Steady State Line (SSL) in contrast to CVR.**

Based on the development of the steady state line, Been and Jeffries (1985) developed a parameter to mathematically explain a soil's relationship with the SSL. They reasoned that even though soils at different confining pressure act differently, soils that were the same distance from the SSL should act similarly. This parameter was called the state parameter, and was calculated as the vertical distance from the SSL in $e\text{-}\log(\sigma')$ space. Mathematically the expression is given as:

$$\psi = e - e_{SS} \tag{3-1}$$

where $e_{SS}$ is the void ratio on the SSL corresponding to an effective confining pressure of interest. Given that soils can plot either above or below the SSL, $\psi$ can be either positive or negative. Positive values of $\psi$ are of most interest to engineers, as these values will represent a soil that is potentially susceptible to liquefaction.

## 3.2    Liquefaction Initiation

Liquefaction initiation, also known as liquefaction triggering is the process of a soil reaching the right conditions to begin to liquefy. From the work of both Casagrande and Castro, it became clear to researchers that liquefaction was a function of both soil susceptibility and shear loading. These two conditions need to both meet certain criteria to allow a soil to enter a liquefied state. Understanding the susceptibility and the initiation potential of soils are key to assigning liquefaction hazard to a potential site. Depending on the properties of a soil at the time liquefaction is triggered there are two potential liquefaction phenomena that can occur, flow liquefaction and cyclic mobility. Because liquefaction initiation will be the focus of this thesis, the evaluation of liquefaction triggering will be discussed in detail in chapter 4.

### 3.2.1 Flow Liquefaction

Flow liquefaction has the potential to cause catastrophic soil deformations. This phenomenon occurs when a liquefied soil's residual shear strength drops below the value required to resist the shear stresses that exist from the weight of the soil. Essentially, during flow liquefaction the soil will suddenly not be able to support its own weight because of the loss of equilibrium in the system. This kind of liquefaction is most common on sloping ground where shear stresses tend to be large. Because of this, slopes, earthen dams and other similar engineered structures can be especially susceptible to flow liquefaction, often with significant consequences.

Flow liquefaction is caused by induced shear stress from an earthquake, which quickly causes a rise in pore water pressure. As the pore pressure buildup occurs, there comes a point where the soil will reach its maximum strength and then will lose strength rapidly. This loss of strength can be visualized in Figure 3-8, which shows the stress paths during liquefaction initiation with either cyclic or monotonic loading. The cyclic loading follows the path A-D-C, while the monotonic loading follows path A-B-C. As strains increase (or fluctuate) the soil eventually becomes unstable. At this point the soil reaches a point called the flow liquefaction surface (FLS).
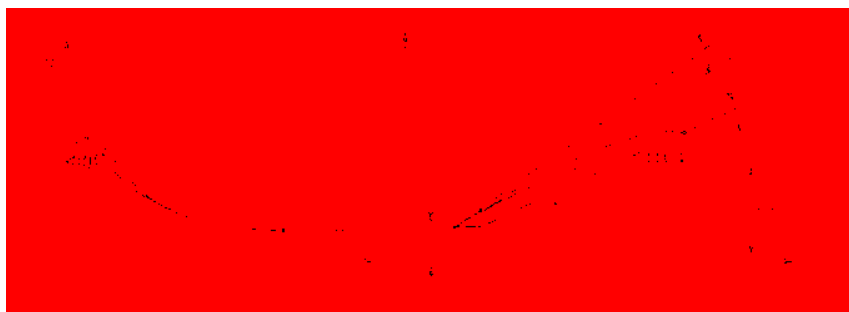


**Figure 3-8: Stress path of soil during liquefaction with both cyclic and monotonic loading (after Kramer, 1996).**

This surface was first defined by Vaid and Chern (1985). This FLS is a line in q – p'

space which separates the behavior of the soil between flow liquefaction and cyclic mobility. It

is at the FLS that flow liquefaction is considered to have been initiated. At this point the soil

quickly loses shear strength as it approaches a steady state strength $S_{Su}$. With the development

of the FLS, it is possible to predict if a soil will be susceptible to flow liquefaction by plotting the

soil's initial stress conditions in p'- q space. If the soil plots in the shaded region as seen in

Figure 3-9, the soil will potentially be susceptible to flow liquefaction.
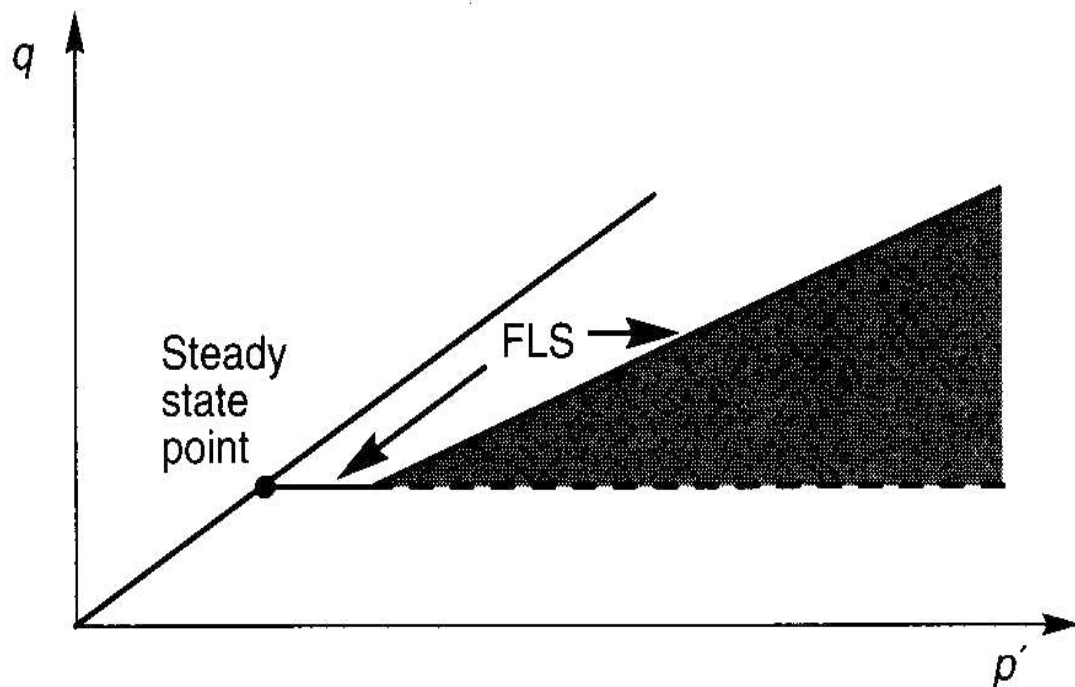


**Figure 3-9: Region of p'-q space where soils are potentially susceptible to flow liquefaction (shaded region) (after Kramer, 1996).**

A significant concern relating to flow liquefaction is the possibility of flow failures. If

the residual strength (strength after end of straining) of the soil is less than the static shear stress

required to keep the soil stable, large displacements will occur as the mass attempts to once again find stress equilibrium. The results of this type of deformation can be seen in Figure 3-10 which shows the flow failure that occurred at the Sheffield dam during the 1925 Santa Barbara earthquake.
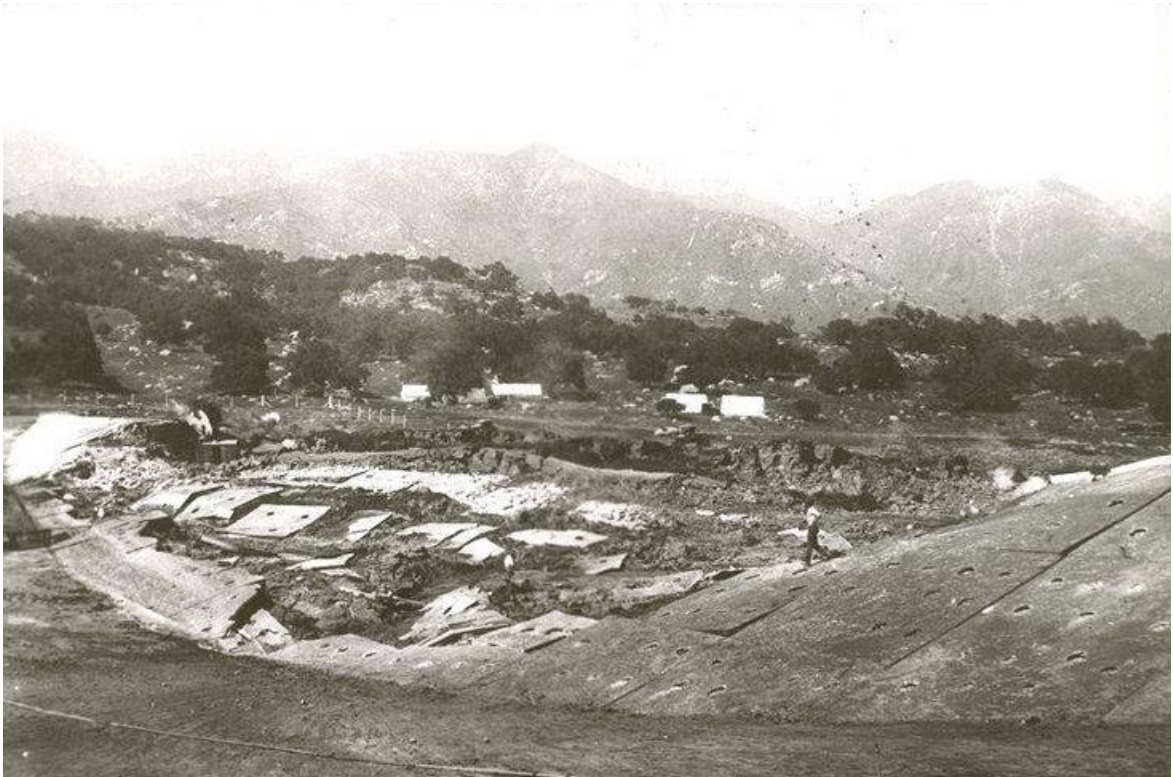


**Figure 3-10: Flow liquefaction failure of the Sheffield Dam Following the 1925 Santa Barbara earthquake (after EERC, Univ. of California).**

### 3.2.2 Cyclic Mobility

Cyclic mobility is defined as the gradual loss of soil strength due to the incremental buildup of pore water pressure from cyclic loading in undrained conditions. Cyclic mobility differs from flow liquefaction in that the static shear stresses remain less than the steady state or residual strength of the soil. During cyclic mobility, the soil does not fail under its own weight, but is weakened by the earthquake loading and eventually deforms to a certain extent. Vaid and

Chern (1985) defined cyclic mobility as "an accumulation of deformations which are limited in magnitude" that can occur during liquefaction initiation. Cyclic mobility is not as limited as flow liquefaction in that it can affect many kinds of soils including dense and dilative soils. The range of initial stress conditions that are susceptible to liquefaction can be seen graphically in Figure 3-11.
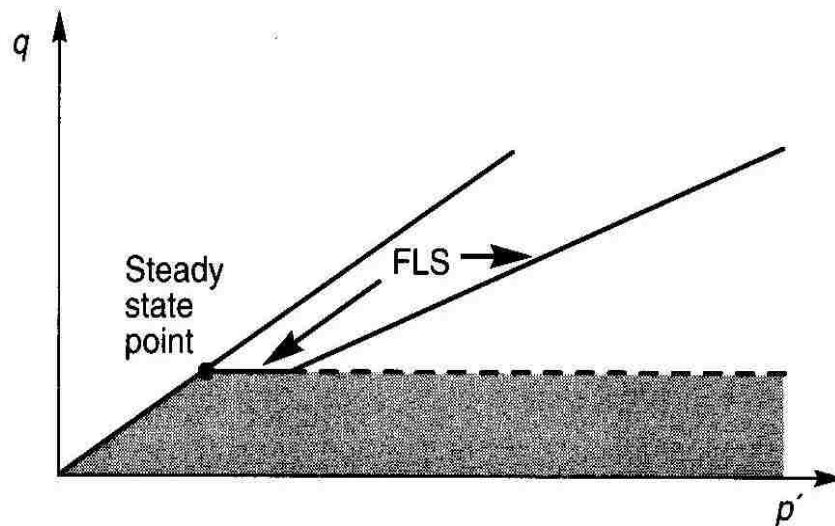


**Figure 3-11: Region of p'-q space where soils are potentially susceptible to cyclic mobility (shaded region) (after Kramer, 1996).**

## 3.3 Liquefaction Effects

When the evaluation of liquefaction triggering at a site is conducted, it is important to consider the potential effects that could result from the triggering of liquefaction. The effects of liquefaction have the potential to decimate structures through differential settlement, lateral spread or other effects. These topics will be briefly discussed in this section.

### 3.3.1 Settlement

Sandy soils have been shown to densify during earthquake loading (Kramer, 1996). This densification of soil layers below the surface can often be visualized in the form of ground settlement. In many cases this settlement can cause enormous damage to structures, lifelines, and other subsurface utilities. Both dry and saturated sands are known to settle during and after earthquake events. The settlement of dry sands occurs very quickly and is often not considered as part of a liquefaction analysis. The settlement of saturated sands however is a crucial part of any liquefaction analysis.

When saturated sands begin to feel earthquake loading, pore pressures will start to build up. Once these pore pressures become strong enough, they can push the sand particles away from each other causing the sand to go into suspension. At this moment, any structure built on this sand will essentially be floating on water. As the pore pressures quickly dissipate, the sands will return into a more natural position. Because of induced loads above, (structures or soil) the sand often settles into a more dense arrangement than before. The sum of this process over large sand layers can cause settlements of up to 1 meter.

An example of the damage that can be caused by liquefaction-induced settlements can be seen in Figure 3-12, where differential settlement under the length of a building has caused it to tilt. These settlements can occur immediately, or can take longer depending on the rate at which the pore pressures are dissipated.

**Figure 3-12: Damage to a Building due to liquefaction-induced differential settlement in Kathmandu, Nepal from 2015 earthquake event (after GEER, 2015).**

The calculation of liquefaction-induced settlement is often done by splitting up the soil profile into smaller increments, calculating the expected strains, and then summing up those strains for the complete soil layer depth.

### 3.3.2 Lateral Spread

Lateral spread is a liquefaction-induced phenomenon caused by cyclic mobility. If cyclic mobility occurs in a region with a significant slope or free face, the conditions may exist to induce lateral spread. During lateral spread, blocks of mostly intact surficial soil displace downslope on top of liquefied soil, these displacements can range from a few centimeters to several meters (Youd and Bartlett 1995). These events often occur in areas near bodies of water such as rivers, lakes, or oceans. Because structures such as bridges, railroad tracks, and port facilities are often built in susceptible regions, they can be particularly prone to damage from

lateral spread.   Figure 3-13 shows an occurrence of lateral spread near a river in Kathmandu, Nepal after the 2015 earthquake event.

To quantify the magnitude of possible lateral spreads, empirically based equations have been developed.   One particularly popular equation used in engineering practice was developed in (Bartlett and Youd, 1995) and (Youd, Hansen et. al., 2002).   This deterministic equation takes into account a potential earthquake scenario (magnitude and distance) along with soil parameters, and site conditions (slope, etc.).   Once the scenario is selected, a possible magnitude for lateral spread is predicted.



**Figure 3-13: Lateral Spread visible near Kathmandu, Nepal after 2015 earthquake events (after GEER, 2015).**

### 3.3.3 Loss of Bearing Capacity

Another effect of liquefaction is the loss of soil bearing capacity. This effect of liquefaction can cause extensive damage to buildings through foundation failure. The reduction in bearing capacity is caused by the buildup of pore pressures during the earthquake. As these pore pressures increase, the liquefied soil will approach a steady state strength which is often less the initial soil strength (Figure 3-8). If the steady state strength becomes less than the required soil shear strength to support the structure a bearing capacity failure can occur. A famous representation of this effect occurred in japan during the Niigata earthquake in 1964 (Figure 3-14). In this event, the structures remained intact from the ground shaking but the buildings rotated and tipped over because the soil could no longer support the weight of the structures and their pile foundations. Ground improvement is often required is cases where bearing capacity from liquefaction is considered as a potential issue. The use of ground improvement can help by raising the minimum liquefied strength above the steady-state strength.



**Figure 3-14: Bearing capacity failure of structures from soil liquefaction in Niigata, Japan (1964) (after NOAA/NGDC - NOAA National Geophysical Data Center).**

### 3.3.4   Flow Failures

As discussed in section 3.2.1, flow failures occur when the steady-state strength of the soil drops below the initial static shear stress of a soil mass.  As the stress state of the soil passes the FLS the strength of the soil decreases very quickly.  Because of the rapidity of this stress transformation, flow failures can be very large and cause catastrophic damage.  A potentially deadly example of this is the Lower San Fernando Dam during the San Fernando earthquake in 1971.  During the earthquake, a flow failure occurred on the upside of the dam which nearly caused a collapse.  Had this caused the complete failure of the dam, thousands of lives could have been lost from flooding in the highly-populated San Fernando valley below.



**Figure 3-15: Flow liquefaction failure of the Lower San Fernando Dam, 1971 (courtesy of the National Information Service for Earthquake Engineering, EERC, University of California, Berkeley).**

### 3.3.5  Other Potential Effects

Other effects of earthquake liquefaction include: sand boils, altered ground motions, and increased lateral earth pressure on retaining wall structures.

Sand boils, sometimes called "sand volcanoes" are a common indicator of soil liquefaction.  These boils are formed when high pore pressures build up in liquefied soils beneath the ground.  If these soils find a seam in the non-liquefied soils above, the pore pressures will dissipate by moving quickly towards the surface.  When these pore pressures are released at the surface, they bring sandy sediments with them from the liquefiable layer to the surface.

Liquefaction can also cause alterations to ground motions.  As liquefaction occurs, a sudden decrease in stiffness will often occur in the liquefied soil layer.  This soil then becomes more likely to filter our high frequency ground motions but allowing low frequency motions to pass through.  These low frequency ground motions can cause large deformations and damage to structures from shaking.

# 4 METHODS FOR ASSESMENT OF LIQUEFACTION INITIATION POTENTIAL

In the early days of the study of earthquake liquefaction laboratory methods were often used to assess liquefaction potential. These methods were useful, but also problematic because of the difficulty in obtaining undisturbed specimens (Seed 1979). Because it is very difficult and expensive to obtain undisturbed samples of many liquefiable soils, engineers have found ways to predict liquefaction based on in-situ soil strength. Methods that use in-situ soil data to correlate liquefaction hazard are called empirical or observation based methods.

Significant research has taken place in the last few decades relating to the creation of methods for estimating liquefaction potential of soils based on empirical data. SPT-based methods were the first to be developed and are commonly used in practice today, but recently the interest in CPT based methods has increased with greater use and availability of CPT data. CPTs have the advantage of providing a nearly continuous soil profile, which allows engineers to then produce a continuous soil profile relating to liquefaction potential. Conversely, SPT methods can provide predictions for liquefaction hazard at only a few select depths in a soil profile. As this thesis is focused on the use of CPT data in liquefaction analysis, these methods will be specifically mentioned in this chapter.

## 4.1 Empirical Deterministic Methods

Empirical methods are often used in the assessment of liquefaction potential. These methods are based on in-situ soil data collected by researchers who then compiled this information into case histories. Because this data is collected in-situ, the uncertainty of the lab methods is replaced by other forms of uncertainty. This thesis will later demonstrate how this uncertainty is considered with different liquefaction initiation models.

In 1971, Seed and Idriss developed a simplified procedure for the evaluation of sites for liquefaction potential. This procedure marked the beginning of the use of empirical methods for liquefaction analysis. The original equations proposed by Seed and Idriss (1971) still form the basis for most of these models today. These methods became available after the occurrence of large earthquakes in Alaska and Japan in 1964. Large amounts of subsurface data were collected at that time which facilitated the development of a liquefaction triggering model based on soils that had been determined to have liquefied or not liquefied during the same earthquake event.

The simplified procedure was based on two basic parameters, the seismic loading on a soil layer and the capacity of the soil to resist liquefaction (Youd et. al. 2001). In this way, the calculation of a factor of safety against liquefaction became a ratio of the loading and capacity of a soil to resist liquefaction.

$$FS_{Liquefaction} = \frac{\text{Resistance}}{\text{Loading}} \qquad (4\text{-}1)$$

To quantify the seismic loading on a soil layer, an expression called the cyclic stress ratio (CSR) is used.

The general equation for CSR is given as:

$$CSR = (\tau_{av} / \sigma_{vo}^{'}) = .65(a_{max} / g)(\sigma_{vo} / \sigma_{vo}^{'})r_d \tag{4-2}$$

where $\tau_{av}$ is the average shear stress, $\sigma_{vo}^{'}$ is the effective stress, $\sigma_{vo}$ is total stress, $a_{max}$ is the maximum acceleration at the ground surface, $g$ is the acceleration of gravity, and $r_d$ is a depth reduction factor. The depth reduction factor in this equation is used to account for changes to the flexibility of the soil profile at depth. The depth reduction factor will be discussed in greater detail later in this thesis.

To quantify the capacity of a soil to resist liquefaction, an expression is defined called the cyclic resistance ratio (CRR). The computation of a CRR is what differentiates most liquefaction initiation procedures. Because of the difficulty in obtaining accurate CRR values from laboratory testing methods, various field tests have become common use in engineering practice to estimate CRR. Examples of field tests commonly used are standard penetration test (SPT), cone penetration tests (CPT), shear-wave velocity measurements ($v_s$), and the Becker penetration test (BPT). Of these tests, SPT and CPT are preferred because their associated liquefaction databases are larger. This thesis will focus almost exclusively on CPT based methods for calculation of CRR.

Once a value for CRR is estimated, it is then possible to calculate a factor of safety against liquefaction ($FS_L$) for a soil layer using equation 4-3.

$$FS_L = \frac{CRR}{CSR} \tag{4-3}$$

The development of the simplified method has greatly improved the ability to estimate if a soil will liquefy. As time progressed, the number of different procedures to calculate CRR increased

significantly. With the development of these different procedures, some confusion began to take place about the consistency and the correct use of different liquefaction resistance methods (Figure 4-1). In 2001, a report was published that summarized the findings of the 1996 NCER and 1998 NCEER/NSF workshops (Youd, Idriss et. at. 2001). The goal of these workshops was to bring together 20 of the world's top experts on liquefaction evaluation and to update the simplified procedure and incorporate research findings from the last decade. The findings from these workshops have been widely adopted in engineering practice and are in common use today.
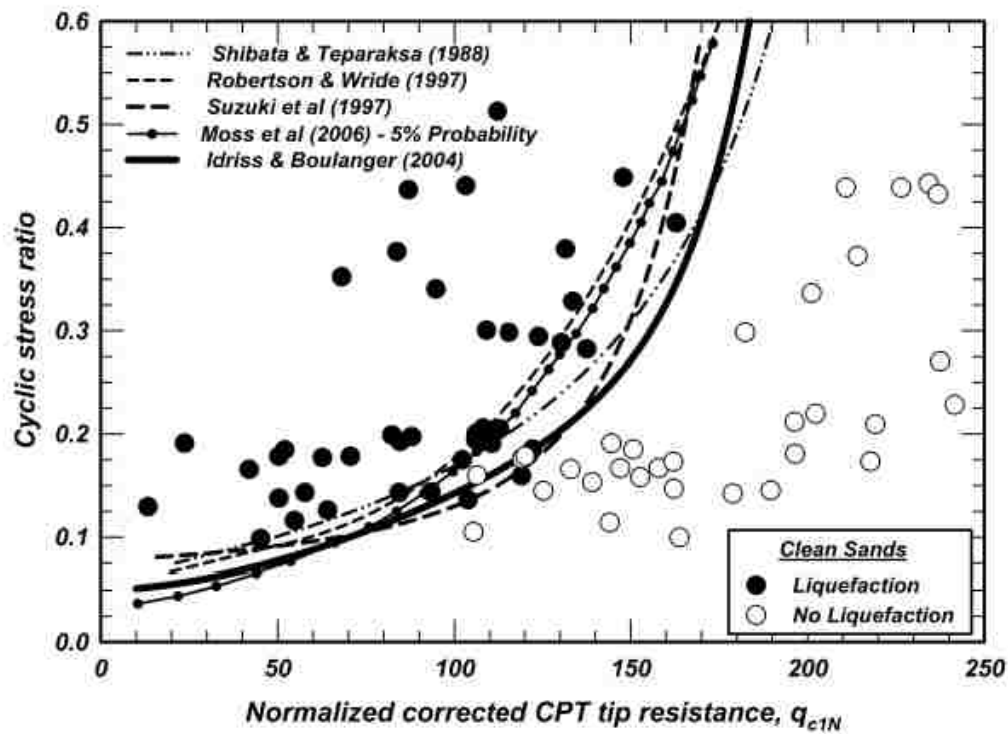


**Figure 4-1: Examples of various CPT-based CRR curves for M=7.5 and $\sigma'_{vo}$ = 1atm (after Boulanger and Idriss 2008).**

### 4.1.1 Robertson and Wride (1998, 2009) [NCEER 2001] Deterministic Procedure

The CPT based liquefaction triggering procedure proposed in a write-up of the 1996 and 1998 NCEER workshops (Youd, Idriss et at. 2001) is based on the work of Robertson and Wride

46

(1998). Findings from researchers such as Skempton (1986) and Robertson (1990) had concerns with using SPT data in the simplified method to estimate CRR values. These concerns were mostly based on the inconsistent nature of the values from the SPT and poor repeatability of results (Kulhawy and Mayne 1990). In this case, the CPT appeared to be a good solution, as it had been seen to be more repeatable than the SPT and to provide a more complete view of a subsurface soil profile. Initial use of the CPT as a tool for analysis of soil liquefaction susceptibility was primarily based on CPT to SPT conversions, but as use of the CPT in engineering practice increased, methods for analysis independent from the SPT models began to be developed.

### *CPT Corrections Factors*

The Robertson and Wride procedure uses several CPT input parameters to estimate the cyclic resistance of the soil at each layer. The major inputs are: cone tip resistance ($q_c$), cone sleeve friction ($f_s$), and the pore pressure measured behind the cone ($u$). This procedure calls for the normalization of the cone tip resistance for both overburden pressure and the units of measure. The normalization process results in a dimensionless soil resistance parameter $q_{c1N}$ defined as:

$$q_{c1N} = \left(\frac{q_c}{P_{a2}}\right)C_N \qquad\qquad (4\text{-}4)$$

In this expression $q_c$ is the measured CPT tip resistance, $P_{a2}$ is a reference pressure in the same units as $q_c$ equal to 0.1 MPa, and $C_N$ is an overburden stress correction factor.

Values for $C_N$ can be found using:

$$C_N = \left( P_a / \sigma_{vo} \right)^n \leq 1.7 \tag{4-5}$$

where $P_a$ is the atmospheric pressure (1 atm.) in the same units as the soil overburden pressure $\sigma_{vo}$, and $n$ is a stress exponent generally set equal to 0.5.

Researchers such as Robertson and Campanella (1985), Seed and de Alba (1986), Shibata and Teparaska (1988), Mitchell and Tseng (1990), Suzuki et al. (2003), and Moss et al. (2006) all developed relationships estimating CRR from corrected values of CPT penetration resistance. The field performance data collected in the 1990's helped to ratify that the CRR estimates from CPT data were reasonable for clean sand values. The 1996 NCEER workshop suggested the following CRR curve in Figure 4-2 based on available CPT data and experience along with SPT correlations. This curve for clean sand values is given along with limiting strains. Although this curve is helpful for estimation of CRR values, it is limited by several assumptions: site conditions similar to the SPT-based database, Holocene age, clean sand deposits; level or gently sloping ground; magnitude M=7.5 earthquake; and depths from 1 to 15 m (Robertson and Wride 1998).
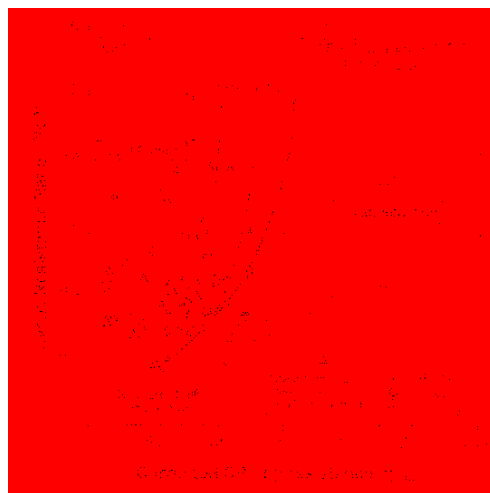


**Figure 4-2: Recommended CRR for clean sands under level ground conditions based on CPT (after Robertson et al 1998).**

Procedures have been developed to estimate soil grain characteristics from CPT data. With the grain characteristics known, correlations to clean sand values can be made, allowing for a direct calculation of CRR for any soil type given as:

$$\left(q_{c1N}\right)_{cs} = K_c \left(q_{c1N}\right) \tag{4-6}$$

where $\left(q_{c1N}\right)_{cs}$ is the normalized clean sand equivalent CPT penetration resistance, $q_{c1N}$ is the normalized CPT penetration resistance, and $K_c$ is a grain characteristics correction factor.

Experience with CPT data shows a relationship between the CPT friction ratio, essentially the ratio of $f_s$ to $q_c$. This ratio was seen to increase with increasing fines content and soil plasticity (Robertson and Wride 1998). Soil behavior charts have been suggested by several researchers (Jefferies and Davies 1993) and (Robertson 1990), which take advantage of the CPT friction ratio and apparent fines content relationship.

Based on the boundaries between apparent soil types on the CPT chart, Robertson (1990) suggests a soil behavior type index $I_c$ defined as:

$$I_c = \left[ \left(3.47 - \log(Q)\right)^2 + \left(\log(F) + 1.22\right)^2 \right]^{0.5} \tag{4-7}$$

where

$$Q = \left(\frac{q_c - \sigma_{vo}}{P_{a2}}\right)\left(\frac{P_a}{\sigma'_{vo}}\right)^n \tag{4-8}$$

and

$$F = \left[\frac{f_s}{q_c - \sigma_{vo}}\right] * 100 \tag{4-9}$$

where $Q$ is the dimensionless normalized CPT penetration with a stress exponent typically set to $n = 1.0$, with $P_a$ and $P_{a2}$ being reference pressures equal to 100 KPa but in same units as $\sigma_{vo}$ and $\sigma'_{vo}$. Depending on the soil type, $Q$ can be, but is not always equal to the previous normalized CPT penetration value $q_{c1N}$ (with $n = 0.5$). A true normalization for soil types requires a stress exponent that varies from about .5 in sands to 1.0 in clays (Robertson and Wride 1998). This calculation requires an iterative procedure that is presented in the Robertson and Wride method and has since been updated in (Robertson 2010). $F$ is the normalized friction ratio and is a function of the cone tip resistance, cone sleeve friction, and soil overburden pressure.
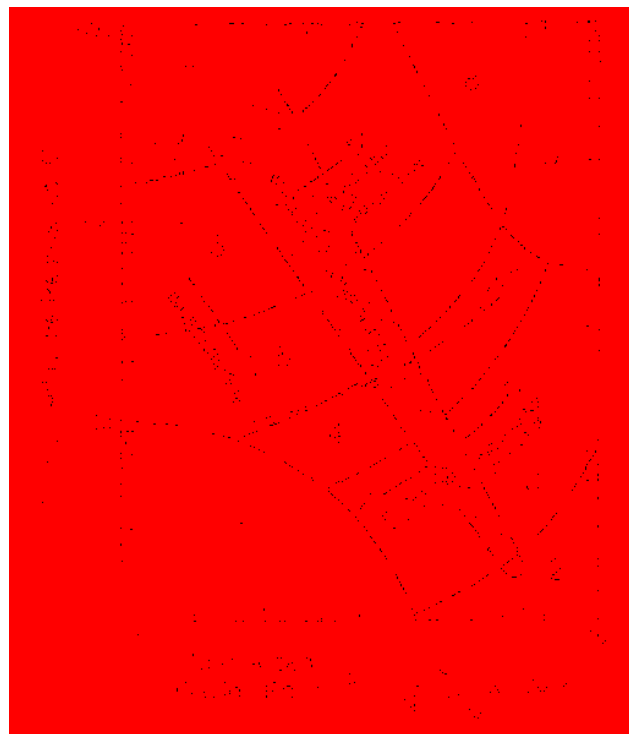


**Figure 4-3: Normalized CPT soil behavior type chart (after Robertson 1990). Soil types: 1, sensitive, fine grained; 2, peats; 3, silty clay to clay; 4, clayey silt to silty clay; 5, silty sand to sandy silt; 6, clean sand to silty sand; 7, gravelly sand to dense sand; 8, very stiff sand to clayey sand; 9, very stiff, fine grained.**

The iterative procedure suggested by Robertson and Wride (1998) begins with setting the stress exponent $n$ equal to 1.0. Next, initial values for $Q$ and $I_c$ are calculated. When $I_c \leq 2.6$ it is suggested to set $n = 0.5$. If the recalculated value then adjusts to $I_c \leq 2.6$ then a value of $n = .75$ should be used. Further clarification on this process can be found in Figure 4-4 which is a flow chart explaining the Robertson and Wride (1998) method.

Once the iterative process is complete, soil grain correction factors should be calculated. The suggested value for $K_c$ is defined as:

$$
\begin{array}{lll}
If: & I_c \leq 1.64 & K_c = 1.0 \\
If: & 1.64 < I_c \leq 2.6 & K_c = -.403 I_c^4 + 5.581 I_c^3 - 21.63 I_c^2 + 33.75 I_c - 17.88
\end{array}
\tag{4-10}
$$

Other options for the calculation of $K_c$ exist, especially if $I_c$ is greater than 2.6. When $K_c$ is used in conjunction with equation (4-6) the result is a value $(q_{c1N})_{cs}$, the normalized clean sand equivalent CPT penetration resistance.

### CRR Procedure

Both the NCEER and Robertson and Wride methods recommend the use of the following expression (4-11) to calculate CRR for a magnitude 7.5 earthquake event using CPT resistance data. Calculation of CRR values for other earthquake magnitudes requires the use of a magnitude scaling factor (MSF) which will be defined later.

$$
\begin{array}{lll}
If: & 50 \leq (q_{c1N})_{cs} < 160 & CRR_{7.5} = 93\left(\dfrac{(q_{c1N})_{cs}}{1000}\right)^3 + 0.08 \\[4ex]
If: & (q_{c1N})_{cs} < 50 & CRR_{7.5} = 0.833\left(\dfrac{(q_{c1N})_{cs}}{1000}\right) + 0.05
\end{array}
\tag{4-11}
$$
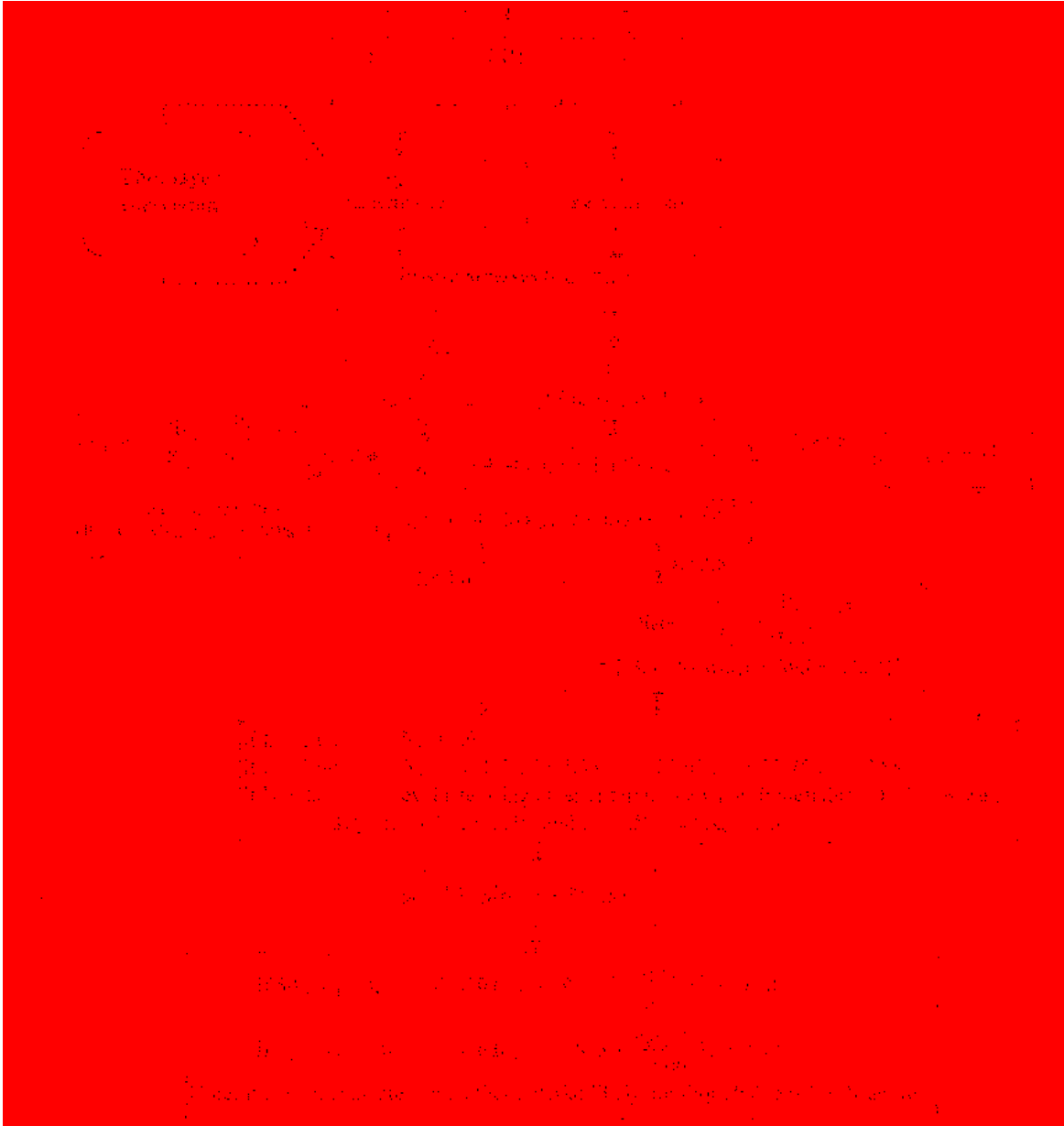
**Figure 4-4: Flow chart describing calculation of CRR (after Robertson and Wride 1998).**

### Recent Updates

An update to the Robertson and Wride method was presented in Robertson (2009). This update presents an improved iterative procedure to calculate the stress exponent ($n$). The following is given:

$$n = 0.381(I_c) + 0.05(\frac{\sigma'_{vo}}{p_a}) - 0.15$$

$$n \leq 1.0$$

(4-12)

This adjustment to the procedure allows for a more precise solution in the iterative calculation of the stress exponent. Values for $I_c$, $Q$, $F$, and $n$ should be recalculated until the change in the stress exponent $\Delta n$ is $\leq 0.01$.

### CSR Corrections

Because of the limited range of conditions associated with case history data, corrections to the CSR are required to interpolate within and extrapolate beyond the available data (Idriss and Boulanger, 2014). With use of these corrections, the liquefaction model can theoretically be used to predict the occurrence of liquefaction over a wide range of conditions.

To correct for different magnitudes of earthquake loadings the CSR should be adjusted by a magnitude scaling factor (MSF) as seen in equation (4-13).

$$CSR_{7.5} = 0.65 \left( \frac{\sigma_{vo}}{\sigma'_{vo}} \right) \left( \frac{a_{max}}{g} \right) (r_d) \left( \frac{1}{MSF} \right) \left( \frac{1}{K_\sigma} \right)$$

(4-13)

Many values for MSF have been suggested by different researchers such as Seed and Idriss (1982) and Ambraseys (1988). The Robertson and Wride method uses the lower-bound equation values suggested in Youd et al. (2001);

$$MSF = 10^{2.24} / M_W{}^{2.56} \tag{4-14}$$

where $M_W$ is the moment magnitude of the earthquake loading. Figure 4-5 shows a range of acceptable values for MSF as presented in Youd et al. (2001).
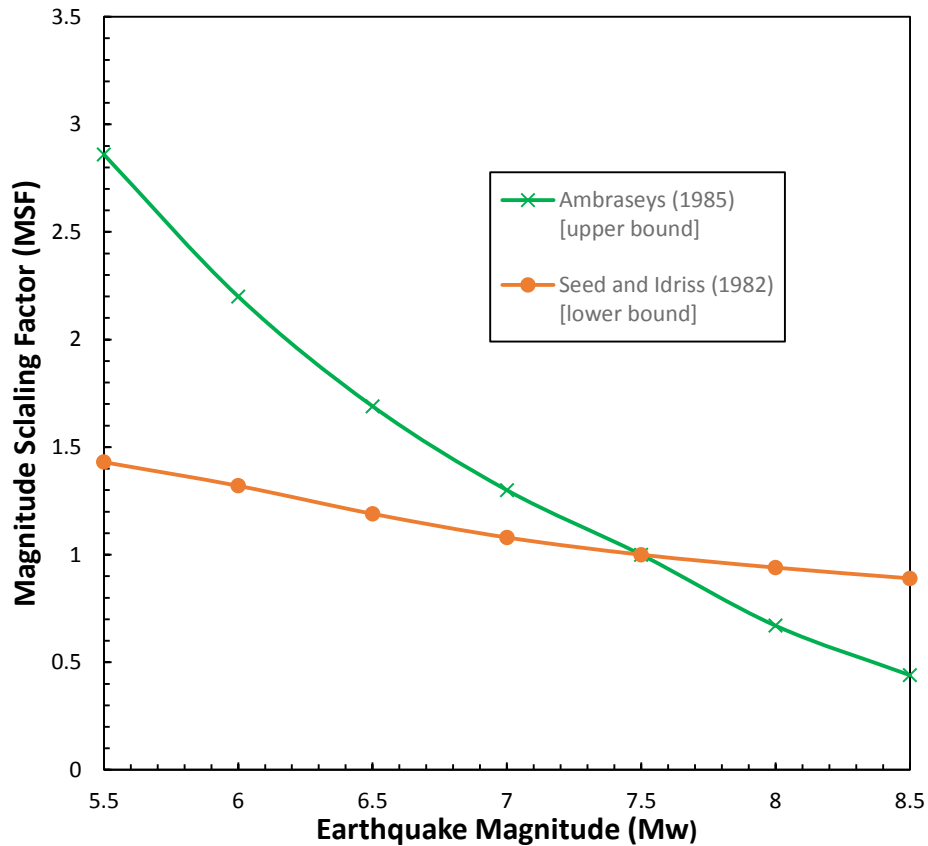


**Figure 4-5: Accepted range of MSF values from Youd et al. (2001).**

The value $r_d$ is a depth dependent shear stress reduction factor. Values for $r_d$ are based on the work of Liao and Whitman (1986), Robertson and Wride (1998), Marcuson (1978), and Seed and Idriss (1971). Mean values are given by the following:

$$r_d = 1.0 - 0.00765z \qquad for \ \ z \le 9.15\,\mathrm{m}$$
$$r_d = 1.174 - 0.0267z \qquad for \ \ 9.15\,\mathrm{m} < z \le 23\,\mathrm{m}$$
$$r_d = 0.744 - 0.008z \qquad for \ \ 23\,\mathrm{m} < z \le 30\,\mathrm{m}$$
$$r_d = .5 \qquad for \ \ z > 30\,\mathrm{m}$$

(4-15)

where $z$ is the depth of interest in meters.

The term $K_\sigma$ in equation (4-13) is a non-linear overburden correction for cyclic stress ratio first suggested by Seed (1983). As presented by Youd, Idriss et al. (2001),

$$K_\sigma = \left( \sigma'_{vo} / P_a \right)^{(f-1)}$$

(4-16)

where $\sigma'_{vo}$ is the effective overburden pressure, $P_a$ is atmospheric pressure in the same units and $f$ is an exponent that is a function of site conditions. The NCEER workshop further suggested that values between $f = 0.6$ and $f = 0.8$ should be used as conservative estimates based on soil relative densities between 80 and 40 percent respectively.
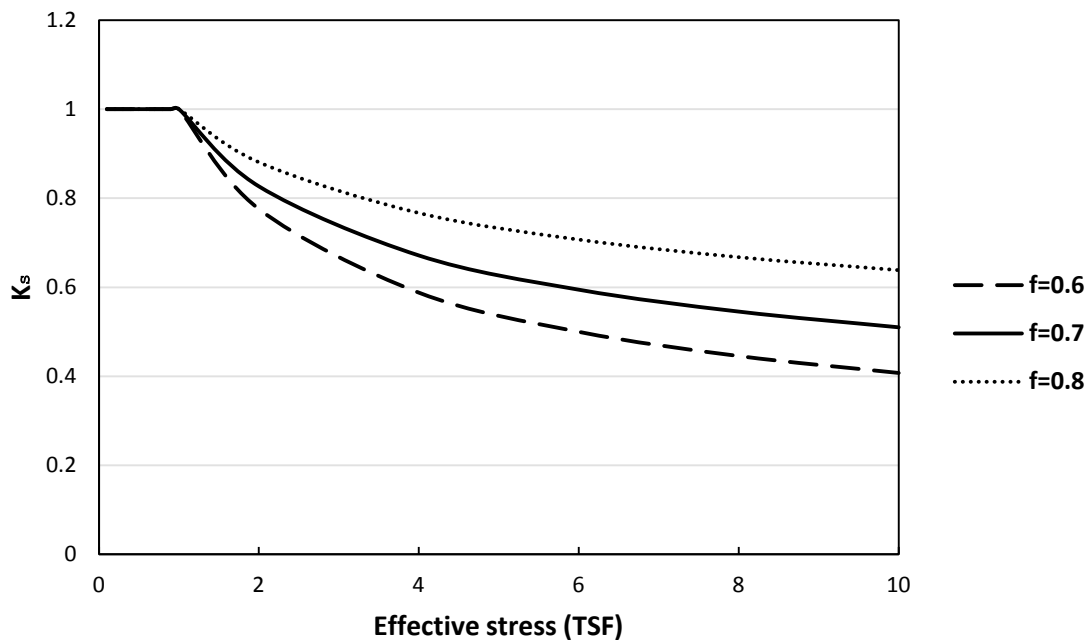


Figure 4-6: Range of values for $K_\sigma$ using the NCEER equation (Youd, Idriss et al. 2001).

Another correction factor for existing shear stresses in the soil, $K_\alpha$ can be found in the literature (Seed 1983, Boulanger and Idriss 2007). Because the liquefaction database was created with cases with mostly level ground or gently sloping ground, this correction is deemed necessary for locations with significant slopes. The case history database is not extensive enough to empirically define this parameter, so the parameter is based mostly on the fundamental understanding of sand behavior (Idriss and Boulanger 2008).

In most cases of level or gently sloping ground, the value $K_\alpha$ will be equal to one, so its consideration makes no change to the equation. Although beyond of the scope of this thesis (which will assume level or gently sloping ground), this factor has been considered in the creation of the liquefaction analysis tool built to facilitate this research.

### *Application of Robertson and Wride Model*

The development of the deterministic CRR curve for the Robertson procedure essentially creates a boundary between cases that are expected to liquefy and those which are not expected to liquefy. Figure 4-7 shows a plot of the Robertson CRR curve along with the case history data used to create the relationship. Once the CRR is defined, it is then possible to make a prediction of whether the soil will or will not liquefy by plotting the CPT resistance and the CSR calculated at a depth of interest for a certain earthquake event. If the point plots right of the CRR curve it is expected that the factor of safety against liquefaction ($FS_L$) will be greater than 1, and thus not expected to liquefy. Conversely, if the point plots to the left of the curve, $FS_L$ will be less than 1 and liquefaction triggering is predicted.
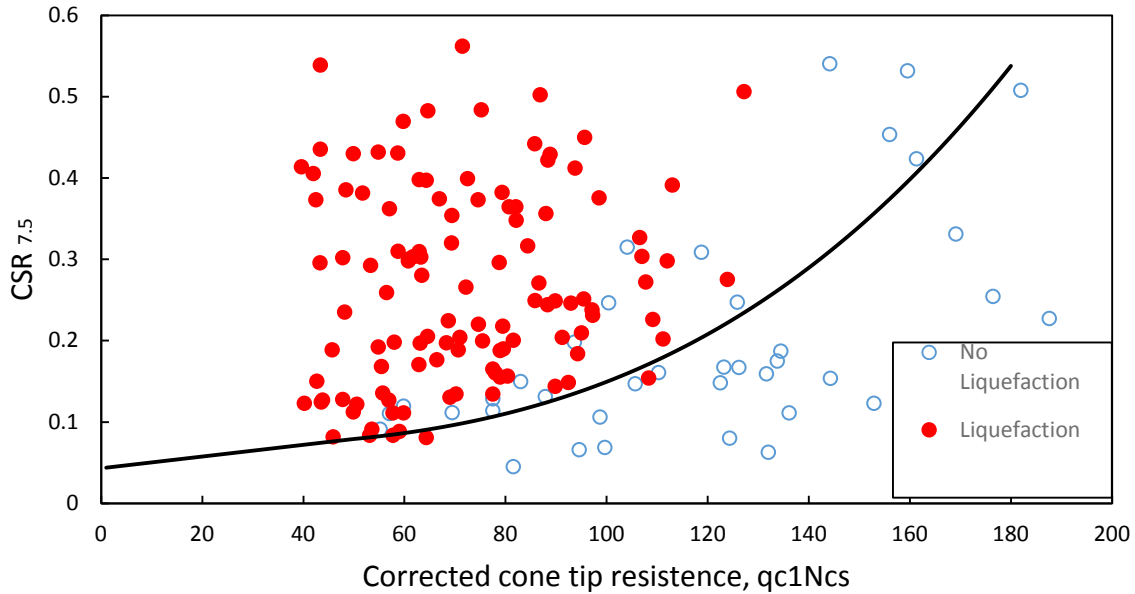
**Figure 4-7: Updated Robertson and Wride Liquefaction triggering curve with case history data points.**

### 4.1.2 Boulanger and Idriss (2008, 2014) Deterministic Procedure

The Idriss and Boulanger CPT Deterministic procedure for liquefaction analysis provides an alternate to the Robertson and Wride procedure. In 2014, Idriss and Boulanger published a new CPT liquefaction triggering database after reconsidering some old data and adding data from recent earthquake events such as the 2011 Tuhoku earthquake and the 2010/2011 Canterbury earthquake sequence. Along with this updated database, a new correlation between CPT resistance and CRR was presented.

Boulanger and Idriss used an identical process with the Robertson and Wride method to correct for overburden effects.

$$q_{c1N} = C_N \frac{q_c}{P_a} \qquad (4\text{-}17)$$

where $q_c$ is the CPT cone tip resistance, $P_a$ is atmospheric pressure, and $C_N$ is an overburden correction factor.

After re-examining past data Idriss and Boulanger suggested a modified overburden correction factor for CPT penetration given as:

$$C_N = (P_a / \sigma_{vo})^m \leq 1.7 \qquad (4\text{-}18)$$

$$m = 1.338 - .0249(q_{c1Ncs})^{0.264} \qquad (4\text{-}19)$$

where $q_{c1Ncs}$ is limited to between 21 and 254. These equations require an iterative process, as a value for $q_{c1Ncs}$ has not yet been calculated and is a function of $C_N$.

Boulanger and Idriss (2014) also published an updated CPT correction for grain characteristics. This correction is similar to corrections used in the Idriss and Boulanger (2008) SPT model, which is based on the fines content of the soil and is empirically derived. The following expression was given for the clean sand equivalent $q_{c1Ncs}$:

$$q_{c1Ncs} = q_{c1N} + \Delta q_{c1N} \qquad (4\text{-}20)$$

where $\Delta q_{c1N}$ is the fines content adjustment factor.

$$\Delta q_{c1N} = \left(11.9 + \frac{q_{c1N}}{14.6}\right) \exp\left(1.63 - \frac{9.7}{FC+2} - \left(\frac{15.7}{FC+2}\right)^2\right) \qquad (4\text{-}21)$$

where FC is the percent fines content.

To obtain an estimate for the fines content of the soil, Idriss and Boulanger suggested the use of a correlation with the soil behavior type index $I_c$ from the Robertson and Wride

procedure. Although useful, Idriss and Boulanger suggested that caution should be used with the application this relationship because of data scatter.

Idriss and Boulanger suggested:

$$FC = 80(I_c + C_{FC}) - 137$$
$$(0\% \le FC \le 100\%)$$

(4-22)

where $I_c$ is the soil behavior type index calculated from the Robertson and Wride procedure, and $C_{FC}$ is a regression fitting parameter that can be used to minimize uncertainty when site-specific fines content data is available. This term is also useful for a sensitivity analysis of penetration resistance with different values for $C_{FC}$. Figure 4-8 is a plot of the relationship between FC and $I_c$ along with the associated data scatter.
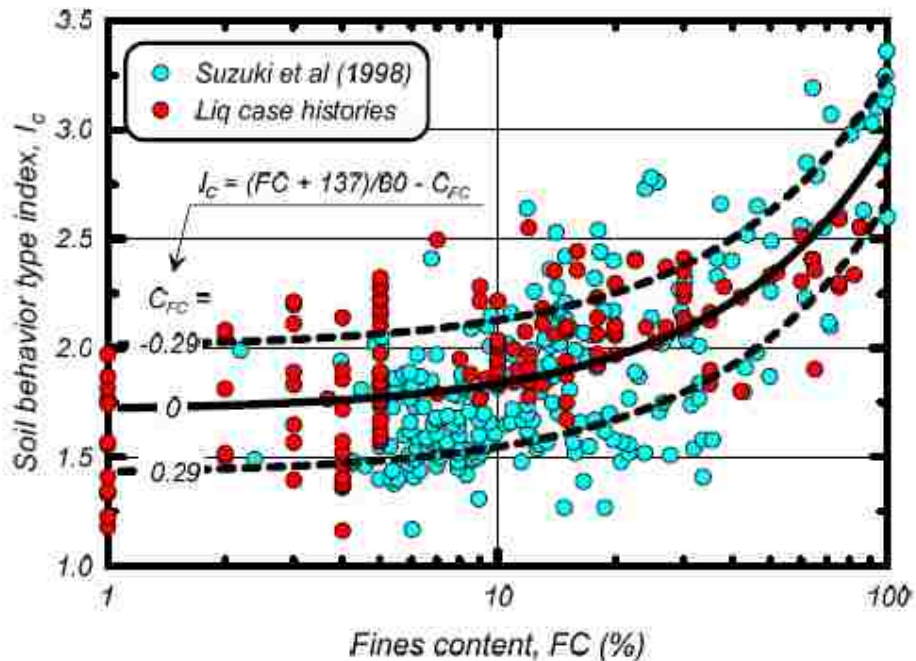


**Figure 4-8: Recommended correlation between $I_c$ and FC with plus or minus one standard deviation against the dataset by Suzuki et al (1998) (after, Idriss and Boulanger 2014).**

Once the iterative procedure from equations (4-18), (4-19), and (4-20) are complete, the deterministic liquefaction triggering curve (CRR) can be calculated. This updated relationship from Idriss and Boulanger (2014) is expressed as:

$$CRR_{M=7.5,\sigma'_{vo}=1atm} = \exp\left(\frac{q_{c1Ncs}}{113} + \left(\frac{q_{c1Ncs}}{1000}\right)^2 - \left(\frac{q_{c1Ncs}}{140}\right)^3 + \left(\frac{q_{c1Ncs}}{137}\right)^4 - 2.8\right) \qquad (4\text{-}23)$$

*CSR Corrections*

Similar to the Robertson and Wride procedure, the Idriss and Boulanger procedure requires the use of CSR correction values to enable proper use of the liquefaction triggering model beyond a very limited set of conditions. As such, the Idriss and Boulanger used a procedure identical to the Robertson and Wride procedure for correcting the CSR, namely:

$$CSR_{M=7.5,\sigma'_{v}=1atm} = 0.65\frac{\sigma_v}{\sigma'_v}\frac{a_{max}}{g}r_d\frac{1}{MSF}\frac{1}{K_\sigma} \qquad (4\text{-}24)$$

which can be compared to equation (4-13), which applies to the Robertson and Wride procedure. Although, equivalent equations are used, Different values are used in the Idriss and Boulanger method for the factors, $r_d$, MSF, and $K_\sigma$.

The magnitude scaling factor in the Idriss and Boulanger procedure has gone through several iterations. Idriss and Boulanger (2008) used the relationship developed by Idriss (1999) for the MSF for sands, namely,

$$MSF_{sand} = 6.9*\exp\left(\frac{-M}{4}\right) - 0.058 \leq 1.8 \qquad (4\text{-}25)$$

where $M$ is the magnitude of the earthquake event.

Idriss and Boulanger (2008) presented another relationship which was found to be more appropriate for clays which tend to have a lower number of stress cycles.

$$MSF_{clay} = 1.12 * \exp\left(\frac{-M}{4}\right) + 0.828 \leq 1.13$$
(4-26)

Figure 4-9 shows a comparison of these equations for a range of values for $M$ and $MSF$.
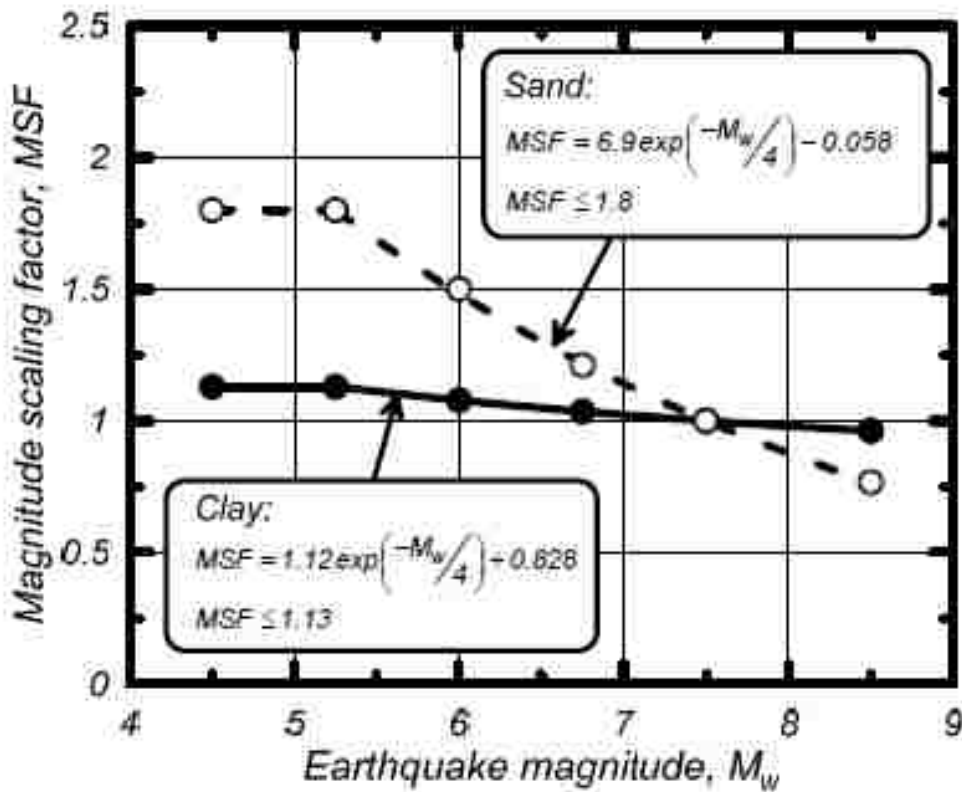


**Figure 4-9: MSF relationship for clay and sand (after, Boulanger and Idriss 2014).**

Having two separate equations for the MSF causes problems, as many soil types are a mix of, or are classified as being somewhere in between sand and clay. Idriss and Boulanger later attempted to better account for the change in the MSF for a range of different soil characteristics.

After significant research into the variation of MSF with the amount of stress cycles Idriss and

Boulanger (2014) presented the following update:

$$\text{MSF} = 1 + \left( MSF_{max} - 1 \right) \left( 8.64 \exp \left( \frac{-M}{4} \right) - 1.325 \right) \tag{4-27}$$

$$MSF_{max} = 1.09 + \left( \frac{q_{c1Ncs}}{180} \right)^3 \leq 2.2 \tag{4-28}$$

Equations (4-27) and (4-28) allow for soil characteristics to be represented by CPT penetration

resistance rather than determination as either sand, or clay. This new relationship was also

shown to improve the degree of fit between revised CPT-based liquefaction triggering

correlation and their respective case history databases (Boulanger and Idriss 2014).

In the Idriss and Boulanger method, $r_d$ is obtained using the equations of Golesorkhi

(1989):

$$r_d = \exp \left[ \alpha(z) + \beta(z) * M \right] \tag{4-29}$$

$$\alpha(z) = -1.012 - 1.126 \sin \left( \frac{z}{11.73} + 5.133 \right) \tag{4-30}$$

$$\beta(z) = 0.106 + 0.118 \sin \left( \frac{z}{11.28} + 5.142 \right) \tag{4-31}$$

where $z$ is the depth below the ground surface in meters, $M$ is the moment magnitude of the

scenario earthquake, and the arguments inside the trigonometric functions are in radians. Figure

4-10 plots a range of possible $r_d$ values.
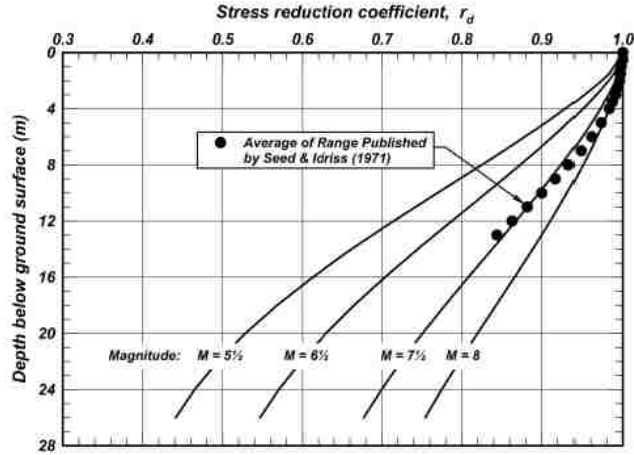
**Figure 4-10: Shear stress reduction factor relationship (after Boulanger and Idriss 2014).**

The $K_\sigma$ relationship used in the Idriss and Boulanger deterministic liquefaction procedure was developed by Boulanger (2003), and is given as:

$$K_\sigma = 1 - C_\sigma \ln\left(\frac{\sigma'_v}{P_a}\right) \leq 1.1 \tag{4-32}$$

$$C_\sigma = \frac{1}{37.3 - 8.27(q_{c1Ncs})^{0.264}} \leq 0.3 \tag{4-33}$$

where $\sigma'_v$ is the vertical overburden pressure, $P_a$ is a reference pressure equal to 1 atm., and $q_{c1Ncs}$ is the clean sand correct CPT resistance calculated from the Idriss and Boulanger method. These relationships were derived from relative state parameter index values. This relationship is especially important when looking at depth greater than 20 meters where $K_\sigma$ begins to vary significantly between methods. Existing methods for obtaining value for $K_\sigma$ have shown to give reasonable conservative estimates (Youd et. al. 2001), so use of this parameter is seen as useful for a conservative liquefaction analysis using the simplified method at depths greater than 20

meters.  Figure 4-11 shows the relationship of $K_\sigma$ with the vertical effective stress at a measured depth increment used by Boulanger and Idriss (2014).
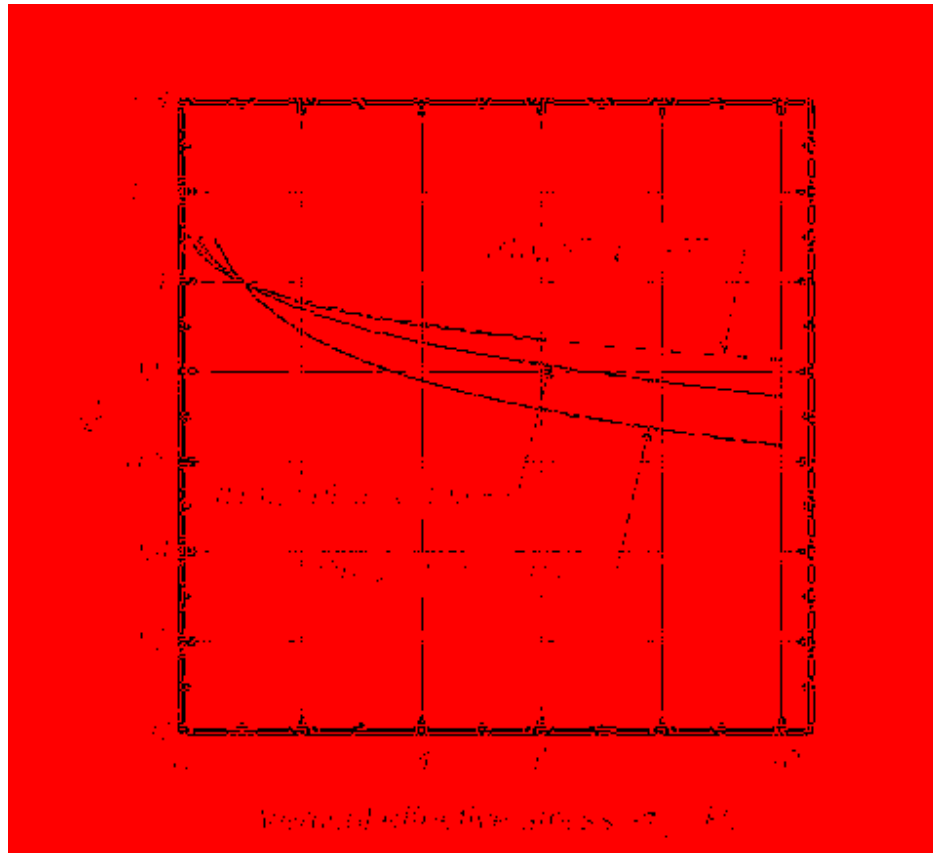


**Figure 4-11: Overburden correct factor relationship (after Boulanger and Idriss, 2014).**

With corrected values of CSR, the liquefaction triggering model is now applicable to a wide range of CPT resistance values and CSR values.  The liquefaction triggering curve for the Idriss and Boulanger deterministic model can be seen in Figure 4-12.  The CRR lines for both Idriss and Boulanger (2014 and 2008) are visible.  As seen in Figure 4-12, almost all the case history values that were observed to have liquefied lie to the left of the CRR line.
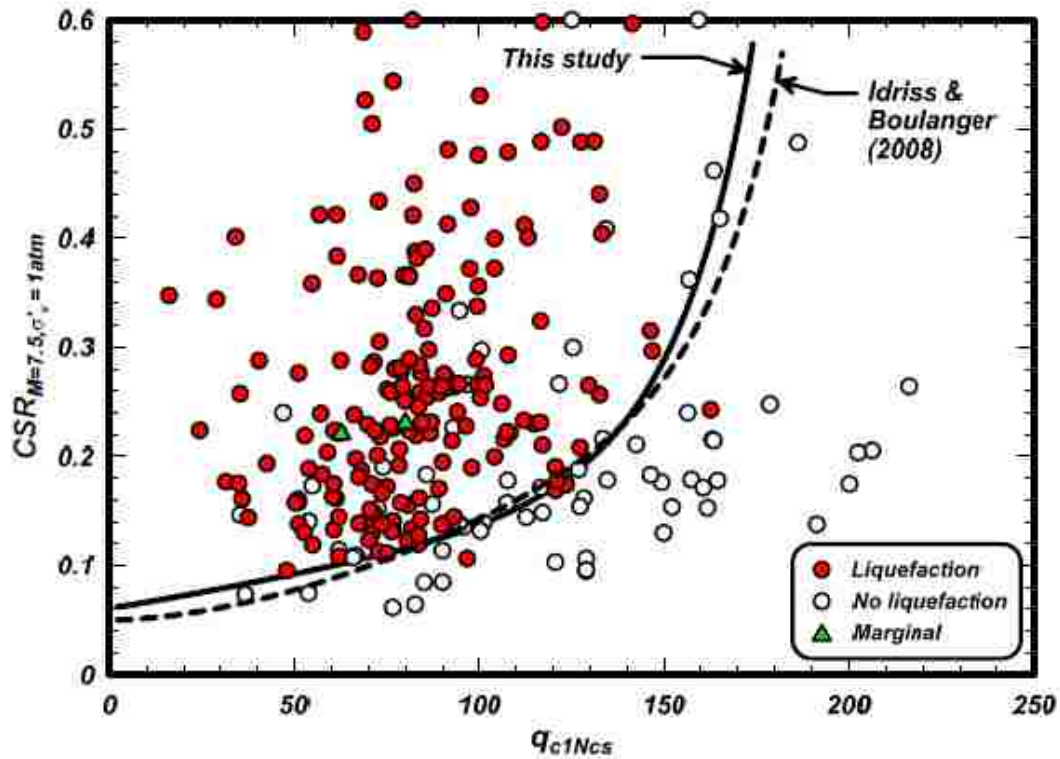
**Figure 4-12: Updated CRR curves and liquefaction case history database (after, Boulanger and Idriss 2014).**

## 4.2 Empirical Probabilistic Methods

In the years following the development of the empirical deterministic methods, researchers began to realize that more information could be derived from the existing case history database. Using statistical analyses, it became possible to estimate not only if a soil would liquefy, but also the likelihood of liquefaction occurring. In this way, depending on the risk level of the project, different probabilities of liquefaction could be considered as a cutoff point for liquefaction initiation. The two following probabilistic methods were developed based on the same case history data as the deterministic methods mentioned previously.

### 4.2.1 Ku et al. (2012) Procedure [Probabilistic Version of Robertson and Wride Procedure]

Because of widespread use and popularity of the Robertson and Wride CPT-based procedure for liquefaction triggering assessment, researchers Ku, Juang, Chang, and Ching attempted to create a probabilistic liquefaction triggering model based on the work of Robertson and Wride. The purpose of the work of Ku et. al. (2012) was to create a probabilistic procedure that required minimal extra effort on the part of the engineer to use a probability of liquefaction occurrence in design (Ku et. al. 2012). Probabilistic methods are often considered by engineers to be too complex for use in practice, but Ku et al. (2012) attempted to create a triggering model that would facilitate the use of probabilistic methods in practice. Also, in developing this liquefaction triggering procedure, the Robertson and Wride liquefaction case history database was augmented with recent data.

To provide a simple transition for engineers from a factor of safety against liquefaction $FS_L$ (from the Robertson and Wride (1998) procedure) to a probability of liquefaction ($P_L$), Ku et al. (2012) created a mapping function to relate the two parameters. Using the principle of maximum likelihood and a Bayesian statistical analysis of the case history database, this expression was defined to relate $FS_L$ and $P_L$:

$$P_L = 1 - \Phi\left[\frac{0.102 + \ln(FS_L)}{0.276}\right] \tag{4-34}$$

where $\Phi$ is the standard normal cumulative distribution function (mean = 0 and standard deviation = 1). Figure 4-13 is a visual representation of this relationship which is seen to decrease significantly from about $FS_L = .75$ to $FS_L = 2$.
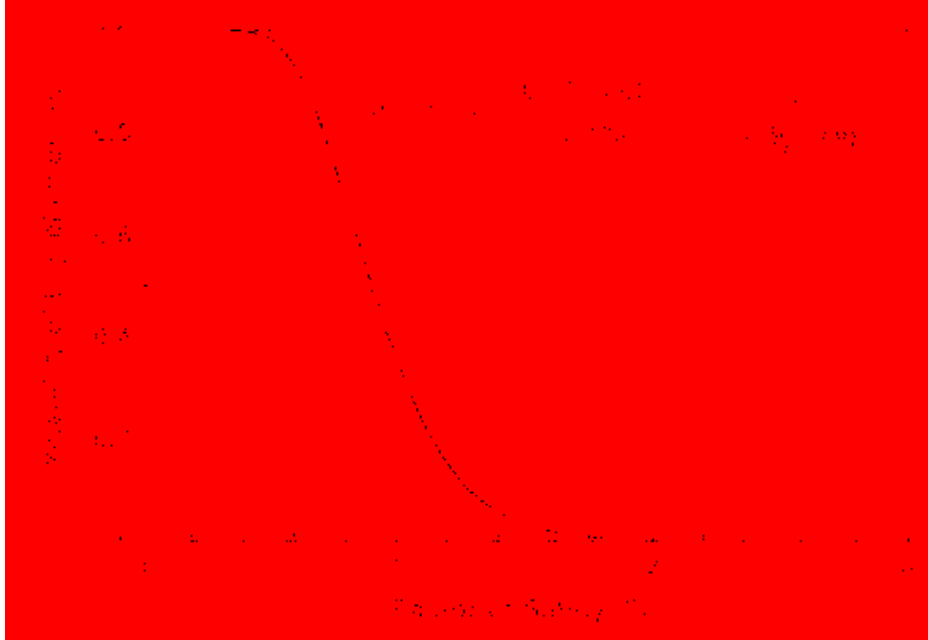
**Figure 4-13: Plot of $P_L$ - $FS_L$ mapping function for values from the Robertson and Wride (1998) procedure, after Ku et al. (2012).**

This equation is very helpful in a back-analysis of a case history or for post-event investigation where conservative bias does not allow for effective analysis (Ku et al. 2012).
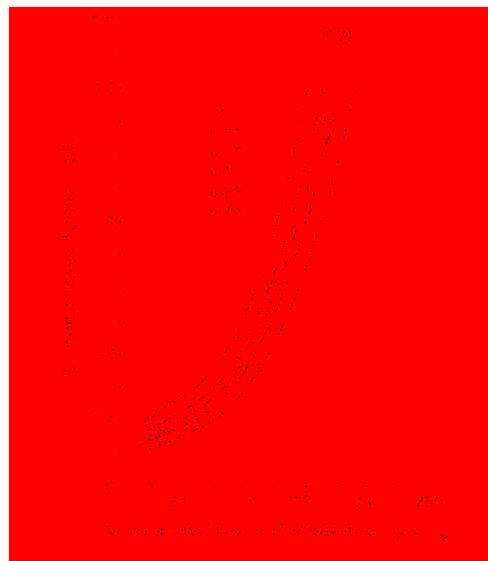


**Figure 4-14: CRR liquefaction triggering curves based on probability of liquefaction ($P_L$).**

**Consideration of Parameter Uncertainty**

Ku et al. (2012) suggests that if the uncertainty in the CPT and non-CPT based input parameters ($q_{c1Ncs}$ , $CSR$, $M_W$, $a_{max}$, MSF, $K_\sigma$) is large, effort should be taken to characterize this uncertainty (Ku et al. 2012). A Monte Carlo simulation analysis is suggested, along with the use of a value for the model uncertainty or bias input into equation (4-34). The consideration of parameter uncertainty in the Ku et. al. (2012) model for the purposes of this study is further explained in chapter 5.

### 4.2.2 Probabilistic Boulanger and Idriss (2014) Procedure

Following the statistical procedure used by Cetin et al. (2002), Boulanger and Idriss (2014) developed a probabilistic version of their SPT liquefaction triggering model (2012a). After developing a deterministic procedure for liquefaction analysis with CPT data, Boulanger and Idriss took on the challenge to develop a CPT-based probabilistic liquefaction triggering relationship.

Using the updated CPT case history database from Boulanger and Idriss (2008), along with a revised MSF relationship; a maximum likelihood analysis was used to develop an equation to estimate the probability of liquefaction. Uncertainty in the liquefaction parameters as well as the liquefaction model are considered. Unlike the equation developed by Ku et. al. (2012), the Boulanger and Idriss (2014) equation is not directly a function the factor of safety against liquefaction, but is a function of $CSR$ and $q_{c1Ncs}$. The expression is given as:

$$P_L = \Phi\left[ -\frac{\frac{q_{c1Ncs}}{113} + \left(\frac{q_{c1Ncs}}{1000}\right)^2 - \left(\frac{q_{c1Ncs}}{140}\right)^3 + \left(\frac{q_{c1Ncs}}{137}\right)^4 - 2.60 - \ln\left(CSR_{M=7.5,\sigma'_v=1atm}\right)}{\sigma_{\ln(R)}} \right] \quad (4\text{-}35)$$

where, $\Phi$ is the standard normal cumulative distribution function, $q_{c1Ncs}$ is the clean sand corrected CPT resistance, $CSR_{M=7.5,\sigma_v=1atm}$ is the corrected $CSR$ value for a standardized magnitude and overburden pressure, and $\sigma_{\ln(R)}$ is the computed model uncertainty for the relationship. Boulanger and Idriss (2014) state that when considering uncertainty in the liquefaction triggering model the value $\sigma_{\ln(R)} = 0.2$ should be used. A warning is given that in a liquefaction analysis, the parameter uncertainties (uncertainty in $CSR_{M=7.5,\sigma_v=1atm}$ and $q_{c1Ncs}$) are often larger than the uncertainty in the triggering model, and for this reason formal treatment of this parametric uncertainty is even more important than acknowledgment of bias towards liquefied sites in the liquefaction model (Boulanger and Idriss 2014).

When using equation (4-35) over a range of values for $q_{c1Ncs}$ and $CSR$, curves can be developed to show the probability of liquefaction correlating to different soil conditions. Examples of these curves can be seen in Figure 4-15. The CRR curve from the deterministic Boulanger and Idriss (2008) relationship correlates approximately with a $P_L$ of 16% if $\sigma = \sigma_{\ln(R)} = 0.2$. The consideration of parameter uncertainty in the Boulanger and Idriss (2014) model for the purposes of this study is further explained in chapter 5.

Another useful equation exists from computing the $P_L$ using the Boulanger and Idriss (2014) model. Based on the derivation shown in (Ulmer et. al. 2015), a function can be derived to compute the $P_L$ directly from a $FS_L$ value, given as:

$$P_L = \Phi \left[ -\frac{\ln(FS_L)}{\sigma_{\ln(R)}} \right] \tag{4-36}$$

where $\Phi$ is the standard normal cumulative distribution function, and $\sigma_{\ln(R)}$ is either the model

or total uncertainty.
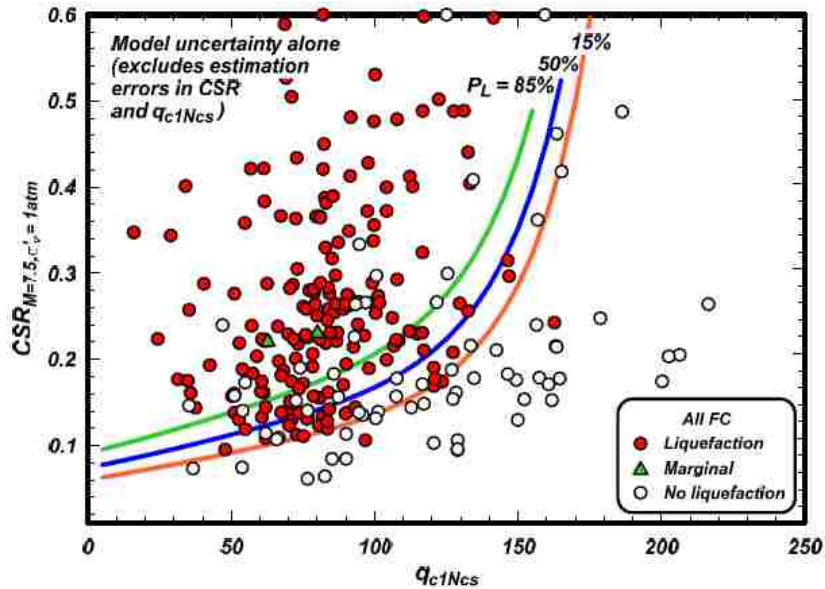


**Figure 4-15: Various CRR liquefaction triggering curves (after, Boulanger and Idriss 2014).**

### 4.3    Examples of Liquefaction Initiation Analysis Methods

Three primary methods exist to compute design values in a liquefaction triggering analysis: deterministic, pseudo-probabilistic, and performance-based.  Each of these methods have been used to some extent by engineers, and each has specific benefits and drawbacks. Examples of computations using the deterministic and pseudo-probabilistic liquefaction triggering methods will be discussed here, while examples of performance-based method will be provided in chapter 5.

### 4.3.1 Deterministic Analysis

As discussed in 2.5.1, a deterministic hazard analysis considers a single governing seismic source and corresponding ground motions to determine the liquefaction design parameters to be assigned to a soil layer. To complete a deterministic analysis, the governing seismic source is found and then the ground motion values are quantified using empirical relationships.

For example, a site was chosen for La Quinta, CA (33.6634, -116.31). The governing fault for this region is the Coachella segment of the San Andreas fault. It is expected that this fault could impart a magnitude of 7.7 and a PGA of 0.7g. For simplicity, in this case it is assumed that PGA is equal to $a_{max}$. When applying these ground motion values to the deterministic liquefaction triggering equations from the Robertson and Wride model discussed in this chapter (specifically using equations (4-3), (4-11), and (4-23)) for an example CPT soil profile, a new profile presenting the factor of safety against liquefaction is computed for each depth increment of the soil profile (Figure 4-16).

The areas of the plot where the deterministic values are less than $FS_L = 1$ (left of the dotted line) represent locations of the soil profile that are expected experience liquefaction for this given scenario. Conversely, anything that plots to the right of the dotted line will represent a condition of $FS_L > 1$ which represents no liquefaction initiation for the specified layers. This analysis is convenient in in terms of simplicity, but is limited in scope, because only takes one potential earthquake scenario into account.
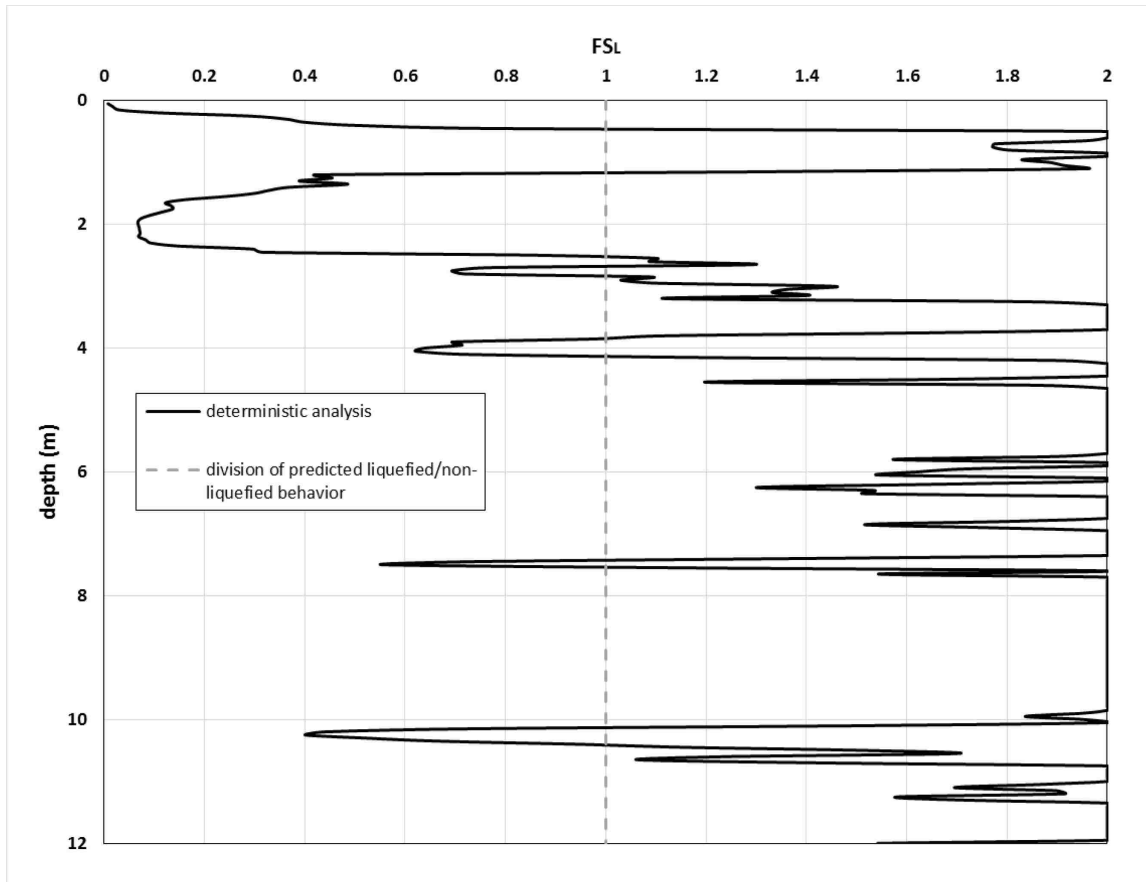
**Figure 4-16: Example results from a deterministic CPT liquefaction triggering analysis.**

### 4.3.2 Pseudo-Probabilistic Analysis

The pseudo-probabilistic approach to liquefaction hazard design is commonly used in practice today. The pseudo-probabilistic method uses parts of both DSHA and PSHA which are discussed in chapter 2. The pseudo-probabilistic method uses a PSHA at a single return period to select design ground motions, and then uses the deterministic liquefaction triggering equations for a simple calculation of the liquefaction hazard. An example of a PSHA that could be used for a pseudo-probabilistic analysis can be found at (https://earthquake.usgs.gov /hazards/interactive/).

Often in design, either mean (average) or modal (most commonly occurring) ground motions values are chosen from the PSHA. Although this method is used widely in practice, it has been criticized by researchers because only one level of seismic loading is explicitly considered from the PSHA (Franke 2014). A truly probabilistic method, should consider all possible combinations of seismic loadings, as well as the corresponding likelihoods of each of those combinations actually occurring.

An example of a pseudo-probabilistic liquefaction hazard analysis is provided here. For the same site used in the previous example La Quinta, CA (33.6634, -116.31), a PSHA was computed using the USGS hazard deaggregation tool (https://earthquake.usgs.gov/hazards/interactive/) and a return period of 2475 years. The mean seismic ground motions were computed and given as: $M_W = 6.87$, and PGA = 0.612 g. Again, for simplicity PGA is assumed to equal $a_{max}$ in this case. When these ground motions are applied to the deterministic liquefaction triggering equations explained in this chapter, specifically equations (4-3), (4-11), and (4-23), design values for the factor of safety against liquefaction are computed for each depth measurement of the example CPT profile.

Results of this particular analysis show that the hazard computed by the pseudo-probabilistic analysis is slightly less than that calculated from the deterministic analysis. This is because the set of values used in the deterministic analysis are similar to "worst case scenario" ground motion values, while the pseudo-probabilistic values represent an "average" of ground motions from several potential sources.
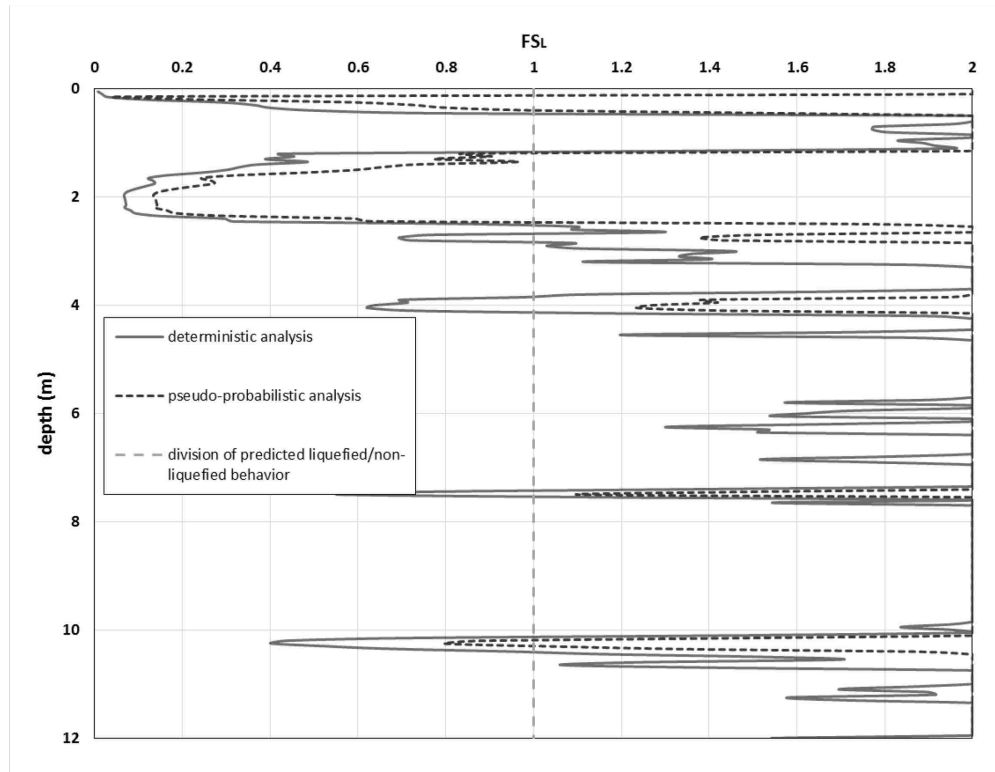
**Figure 4-17: Example of results from a pseudo-probabilistic CPT liquefaction triggering hazard analysis.**

Although many engineers use the pseudo-probabilistic approach because of simplicity and ease of use, there are several drawbacks that should be considered such as:

*Incompatible pairs*

The use of a pseudo-probabilistic approach can create incompatible pairs of ground motions ( $a_{max}$ , $M_W$ that would never occur together). These values are critical for the prediction of liquefaction hazards. It is somewhat counter-intuitive to use these values for design, when it is believed that those ground motions could never occur in conjunction.

*Consideration of only one return period*

When computing design values in this analysis, ground motions values are chosen for just one return period. A PSHA considers a wide range of seismic sources and their corresponding return

periods, so by considering only one return period in the analysis, part of the benefit of the PSHA is lost.

*Uncertainty not explicitly considered*

Uncertainty is an important part of any truly probabilistic procedure. In a liquefaction analysis, large amounts of uncertainty are involved in the computation of ground motions all the way to the computation of the factor of safety against liquefaction. In a pseudo-probabilistic analysis, neither uncertainty in the liquefaction triggering model nor the uncertainty in site amplification are explicitly considered. This can cause engineers to use excessive amount of conservatism in design in an attempt to factor in this uncertainty. This can in some cases lead to overdesign.

*Confusion in interpretation of results*

The results from a pseudo-probabilistic liquefaction hazard analysis do not necessarily correlate with the return period used to obtain the design ground motions. Many engineers are confused by this fact and often use these values incorrectly. This can be problematic if a structure is required to be built to certain design-life. Misinterpretation of results can lead to either overdesign or even under design.

# 5    PERFORMANCE-BASED EARTHQUAKE ENGINEERING DESIGN

Because of the extreme cost to life and property that can occur from earthquake induced liquefaction, design procedures have been established to minimize these risks.  In the past 100 years various design codes have been developed to guarantee that seismic loading is sufficiently accounted for in structural design.  Unfortunately, the application of these design codes has led to a very narrow view of potential liquefaction hazards.  The current state of design generally considers a deterministic approach which is limited because it considers only one potential earthquake scenario (Kramer and Mayfield 2007).  Although building codes have produced safer structures, a more refined process is required to properly analyze the risk that should be considered from all possible earthquake scenarios.

To more efficiently consider earthquake hazards in the design of structures, a whole new approach has been developed called performance-based design.  Performance-based engineering seeks to provide more rational, complete and accurate estimates of earthquake losses by integrating the prediction of ground motions and other parameters (Kramer and Mayfield 2007).  As time has gone on many engineers have held tight to the cookie-cutter approach to earthquake design, leaning on extreme conservatism when considering seismic loads.  Performance-based design is a much more flexible process that allows the engineer to consider different levels of acceptable risk in design.  In the last 20 years much research has been focused on showing how the current state of seismic design is flawed and that a new

design process is needed. The Pacific Earthquake Engineering Research (PEER) Center has applied this new approach to the realm of seismic design (Cornell and Krawinkler, 2000; Krawinkler, 2002; Deierlein et al. 2003), and has named this approach performance-based earthquake engineering (PBEE).

## 5.1 PEER PBEE Framework

The framework proposed by PEER can be simplified to the use of several parameters associated with different parts of a project, and a desired outcome. These parameters are defined as:

- Intensity Measure (IM): a description of potential ground motions. Examples of this can include $a_{max}$ and PGA.

- Engineering Demand Parameter (EDP): a design value used by engineers to account for potential IM values. Examples of EDP's are $FS_L$ or CPT cone-tip resistance required to resist liquefaction ($q_{req}$).

- Damage Measure (DM): a physical measurement that can also be useful for design. Examples of DM's can include magnitudes of building settlement, building tilt, cracking, etc.

- Decision Variable (DV): a parameter used by decision-makers that takes into account the risk and potential effects caused by DM's. Examples of DV's are casualties, economic loss, and downtime.

These values can be used in an analysis using the total probability theorem. The following equation has been devised by PEER to consider these parameters.

$$\lambda_{DV} = \sum_{k=1}^{N_{DM}} \sum_{j=1}^{N_{EDP}} \sum_{i=1}^{N_{IM}} P[DV > dv \mid DM = dm_k] * P[DM > dm_k \mid EDP = edp_j] * \tag{5-1}$$

$$P[EDP > edp_j \mid IM = im_i]\Delta\lambda_{im_i}$$

where $P[a \mid b]$ represents the conditional probability of a value $a$ given $b$ ; $N_{DM}, N_{EDP}, N_{IM}$ represent the number of increments of the DM, EDP, and IM respectively; and $\Delta\lambda_{im}$ is the incremental mean annual rate of exceedance for the intensity measure ($im_i$). This equation incrementally creates a hazard curve in terms of desired output parameters. In the case of liquefaction analysis, the PBEE framework allows the creation of a hazard curve relating an EDP (usually $FS_L$) to an intensity measure of $a_{max}$ or PGA. Uncertainty in each of the different parameters is built into this calculation by use of the $P[a \mid b]$ term.

### 5.1.1 Fragility Curves

The framework of PBEE, uses the same probabilistic principles used in a PSHA (section 2.5.2). To compute a design hazard curve from equation (5-1), the process must be taken one step at a time using a fundamental equation (in this case using $EDP$ and $IM$).

$$\lambda_{edp} = \int P[EDP > edp \mid IM]\Delta\lambda_{IM} \tag{5-2}$$

which can be approximated as:

$$\lambda_{edp} \approx \sum_{i=1}^{N_i} P[EDP > edp \mid IM = im_i]\Delta\lambda_{IM} \tag{5-3}$$

where $\sum_{i=1}^{N_i} P[EDP > edp \mid IM = im_i]$ can be obtained from a cumulative density function (CDF) that relates the probability of the engineering design parameter being exceed with a given

intensity measure.  This type of CDF is called a fragility curve.  An example of how fragility

curves can be used to create a hazard curve can be seen in Figure 5-1.  The fragility curve in this

example relates the probability of an $EDP(D)$ exceeding a threshold value ($d_i$) given an $IM$

(PGA).  Using equation (5-3), a hazard curve relating the $EDP$ to the $IM$ can be created.
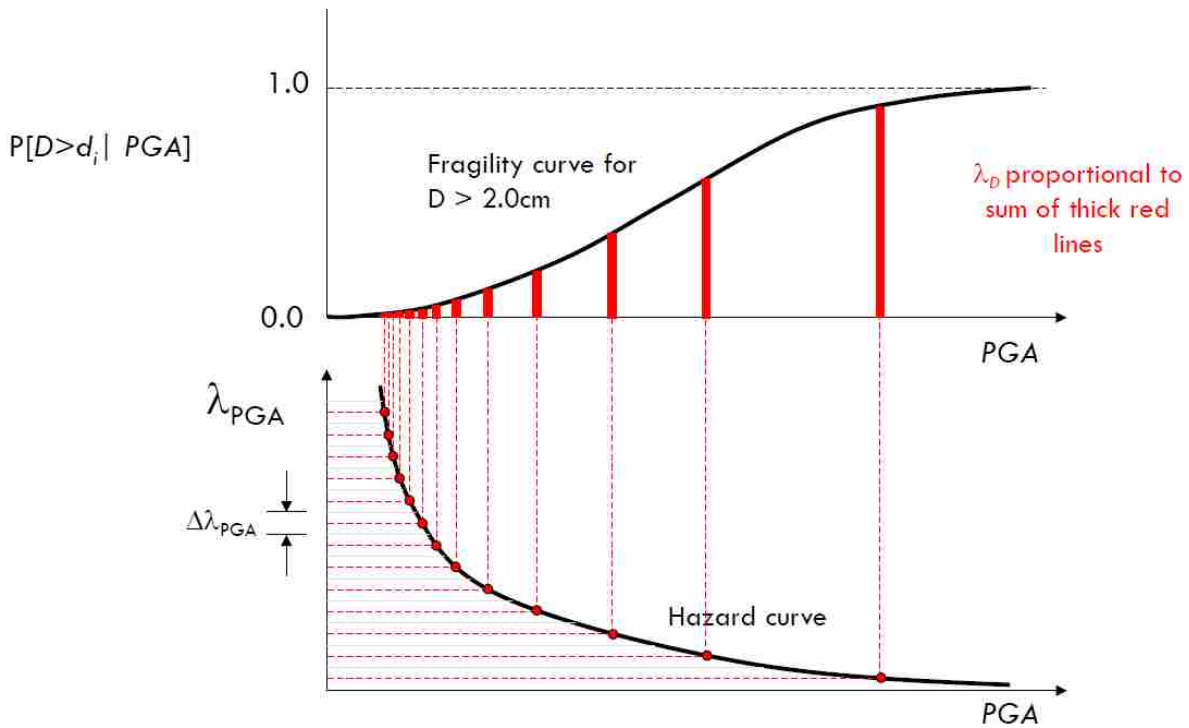


**Figure 5-1: Relationship between a fragility curve and a hazard Curve (courtesy of Steven Kramer, from a NEES presentation in 2005).**

The hazard curves produced by this performance-based method can allow engineers to

more appropriately select the design parameters that should be used on a project.  For projects of

great importance (i.e. a hospital), greater care may be taken to consider a less frequent but more

severe liquefaction event.  In contrast, for a low importance project, it is possible that a less

stringent earthquake design criteria should be used better balance the economics of the project.

Figure 5-2 is a chart that represents one way an earthquake design level could be chosen given a

desired earthquake performance level. For critical structures, a longer return period (inverse of mean annual rate of exceedance) should be considered to satisfy the proper performance over a non-critical structure.
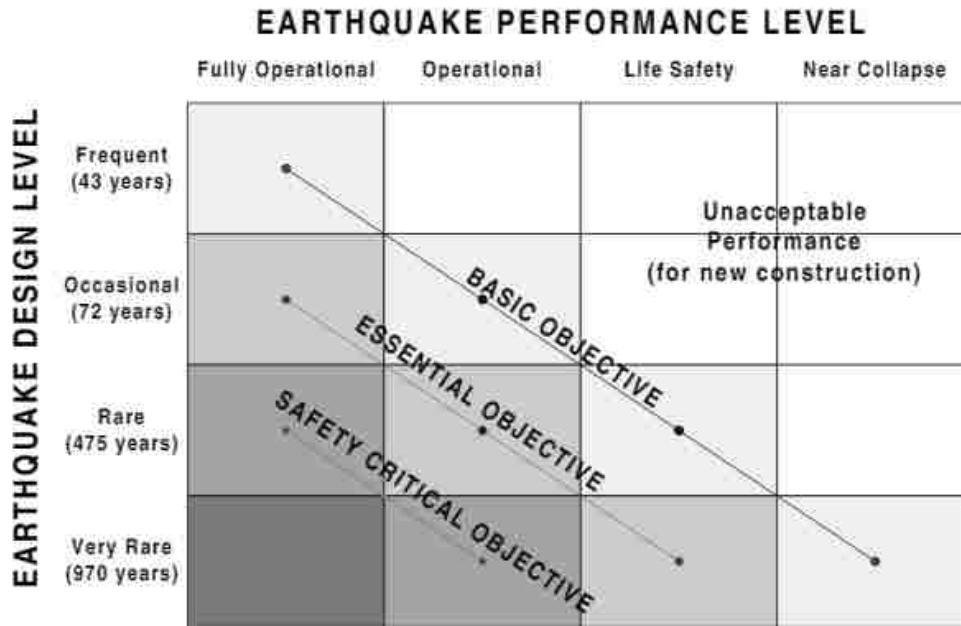


**Figure 5-2: Acceptable earthquake performance level (after Bertero and Bertero, 2002).**

## 5.2 Performance-Based Liquefaction Initiation

In dealing with liquefaction analysis, the principles of PBEE can be applied specifically to the problem of liquefaction initiation. A liquefaction triggering analysis deals mainly with intensity measures such as $a_{max}$ and earthquake magnitude, which can be obtained from a PSHA. The use of fragility curves that incorporate the probability of liquefaction, a hazard curve for an engineering design parameter can be developed. The EDP's most commonly used in this type of analysis are factor of safety against liquefaction ($FS_L$), or the required CPT cone-tip resistance to resist liquefaction ($q_{req}$). An example of a possible hazard curve from this process is shown

in Figure 5-3. This provides a convenient design tool, as a mean annual rate of exceedance (or corresponding return period) can be selected, and then the corresponding *EDP* value from the hazard curve can be used for design. This process allows for much greater flexibility in design. For example, using the hazard curve in Figure 5-3 for a return period of 100 years (i.e. $\lambda = \frac{1}{100}$ years) would predict $FS_L \approx 2$, which signifies that liquefaction will not be expected to initiate. An example of the process to create a liquefaction initiation hazard curve will be shown later in this chapter.
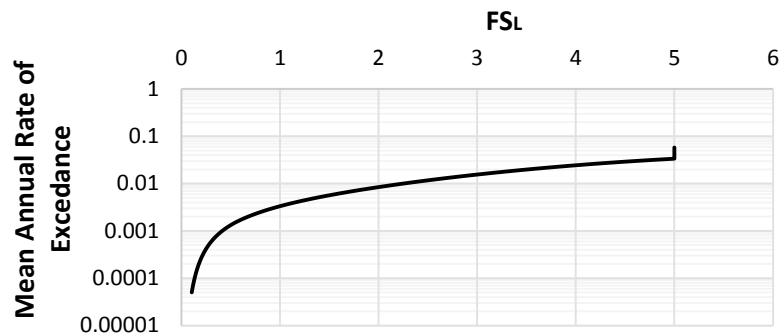


**Figure 5-3: Design hazard curve output from PBEE using Boulanger and Idriss (2014) model.**

### 5.2.1   Incorporation of Probabilistic Models into PBEE

Kramer and Mayfield (2007) first attempted to apply a SPT based liquefaction triggering model by Cetin et al. (2004) into the PBEE framework. To apply the framework to consider liquefaction triggering, some small changes were made in the framework. The first step to this modification was to change the main equation to solve for a probability of non-exceedance, rather than probability of exceedance. This was required because $FS_L$ unlike other *EDP*'s is more favorable as a higher value rather than a low value. Because of this fact, engineers are

more interested in when $FS_L$ is expected to **not** exceed a certain value. The equation for the non-exceedance of $FS_L$ is:

$$\Lambda_{FS_L^*} = \sum_{i=1}^{N_{IM}} P\left[FS_L < FS_L^* \mid IM_i\right]\Delta\lambda_{IM_i} \tag{5-4}$$

This equation assumes that the *IM* describes the probability of $FS_L$ term of being exceeded. Because the simplified method derived by Seed and Idriss requires the use of two different *IM* values another modification is required. To account for both $a_{max}$ and $M_W$, Kramer and Mayfield (2007) provided the following expression:

$$\Lambda_{FS_L^*} = \sum_{j=1}^{N_{Mw}} \sum_{i=1}^{N_{a_{max}}} P\left[FS_L < FS_L^* \mid a_{max}, m_j\right]\Delta\lambda_{a_{max_i},m_j} \tag{5-5}$$

where $N_{M_W}$ and $N_{a_{max}}$ are the number of subdivided magnitude and peak acceleration increments respectively, and $\Delta\lambda_{a_{max_i},m_j}$ is the incremental mean annual rate of exceedance for a given $a_{max}$ and $M_W$. This equation brings the analysis into the truly probabilistic realm by considering all possible combinations of $a_{max}$ and $M_W$. To solve the conditional probabilities in this equation, the probability of liquefaction equations can be used.

Kramer and Mayfield also related performance based methodology to in-situ soil resistance. Kramer and Mayfield provided an expression for a relative penetration resistance given as:

$$\Delta N_L = N_{site} - N_{req} \tag{5-6}$$

where $N_{site}$ is the corrected in-situ SPT resistance and $N_{req}$ is the corrected SPT resistance required to cause a condition where $FS_L = 1$. For CPT-based analyses, the analogous expression can be used:

$$\Delta q_L = q_{site} - q_{req} \tag{5-7}$$

where $q_{site}$ is the corrected in-situ CPT cone-tip resistance and $q_{req}$ is the corrected CPT cone-tip resistance required to cause a condition where $FS_L = 1$.

The calculation of $N_{req}$ at each depth increment of a soil profile can be helpful to engineers when considering liquefaction hazards. The difference between a computed value of $N_{req}$ and the actual in-situ SPT resistance would provide an indication of the amount of ground improvement required to bring a particular site to an acceptable factor of safety (Kramer and Mayfield 2007). These same principles apply for the CPT, thus the term $\Delta q_L$ can be used by engineers to consider how much ground improvement may be needed at a site to negate a liquefaction hazard (bring $FS_L \geq 1$). The relationship between $FS_L$ and $\Delta N_L$ is shown visually in Figure 5-4. As seen in the left frame (a) of Figure 5-4, $\Delta N_L$ is the departure from the $FS_L$ when considering a required soil resistance to prevent liquefaction. Part (b) of Figure 5-4 shows that $\Delta N_L$ can be negative when $FS_L$ is less than 1, or in other words, liquefaction is expected to occur. $\Delta N_L$ will be positive for value where $FS_L$ is greater than 1, or liquefaction is not predicted to be triggered.
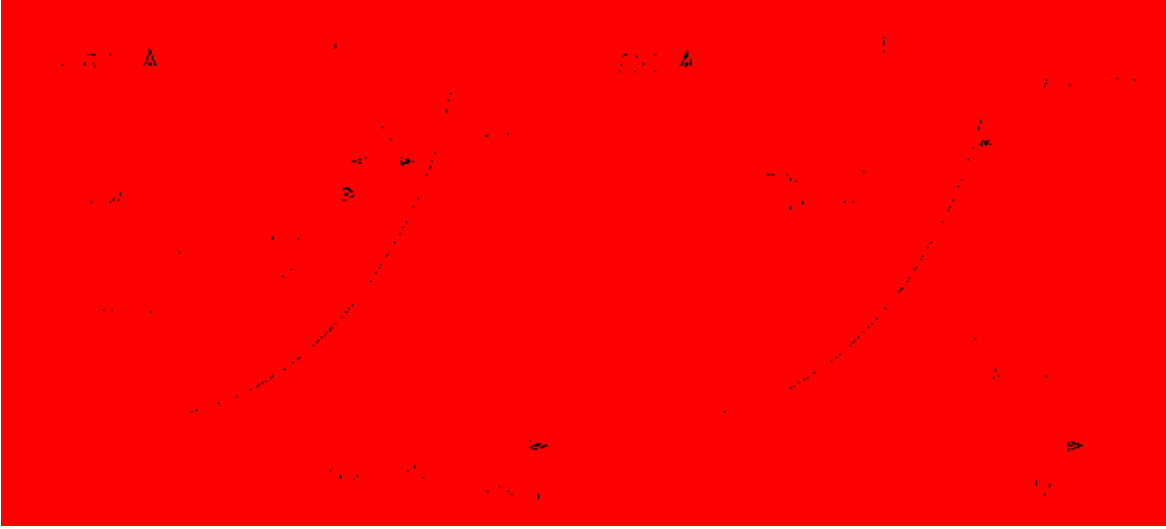
**Figure 5-4: Relationship between $FS_L$ and $\Delta N_L$ (after Kramer and Mayfield, 2007).**

When considering the parameter $N_{req}$ in PBEE, Kramer and Mayfield developed an expression to compute the mean annual rate of exceedance of an incremental value of $N_{req}$ ( $N_{req}^{*}$ ). In terms of the CPT, the mean annual rate of exceedance of an incremental value $q_{req}^{*}$ at a depth of interest can be defined as:

$$\lambda_{q_{req}^{*}} = \sum_{j=1}^{N_{Mw}} \sum_{i=1}^{N_{a_{max}}} P\left[q_{req} > q_{site} \mid a_{max}, m_j\right] \Delta\lambda_{a_{max_i}, m_j} \tag{5-8}$$

where

$$P\left[q_{req} > q_{site} \mid a_{max}, m_j\right] = P_L \tag{5-9}$$

Equations (5-8) and (5-9) facilitate the computation of all hazard curves used in this study. An example of this computation will be shown later in this chapter.

Because $FS_L$ and $\Delta N_L$ essentially provide the same information, Kramer and Mayfield provides a useful conversion between the two.

$$FS_L^{site} = \frac{CRR}{CSR} = \frac{CRR(N_{site})}{CRR(N_{req}^{site})} \tag{5-10}$$

When using CPT data becomes:

$$FS_L^{site} = \frac{CRR}{CSR} = \frac{CRR(q_{site})}{CRR(q_{req}^{site})} \tag{5-11}$$

where, $q_{site}$ is the measured corrected clean-sand equivalent CPT cone-tip resistance, and $q_{req}^{site}$ is the computed corrected clean-sand equivalent CPT cone-tip resistance required to resist liquefaction at the site of interest. This equation can be applied to both the Ku et. al., and Boulanger and Idriss liquefaction triggering models, by applying their corresponding *CRR* equations in terms of both $q_{site}$ or $q_{req}^{site}$.

### 5.2.2  Implementation of Ku et al. (2012) Model in PBEE

To use the Ku et al (2012) model (probabilistic version of the Robertson and Wride deterministic model) in the framework established by Kramer and Mayfield (2007), some modification is required to the given probabilistic relationship such that it will be in the terms of $a_{max_i}$ and $m_j$ .

$$P_L = 1 - \Phi \left[ \frac{0.102 + \ln(\frac{CRR}{CSR})}{\sigma_{tot}} \right] \tag{5-13}$$

where CSR in this equation is in terms of $a_{max_i}$ , $m_j$, and CRR is in terms of the incremental value $q_{c1Ncs}^{*}$ .

To account for uncertainty related to the calculation of $P_L$ using (5-13), a single term $\sigma_{tot}$ can be used. Two cases are often considered when doing a liquefaction analysis. First, where

uncertainty in the parameters (*CRR*, *CSR*, $q_{req}$) are considered along with model uncertainty; and second, where only uncertainty in the liquefaction model is considered. For the purposes of this thesis, values for uncertainty in Table 5-1 were statistically computed from the Ku et. al. database by resolving their maximum likelihood function, but without removing uncertainty for parameters such as $q_{c1Ncs}$ or *CSR*. By allowing the MLE solution to solve for $\sigma_{tot}$ in this manner, the total (ie, the model + parameter uncertainty) is computed. Total uncertainty is denoted as $\sigma_{tot}$. By including $\sigma_{tot}$ in a simplified probabilistic liquefaction analysis, the engineer does not need to assume that his/her specified CPT sounding values are the true CPT values. Rather, the use of $\sigma_{tot}$ indirectly accounts for the possibility of varying CPT values by means of a larger uncertainty value. Therefore, resolving the Ku et al. (2012) maximum likelihood equation for total uncertainty yields $\sigma_{tot} = 0.3537$.

**Table 5-1: Ku et. al. standard deviation with and without parameter uncertainty included**

| criteria | $\sigma_{tot}$ |
|---|---|
| Parameter uncertainty + model uncertainty | 0.3537 |
| Model uncertainty only | 0.276 |

In attempting to implement the Ku et. al. (2012) model into a performance-based setup, certain limitations to the model were detected. The use of the suggested equations from Ku et al. (2012) was seen to give reasonable prediction of the probability of liquefaction for values within the range of $q_{c1Ncs}$ between 1 to about 165. However, the calculated probability of liquefaction was seen to be considerably conservative for values beyond this range. This issue was found to be caused by the limitations of the CRR equations which come from the deterministic Robertson

and Wride (1998) procedure. The CRR equations were developed to match the case history data up to the range of

$q_{c1Ncs} \approx 165$. This was seen to cause issues when used in a probabilistic sense. When using the model in areas of very high seismicity (CSR > 1.5), it becomes possible for significant contribution to the liquefaction hazard to come from $q_{c1Ncs}$ values above 200. Dr. Peter Robertson was consulted on this issue, and was of the opinion that a cap should be placed near a value of $q_{c1Ncs} \approx 175$ (personal communication, April 5, 2017). However, applying a cap is detrimental in a probabilistic analysis because the construction of hazard curves relies on a probability function that is continuous from 100% to 0%. Implementing a cap essentially will end the hazard curves prematurely, limiting their effectiveness in analysis over a complete range of potential return periods.

To solve this problem, an equation was provided to represent the cyclic resistance for values beyond $q_{c1Ncs} \approx 165$. This equation is based on the CRR equation used in the probabilistic Boulanger and Idriss model, which more accurately represents the cyclic resistance of a soil at very high values of seismic loading. The results of this change can be viewed in Figure 5-5, where the solid line represents the CRR curve with the practical limit and the dotted line shows the CRR curve using the original CRR equations beyond their original bounds. The area between the two lines represents unrealistic values that would be expected to liquefy in the performance-based analysis without the use of a practical limit.
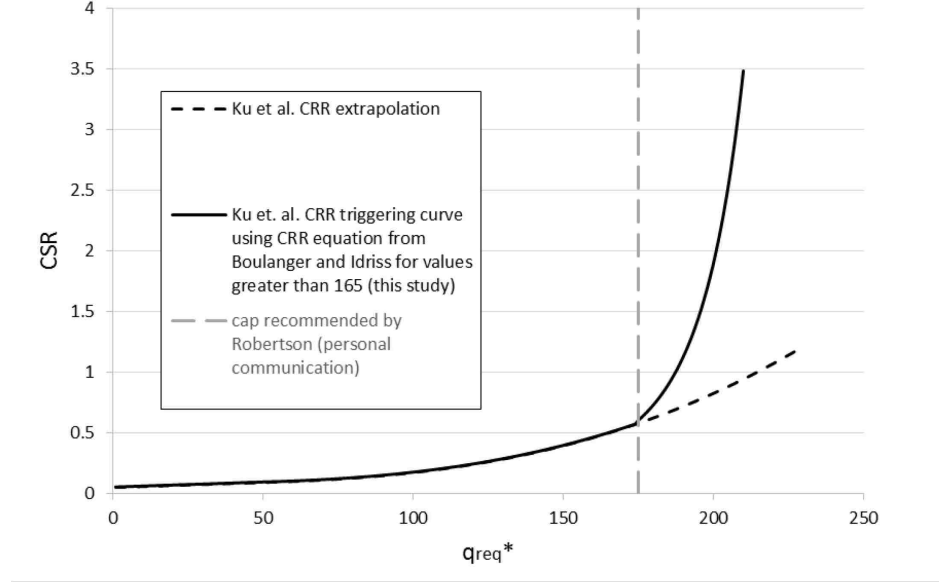
**Figure 5-5: Comparison of Ku et. al. CRR values at high values of CSR.**

### 5.2.3 Implementation of Boulanger and Idriss (2014) Model in PBEE

An alternative to the Ku et al model is the Boulanger and Idriss 2014 probabilistic model. This model follows a more typical approach in that the functions in this model do not try to map $FS_L$ as $P_L$, but calculates a value for $P_L$ directly from CPT penetration resistance. To apply the Boulanger and Idriss (2014) equation to PBEE only a minor adjustment must take place, replacing $q_{c1Ncs}$ with $q_{c1Ncs}{}^*$, which is an incremental value which covers all possible values of $q_{req}$. The expression then becomes:

$$P_L = \Phi\left[-\frac{\dfrac{q_{c1Ncs}^*}{113}+\left(\dfrac{q_{c1Ncs}^*}{1000}\right)^2-\left(\dfrac{q_{c1Ncs}^*}{140}\right)^3+\left(\dfrac{q_{c1Ncs}^*}{137}\right)^4-2.60-\ln\left(CSR_{M=7.5,\sigma'_v=1atm}\right)}{\sigma_{tot}}\right] \qquad (5\text{-}14)$$

where $a_{max_i}$ and $m_j$ are represented in the term $CSR_{M=7.5,\sigma'_v=1atm}$.

To account for uncertainty related to the calculation of $P_L$ in equation (5-14), a single term $\sigma_{tot}$ can be used. Boulanger an Idriss (2014) present a value for model uncertainty that should be used in this relationship as seen in Table 5-2. To estimate a value for the uncertainty when considering both model and parameter uncertainty, a re-analysis of the case history database was required. This re-analysis was done by resolving their maximum likelihood function, but without removing uncertainty for parameters such as $q_{c1Ncs}$ or $CSR$. A fitting parameter ($C_0$), such as described in Boulanger and Idriss (2014) was locked at a value of 2.6. By allowing the MLE solution to solve for $\sigma_{tot}$ in this manner, the total (ie, the model + parameter uncertainty) is computed. Total uncertainty is denoted as $\sigma_{tot}$. By including $\sigma_{tot}$ in a simplified probabilistic liquefaction analysis, the engineer does not need to assume that his/her specified CPT sounding values are the true CPT values. Rather, the use of $\sigma_{tot}$ indirectly accounts for the possibility of varying CPT values by means of a larger uncertainty value. Therefore, resolving the Boulanger and Idriss (2014) maximum likelihood equation for total uncertainty, given $C_0 = 2.6$ yields $\sigma_{tot} = 0.506$.

**Table 5-2: Boulanger and Idriss (2014) standard deviation values with and without parameter uncertainty included.**

| criteria | $\sigma$ tot |
|---|---|
| Parameter uncertainty + model uncertainty | 0.506 |
| Model uncertainty only | 0.2 |

## 5.3 Example Computation of Liquefaction Triggering Hazard Curves

To better illustrate the process of how the Ku et. al. (2012) and Boulanger and Idriss (2014) performance-based models can be used to compute hazard curves for $FS_L$ and $q_{req}$ an example calculation is provided.

*Step 1: ground motions*

Ground motions must be obtained for a range of return periods from a PSHA. Generally, these values are in the form of PGA values. Site amplification can be considered as described in chapter 2, but in order to consider uncertainty in site amplification ( $F_{pga}$ ) a probabilistic procedure should be used. The procedure to consider uncertainty in $F_{pga}$ begins by obtaining PGA values and their corresponding annual rates of exceedance ( $\lambda$ ), as provided in a PSHA. When plotting these points, each can be connected to create a PGA curve.

The PGA curve should then be divided into increments of $\Delta\lambda$ (Figure 5-6). For each of these increments, a corresponding PGA value should be selected from the PGA curve. Each of these many PGA values should be applied to equation (2-3), without use of the uncertainty term.
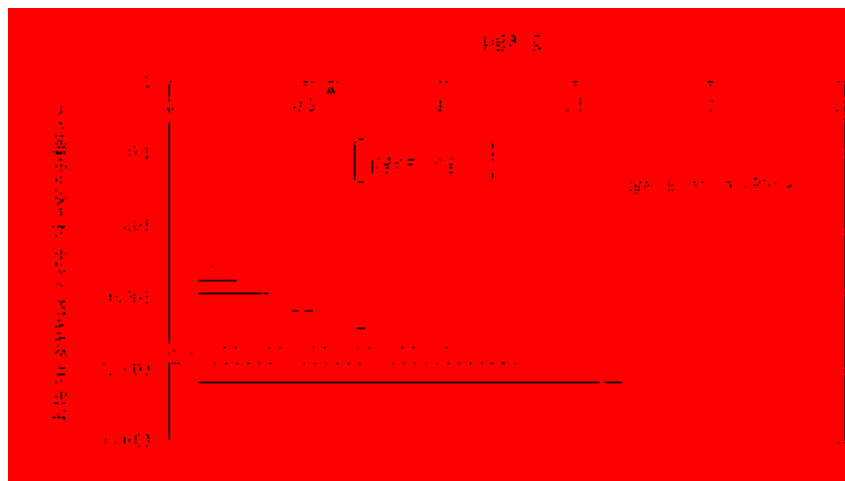


**Figure 5-6: Beginning of process to consider uncertainty in site amplification.**

The results of that calculation will be represented as a value ($x$) Next, a wide range of possible $a_{max}$ values should be computed from about .01g to 4g. These $a_{max}$ values will represent all possible accelerations, and can be termed $a_{max}^{*}$.

With a large list of values for $x$ and $a_{max}^{*}$, a z-score relating these two values can be computed using:

$$z = \frac{x - \ln(a_{max}^{*})}{0.3} \qquad (5\text{-}15)$$

where 0.3 is a suggested uncertainty value representing the uncertainty in site amplification. Next, the probability that the $a_{max}^{*}$ value will be the true $a_{max}$ value can be computed as:

$$P = \Phi(z) \qquad (5\text{-}16)$$

where $\Phi$ is the normal standard cumulative distribution. By computing a probability value for each possible combination of $x$ and the $a_{max}^{*}$ value currently under consideration, a new value for the mean annual rate of exceedance of $a_{max}^{*}$ is given as:

$$\lambda_{a_{max}^{*}} = \sum P(\Delta\lambda) \qquad (5\text{-}17)$$

This will result in a point ($a_{max}^{*}, \lambda_{a_{max}^{*}}$) that can be plotted as the beginning of an $a_{max}$ hazard curve. This process should be repeated for each value of $a_{max}^{*}$ until a full $a_{max}$ hazard curve is completed.

Once the probabilistic procedure for site amplification is completed, ground motions from $a_{max}$ hazard curve are then deaggregated (deconstructed) for various magnitude bins. Figure 5-7 shows what deaggregated values from two magnitude bins might look like. Next, a new

increment $\Delta\lambda$ is chosen from which to incrementally pick values from off the curve (Figure 5-7). The smaller the size of this increment, the more accurate the calculation will become, as a more complete view of all possible ground motions will be considered.
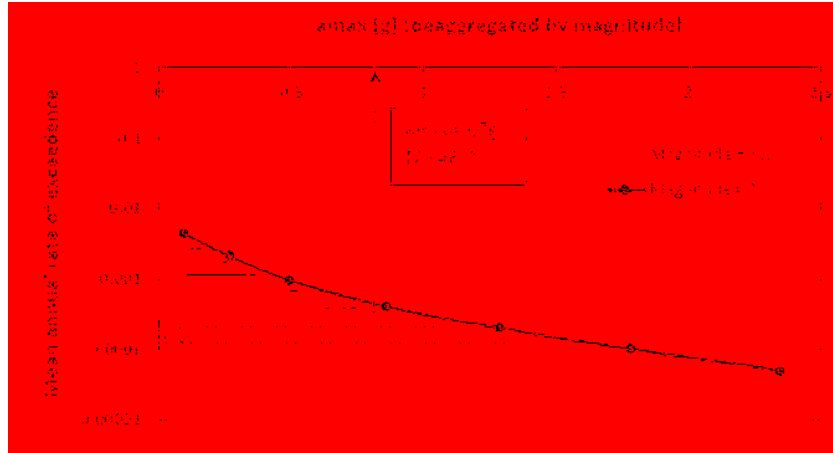


**Figure 5-7: Example of deaggregated $a_{\max}$ values from a PSHA**

*Step 2: Compute* $P\left[q_{req} > q_{site} \mid a_{\max}, m_j\right] = P_L$

Given an incremental value for $a_{\max}$ and $m_j$, compute the probability that the CPT cone-tip resistance required to resist liquefaction $q_{req}$ is greater than a value of interest $q_{site}$. To compute this probability simply use the equations given for the probability of liquefaction for each model. For the Ku et. al. (2012) model use (5-13), for Boulanger and Idriss (2014) use (5-14) with given input values, $a_{\max}$, $m_j$, and $q_{site}$. When computing the probability over a wide range of values for $q_{site}$, a fragility curve, like the example shown in Figure 5-8 can be produced. As seen in Figure 5-8, the probability that the required CPT resistance to prevent liquefaction drops significantly as the selected values of $q_{site}$ increases.
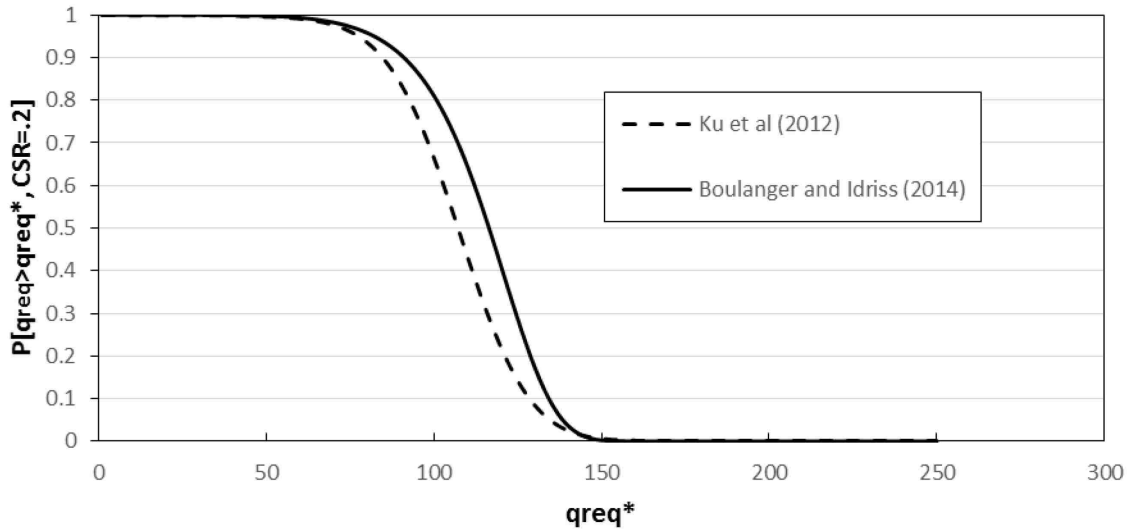
**Figure 5-8: Example fragility curve for hypothetical site, given CSR=.2.**

*Step 3: Compute Sum of products of* $P\left[q_{req} > q_{site} \mid \mathrm{a}_{max}, m_j\right]$ *and* $\Delta\lambda$.

For each of set of ground motions ($a_{max}$, $m_j$) compute a probability value. Next, move on the next set of $a_{max}$ and $m_j$ values (using same $q_{site}$) and sum the probabilities together. After all the sets of ground motions are computed for one magnitude bin (Figure 5-7) multiply the sum of probabilities by $\Delta\lambda$. Next, repeat this process with the next magnitude bin. Once all possible combinations of $a_{max}$ and $m_j$ are used in conjunction with one value $q_{site}$, a value for the mean annual rate of exceedance of $q_{req}$ ($\lambda_{q_{req}^*}$) can be computed by using the equation (5-6). The set of the two values ($q_{req}$, $\lambda_{q_{req}^*}$) now become the first point that can be plotted on a $q_{req}$ hazard curve.

*Step 4: Compute $q_{req}$ hazard curve*

Once the process for the computation of one point of the hazard curve is complete, the entire process should be repeated, but using a different value for $q_{req}$. Once these calculations are run for a wide range of $q_{req}$ values, a hazard curve as seen in Figure 5-9 is created.
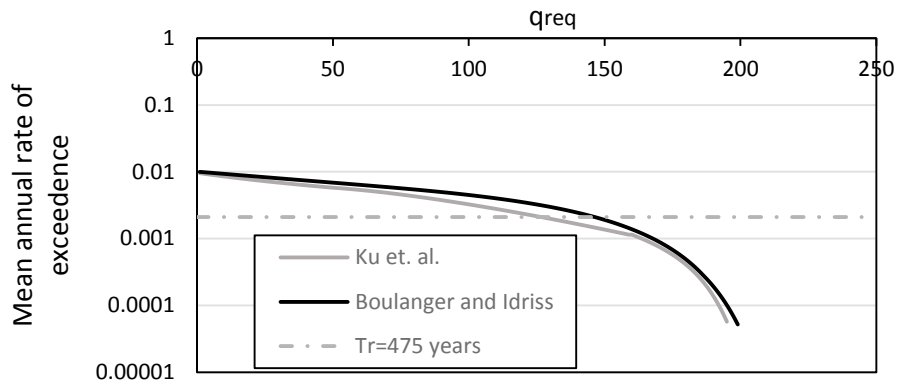


**Figure 5-9: Example $q_{req}$ hazard curve.**

*Step 5: convert $q_{req}$ hazard curve to $FS_L$ hazard curve.*

To compute a $FS_L$ hazard curve, a conversion must be made from the $q_{req}$ curve already computed. Using equation (5-9) and real site-specific CPT cone-tip resistance values from a CPT sounding, a correlating value of $FS_L$ can be computed for each value of $q_{req}$. When $q_{req}$ is converted to $FS_L$ the value $\lambda_{q_{req}^*}$ is automatically converted to an annual rate of non-exceedance of $FS_L$ ($\Lambda_{FS_L}$). The sets of ($FS_L$, $\Lambda_{FS_L}$) create a new hazard curve as seen in Figure 5-10. For example, the following hazard curve shows that at a return period of 475 years, the Boulanger and Idriss liquefaction triggering model will not be expected to exceed $FS_L = 0.4$. Because a

condition of non-liquefaction is correlated with $FS_L \geq 1$ in this case it would be predicted that liquefaction would occur.
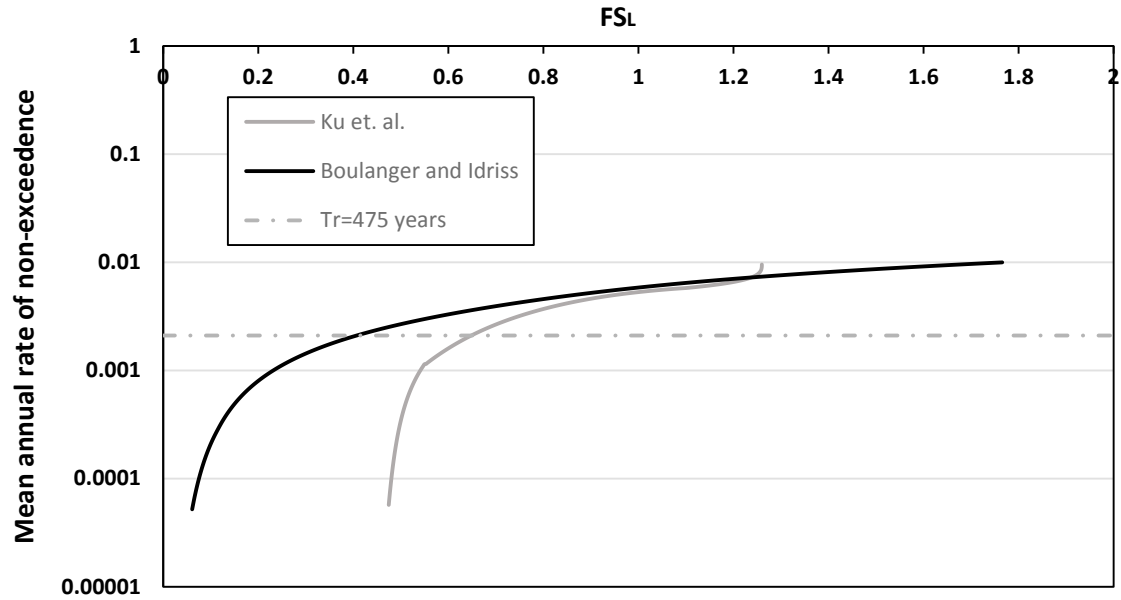


**Figure 5-10: Example of a factor of safety against liquefaction hazard curve.**

# 6    COMPARATIVE STUDY

To compare the performance-based liquefaction method to the conventional pseudo-probabilistic liquefaction method, a study was conducted to compare liquefaction triggering results from each method.  To appropriately consider the intricacies of both the Ku et. al. (2012) and Boulanger and Idriss (2014) liquefaction triggering models, the analysis was conducted over a wide range of soil parameters and a variety of site locations / seismic loadings.  Myself, along with two other students created a computational tool called CPTLiquefY to facilitate the computation of both performance-based, and conventional CPT-based liquefaction triggering results.  Results from CPTLiquefY are then compared and presented in a graphical format from Microsoft Excel.  A brief statistical analysis of the distribution of the liquefaction triggering predictions between the conventional and performance-based methods was also conducted.

## 6.1    CPTLiquefY

To facilitate a complex performance-based liquefaction analysis, a research tool called CPTLiquefY has been developed.  This tool was developed by myself, Mikayla Hatch, and Tyler Coutu.  This tool has the capacity to run the heavy computational load that comes with a performance-based analysis.  This process becomes more complex when dealing with CPT data which can give a nearly continuous profile of a soil down to a desired depth.  For this type of analysis, all possible site conditions must be analyzed with their corresponding probabilities of occurrence.  This process involves millions of calculations which must be repeated for

potentially hundreds of CPT readings for one soil profile. Because of the heavy computational load on this program, C++ was used as the coding language over other options for greater speed and flexibility. This program was coded in the Visual Studio C++ to allow the program to be stand-alone. Problems with Microsoft updates have proved problematic for past liquefaction tools (Franke et. al. 2014), but this should be resolved by the stand-alone nature of CPTLiquefY. The purpose of this tool is primarily to allow researchers to perform performance-based analyses with CPT data, and to potentially be used in design if deemed appropriate by funding sponsors of this research. My contribution to the development of this program was focused on the development of the initial CPT calculations, inclusion of PSHA data from the USGS database, and the development of the site amplification and liquefaction triggering calculations and methods.

The general concept of CPTLiquefY is primarily modeled after the SPT liquefaction analysis tool PBliquefY (Franke et. al. 2014). As such, CPTLiquefY has been designed to run both conventional pseudo-probabilistic calculations along with performance-based liquefaction analyses. These calculations are based on established CPT deterministic empirical liquefaction models (Robertson and Wride (1998), Boulanger and Idriss (2008)) along with probabilistic models (Ku et. al. (2012), Boulanger and Idriss (2014)). Along with liquefaction triggering capabilities, CPTLiquefY also has the capability to compute values for liquefaction effects including settlements and lateral spreads. Additional options are available for users to modify the conditions of the analysis. In order to facilitate a large comparative study, CPTLiquefY has the capability to run analyses in large batches. Further explanation of the program capabilities can be found in Appendix A.

### 6.1.1   Analysis Process

To begin an analysis, a soil profile of interest is selected.  This can be done for one soil profile or multiple (see Appendix A)  This profile should at the minimum represent standard CPT data with the following data present for each layer: depth from ground surface, cone tip resistance ($q_c$), cone sleeve friction ($f_s$), and pore pressure measured behind the cone ($u$). Next, a location for the analysis should be chosen.  This can be done for one location or multiple sites.  Once a site location is chosen, a pseudo-probabilistic analysis can be run.  This analysis will require the selection of a return period of interest, or an exceedance percentage and a range of years.  Using these selections, values will be automatically selected from a PSHA for the governing ground motions scenario ($a_{max}$, $M_W$).  After this data is obtained, values for the pseudo-probabilistic analysis will be calculated.  After the pseudo-probabilistic analysis is complete, the user can begin a performance-based analysis.

*NSHMP-haz*

To begin the performance-based analysis, the user must download USGS deaggregation data.  Previously, this data has been obtained by means of downloading deaggregation values from an online USGS resource.  (As of early 2017 the USGS deaggregations site has been decommissioned and replaced with a unified hazard tool).  With the transition of the USGS to the new unified hazard tool, deaggregations are no longer available in the same format as previously.  To combat this issue, USGS has provided an offline version of their deaggregation tool, which creates output deaggregations that can be easily applied to site specific liquefaction analyses.  This tool is called NSHMP-haz.  CPTLiquefY is equipped to use this new tool to obtain deaggregation data in real time without access to the internet. For more information on NSHMP-haz view Appendix A.

Figure 6-1 shows the basic process followed for a conventional and a performance-based analysis in CPTLiquefY. The program must run the NSHMP-haz tool for a range of return periods (usually about 50 years to 20,000 years). Once the values from about 10 return periods of the NSHMP-haz deaggregation tool have been run, the data is loaded into CPTLiquefY. Next, the site amplification is taken into account. In the conventional procedure, site amplification is considered using an amplification factor as described in section 2.4.2.

For the purposes of the analysis described in this thesis values for $F_{pga}$ were chosen which correspond to a NEHRP site class D. For a performance-based analysis, site amplification is considered using a probabilistic procedure discussed in 5.3 (Step 1). Once the $a_{max}$ values are calculated, both the conventional and performance based-calculations can begin. Once complete, the results from the performance-based analysis are available in the program setup. After all calculations are finished, the data can be exported into a clean excel format to better enable comparison of liquefaction analysis results.

To run a performance-based analysis, many iterations must be completed. In CPTLiquefY the time required to obtain the performance-based results is a function of computing speed and the number of depth increments in the selected soil profile. Depending on the computing speed of the computer system being used, a complete performance-based analysis with about 150 depth increments can be completed in about 7 to 10 minutes.
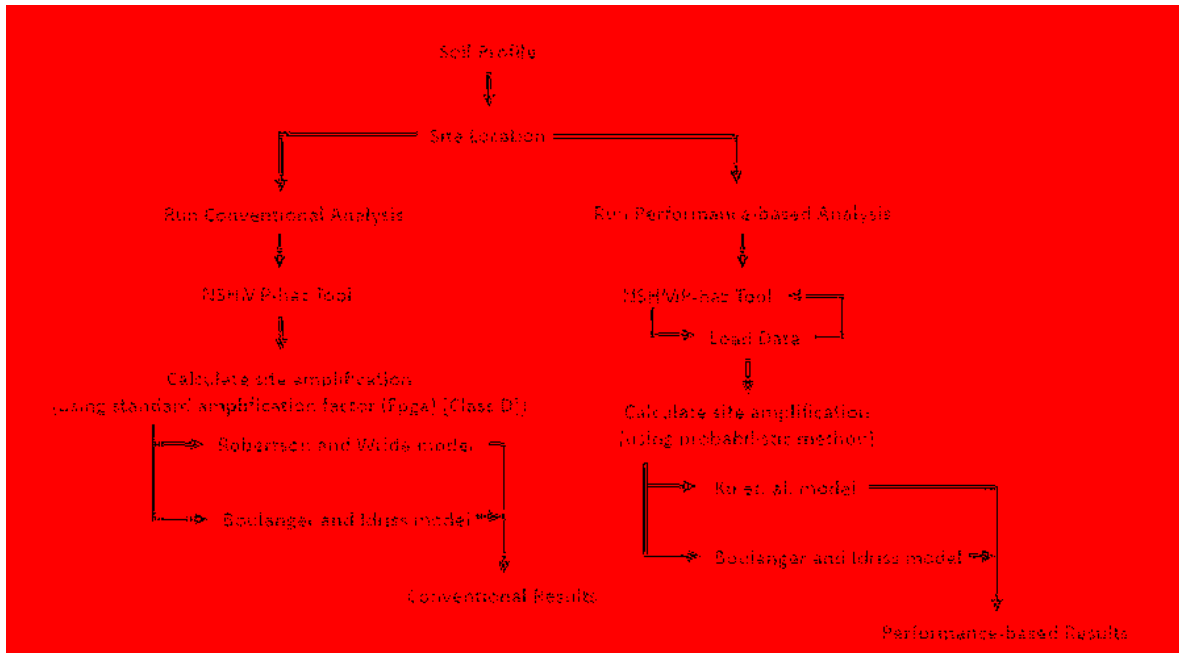
**Figure 6-1: Basic program flow chart for CPTLiquefY.**

## 6.2 Site Locations

Site selection is an important step in a liquefaction susceptibility analysis. For consistency, the sites used in this analysis are the same as those used in previous performance-based liquefaction research (Kramer and Mayfield, 2007). These sites were chosen to represent a range of different seismic environments that can be found throughout the continental United States. In this way, the analysis can be seen as applicable to most any possible analysis location within the continental region.

The 10 sites chosen are distributed as such: 4 on the west coast near the San Andreas Fault system, 2 in the Pacific north-west near the Cascadia Subduction zone and associated faults, 2 near the Wasatch fault and rocky mountain region, 1 near the New Madrid fault system,

and 1 near the Charleston liquefaction features.  A map of these locations can be found in this section (Figure 6-2).

Recently, USGS has released a new version of its seismic source model.  This release provides several updates to probabilistic earthquake hazard calculation for the conterminous United States (Peterson et. al. 2015).  The 2014 model has now replaced the 2008 USGS seismic source model as the most current version of the USGS National Seismic Hazard Mapping Project (NSHMP).  Using the 2014 USGS seismic source model; analyses were conducted for each of these locations.  This is the first time the 2014 USGS seismic model update has been used in conjunction with research related to performance-based liquefaction triggering analysis. The resulting values for earthquake magnitude (mean and modal) and mean maximum acceleration for each location are shown in Table 6-1.  These values represent results from the 2014 PSHA. For comparative purposes, values correlating to a 2475-year return period are presented here.



**Figure 6-2: Geographical distribution of sites used for liquefaction analysis.**

**Table 6-1: Mean and modal magnitude values along with acceleration from PSHA (USGS 2014) corresponding to $T_R = 2475$ years.**

| Number | Location | Pga [g] | Mw (mean) | Mw (modal) |
|--------|----------|---------|-----------|------------|
| 1 | Butte | 0.179 | 6.25 | 5.5 |
| 2 | Charleston | 0.729 | 6.77 | 7.3 |
| 3 | Eureka | 1.400 | 7.93 | 6.99 |
| 4 | Memphis | 0.571 | 6.88 | 7.55 |
| 5 | Portland | 0.437 | 7.49 | 9.3 |
| 6 | Salt Lake City | 0.671 | 6.81 | 6.89 |
| 7 | San Francisco | 0.725 | 7.48 | 7.7 |
| 8 | San Jose | 0.691 | 7.04 | 6.8 |
| 9 | Santa Monica | 0.742 | 6.93 | 7.31 |
| 10 | Seattle | 0.643 | 7.05 | 7.09 |

Most of the sites are distributed in the moderate to high seismicity range. As seen in Figure 6-3, obvious outliers exist in the form of Eureka and Butte which can be classified as very high seismicity, and low seismicity areas respectfully. The values of $a_{max}$ seen below were applied to the conventional pseudo-probabilistic analysis to represent the relative ground acceleration expected to possibly occur at each location.
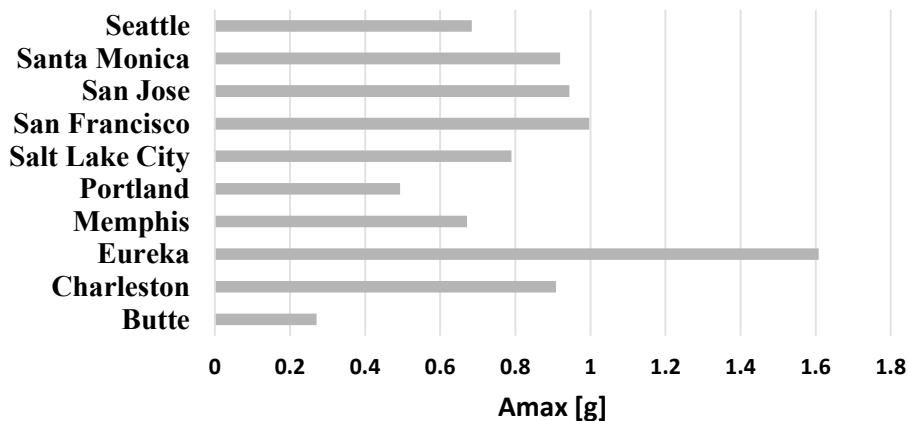


**Figure 6-3: Comparison of mean max ground surface acceleration for each site from PSHA corresponding to a return period of 2475 years, and site amplification factors for AASHTO site class D.**

Figure 6-4 shows a comparison of the mean and modal magnitude values obtained from the PSHA. These values are crucial in a conventional pseudo-probabilistic liquefaction hazard assessment which considers one earthquake scenario (one set of $a_{max}, M_W$ ). As seen below Portland had very high values in the modal category. This is likely due to the updates in the USGS 2014 deaggregations which contains a significant update to the seismic hazard in the southern part of the Cascadia subduction zone (Peterson et. al. 2015).
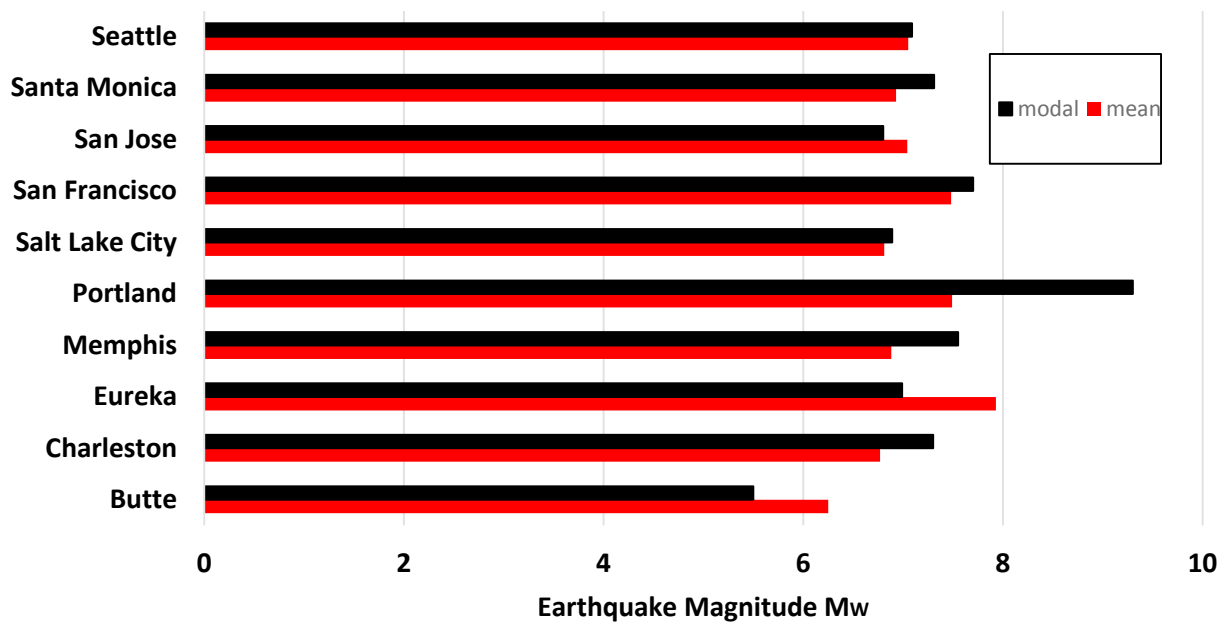


**Figure 6-4: Comparison of mean and modal magnitude values from PSHA for each site.** $T_R = 2475$ **yrs.**

## 6.3   Soil Profiles

20 Soil profiles were chosen to represent a wide variety of possible field conditions that could be found throughout the continental United States. To attempt to capture the natural variability of soil profiles in nature, real CPT data was used in this analysis. The data used in

this analysis were obtained from the USGS seismic cone project, which maintains a database of over 1000 CPT profiles collected in the last 50 years (https://earthquake.usgs.gov/research/cpt/data/). This subsurface data is also freely accessible to the public.

Profiles were selected from several different regions and depositional environments around the United States. Figure 6-5 shows the geographical distribution of these profiles. Because saturated sandy soils are often required for liquefaction to initiate, another factor used in the selection of soil profiles was the prevalence of sand-like soils in the profile. Although some profiles contain data down to greater depths, for the purposes of this thesis, data were only considered down to a depth of 12 meters, as case histories for both the Robertson and Wride and Boulanger and Idriss models are largely taken from depths of 12 meters or less. Only CPT data from the year 1990 and on were used in the analysis. Older profiles, although useful in some applications were not considered in this research.

Profiles were also selected based on a desired range of CPT clean sand resistance values. Figure 6-6 shows the distribution of $q_{t1Ncs}$ values according to depth for the full profiles. Table 6-2 also gives a summary of other properties related to each soil profile.

Although the analysis tool CPTLiquefY has the capability to vary these properties, the following were held constant for the purposes of the analysis:

Ground water table depth = 0 m (at ground surface)

Pore water pressure behind cone $u$ = 0 KPa (for all depths)

Tip resistance units: MPa

Sleeve Friction units: KPA

Net area ratio = .8

Uncertainty considered in performance based analysis = total uncertainty

The effect of pore water pressure behind the cone was not considered, as the data from the USGS database did not contain these data. Although the omission of this data, and the assumption of the ground water table at the surface will have a significant effect on the soil resistance and liquefaction hazard, the purpose of this study is to analyze the difference between two liquefaction analysis methods. As long as these factors are kept constant throughout the study, the validity of the results of this comparative study will be preserved, even if the values do not represent the exact in-situ soil resistance values.

In the future, a site-specific analysis may be helpful in determining the agreement between the performance-based method and actual case history data. In that case, higher quality CPT data would be required to make an effective comparison. CPTLiquefY, as created by my colleges and I has the capability to analyze more complete CPT data for such an analysis.

**Table 6-2: CPT Profile information**

| Profile | Name | Location | Latitude | Longitude | Source | Sand Content | Stiffness | Full Depth (m) | Date Collected |
|---|---|---|---|---|---|---|---|---|---|
| 1 | SFO029 | San Francisco, CA | 37.824 | -122.364 | USGS | Medium | soft/very soft | 17 | 1/21/1994 |
| 2 | LWE001 | Lawrenceville, Ill | 38.747 | -87.511 | USGS | High | med to hard | 12.5 | 10/6/2004 |
| 3 | HNC005 | Evansville, IN | 37.872 | -87.702 | USGS | Medium | med | 20 | 12/6/2003 |
| 4 | BDY002 | Arkansas | 33.278 | -92.333 | USGS | Medium | med | 12 | 12/14/2005 |
| 5 | SBC030 | Riverside,CA | 34.070 | -117.290 | USGS | High | med/hard | 19 | 3/24/2001 |
| 6 | BKY006 | Charleston, SC | 32.905 | -79.924 | USGS | High | soft | 20 | 11/6/2004 |
| 7 | MGA003 | Matagorda, TX | 28.765 | -95.787 | USGS | Low | soft | 18.15 | 1/5/2006 |
| 8 | SCR001 | East St. Louis, Ill | 38.620 | -90.162 | USGS | High | med | 24 | 10/6/2008 |
| 9 | SOC024 | Oceano, CA | 35.104 | -120.631 | USGS | High | med/hard | 15 | 3/2/2004 |
| 10 | POR006 | Chesterton, IN | 41.660 | -87.051 | USGS | Medium | soft/med | 15 | 9/24/2004 |
| 11 | HTN003 | Upper peninsula, MI | 47.159 | -88.245 | USGS | High | soft to hard | 17 | 9/15/2004 |
| 12 | SYC001 | Memphis, TN | 35.195 | -89.987 | USGS | Medium | soft/med | 20 | 10/29/2003 |
| 13 | BZA001 | Freeport, TX | 28.979 | -95.285 | USGS | low(interbedded) | soft | 30 | 1/3/2006 |
| 14 | CMN002 | Rio grande valley, TX | 25.953 | -97.560 | USGS | Medium | soft | 20 | 1/14/2005 |
| 15 | LAC076 | Northridge, CA | 34.227 | -118.560 | USGS | Low | soft | 14 | 6/18/1996 |
| 16 | RCD052 | Fargo, ND | 46.471 | -96.834 | USGS | very low | very soft | 18 | 9/8/2008 |
| 17 | SCC097 | Santa Clara, CA | 37.427 | -122.041 | USGS | Low | soft | 18 | 6/26/2000 |
| 18 | Oak061 | Oakland, CA | 37.818 | -122.281 | USGS | very low | very soft | 20 | 3/30/1999 |
| 19 | SCS001 | St. Charles, MO | 38.856 | -90.212 | USGS | very high | medium | 24 | 10/6/2008 |
| 20 | BKY021 | North Charleston, SC | 33.036 | -79.736 | USGS | Low | medium | 20 | 11/14/2004 |

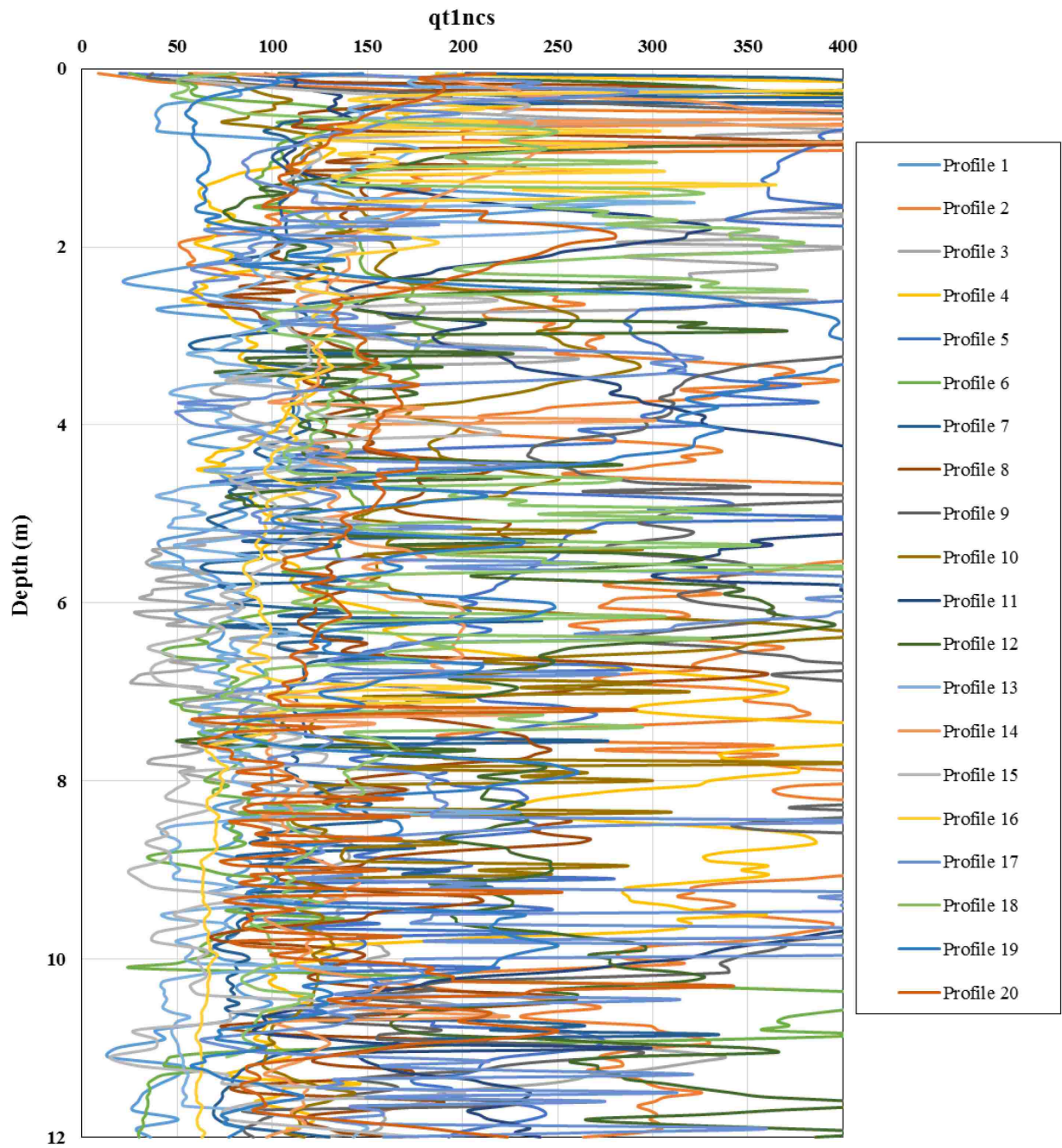**Figure 6-5: Geographical distribution of CPT profile used in study.**

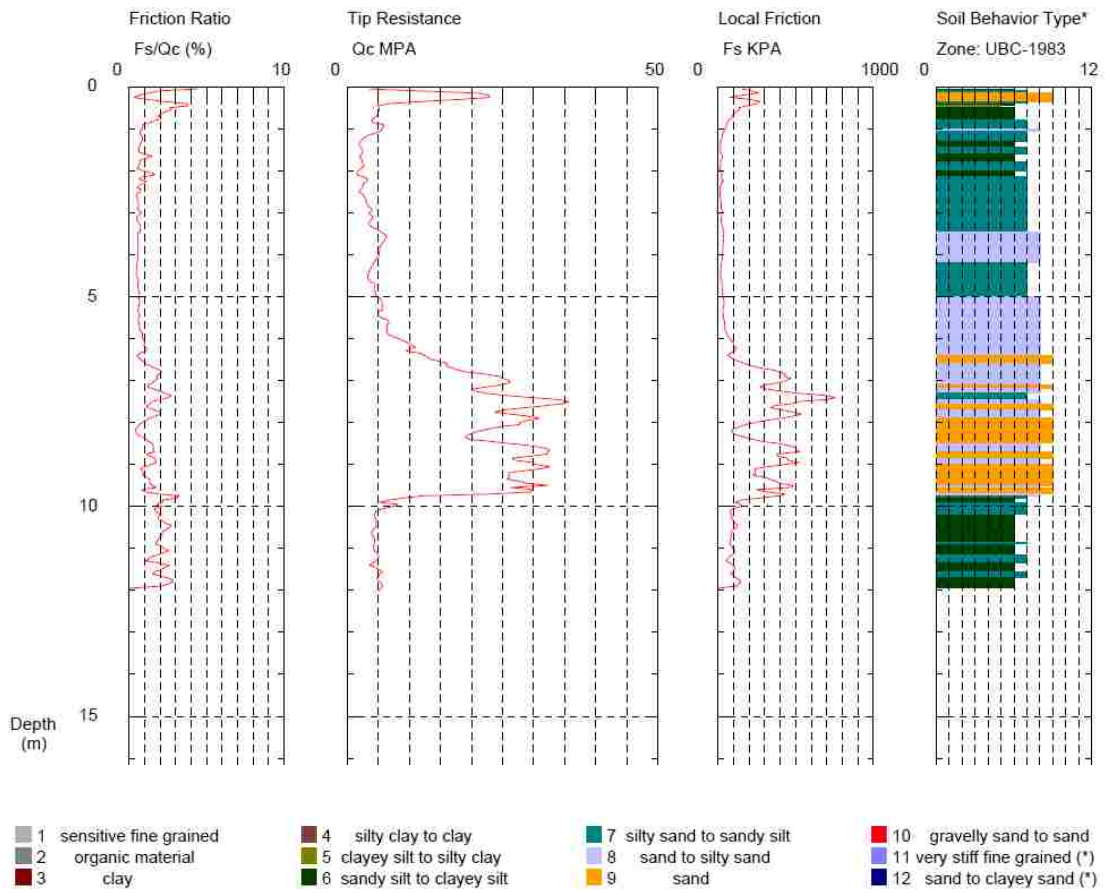**Figure 6-6: Range of** $q_{t1Ncs}$ **values represented by 20 soil profiles used in study.**

**Figure 6-7: Example of CPT data obtained from USGS CPT Database (Profile 4.).**

# 7    RESULTS OF COMPARITIVE STUDY

The comparison of the conventional pseudo-probabilistic and performance-based liquefaction triggering methods is useful when considering the difference between design values that are currently computed by engineers and researchers relating to liquefaction triggering hazards. A comparison of CPT-based methods has up to this point not been considered because of the lack of an established performance-based procedure that incorporates CPT data. This thesis has presented a new performance-based procedure to allow this comparison. In this comparison, both mean and modal values were obtained from a PSHA for use the pseudo-probabilistic method.

It is also useful to briefly compare the two new performance-based liquefaction triggering models to each other. The results of this comparison can also potentially aid engineers as performance-based methods become more widely accepted. This brief comparison of performance-based results will be presented first, while the results from the comparison between conventional and performance-based methods with be discussed second.

## 7.1    Outputs of Performance-Based Analysis

The performance-based method provides an output in the form of a design hazard curve. A hazard curve can be used to analyze the site-specific liquefaction triggering hazard for a soil layer of a considered soil profile. These hazard curves can be converted into a performance-

based design soil profile, which can then be compared directly to the conventional liquefaction triggering analysis results.

### 7.1.1   Liquefaction Triggering Design Hazard Curves

The results from both performance-based models resulted in liquefaction triggering design hazard curves. These hazard curves are generally presented based on 1 of 2 parameters: factor of safety against liquefaction ($FS_L$), or CPT resistance required to resist liquefaction ($q_{req}$), these hazard curves are created for each depth measurement from a CPT sounding. An example of each of these hazard curves can be seen in figures 7-1 and 7-2.

Hazard curves for $FS_L$ tend to have a similar appearance to those seen in figure 7-1. As the mean annual rate of exceedance (inverse of return period) decreases, the factor of safety against liquefaction will decrease. This occurs because lower annual rates of exceedance correlate with stronger earthquake events, which are more likely to initiate liquefaction. For hazard curves plotting $q_{req}$ (figure 7-2), this trend is reversed, as greater values of $q_{req}$ correlate with decreasing annual rates of exceedance. This occurs because for larger earthquake events (smaller annual rate of exceedance) a larger value of CPT cone tip-resistance is required to prevent liquefaction from being triggered.

In general, the Boulanger and Idriss model (2014) appears to give smaller values for $FS_L$ when compared to the Ku et. al (2012) model. Also, the difference between the two models increases at higher return periods. The only exception to this is at the very top of the hazard curve (low return periods, i.e. 100 years). This trend was consistent throughout all profiles and locations. The soil layer presented in Figure 7-1 would likely be classified as very liquefiable,

seeing as the values for $FS_L$ interpolated from either curve at the 475 year return period are significantly less than $FS_L = 1$, which represents the expected boundary between liquefied and non-liquefied behavior.
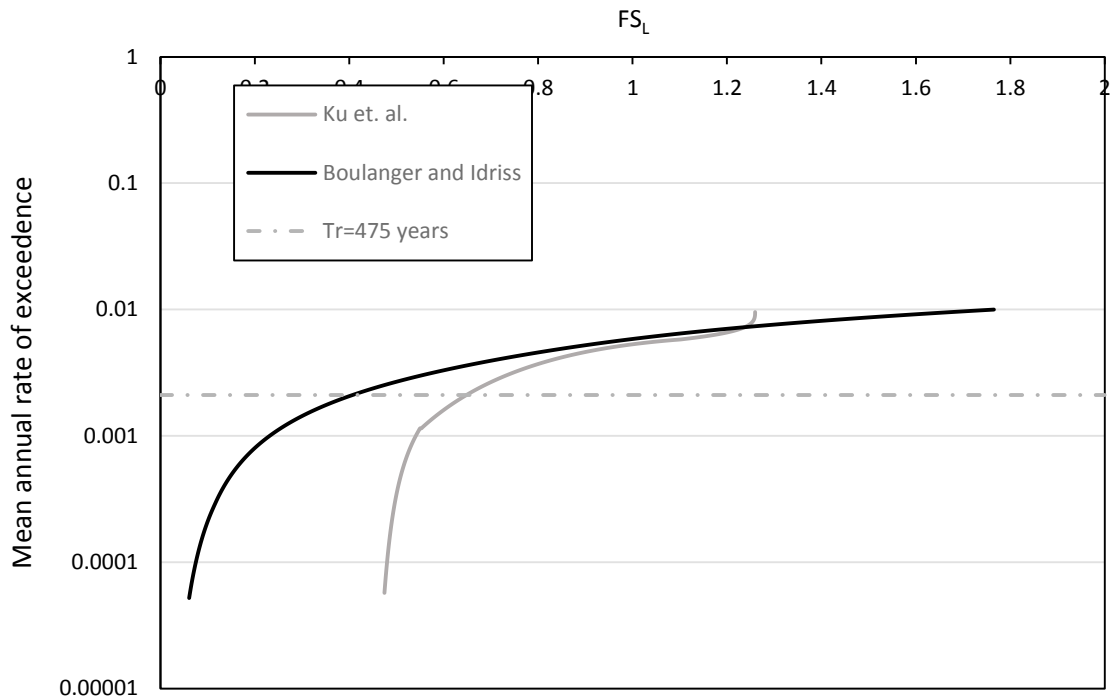


**Figure 7-1: Example hazard curve output for $FS_L$ (profile 6, layer 150, Salt Lake City).**

When comparing the two models in the realm of $q_{req}$, a similar trend is produced. Throughout all ranges of conditions and return periods, the Ku et. al. (2012) results consistently give slightly smaller values than Boulanger and Idriss (2014) for $q_{req}$. In other words, the Ku et. al. (2012) model will most always predict that less soil stiffness will be required to resist liquefaction than the Boulanger and Idriss (2014) method will predict. Figure 7-2 shows that in this situation, both methods predict that at a return period of 475 years ($T_R = 475$) the required

stiffness of the profile must be about 125 to 140 $q_{c1Ncs}$ respectively to resist the occurrence of liquefaction.
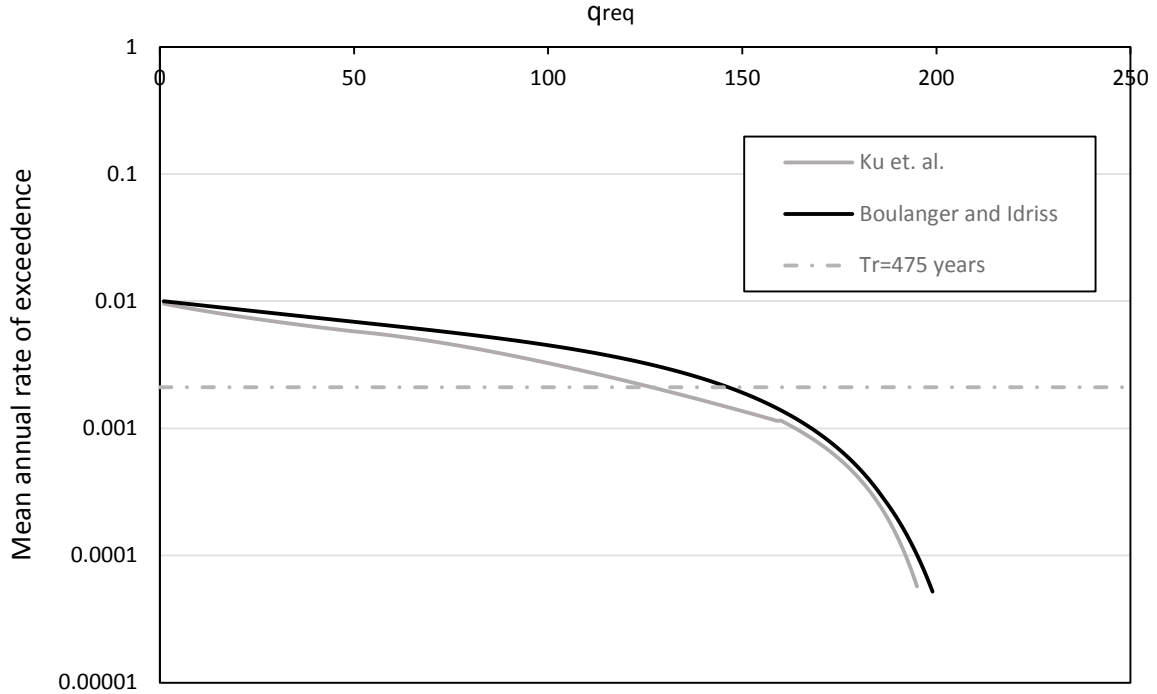


**Figure 7-2: Example Hazard curve output for $q_{req}$ (profile 6, layer 150, Salt Lake City)**

### 7.1.2  Factor of Safety Profiles

When considering the hazard curves created by the CPT performance-based analysis for each soil layer, it is possible to create a continuous soil profile relating to a liquefaction design parameter at a certain return period of interest (i.e. 475 years). Because of their common use in conventional engineering practice, soil profiles for $FS_L$ vs. depth were created from the output files of CPTLiquefY. Figure 7-3 presents an example of a factor of safety against liquefaction profile. The analysis of these profiles allows other trends to be found from these data. To provide further clarification, the CPT soil behavior type profile is provided on the right side of

Figure 7-3.  Below the figure a legend describing which colors represent which soil types is given.

Figure 7-3 further describes some of the trends discussed previously when looking at the factor of safety hazard curves for the two models.  The plot below represents a moderately stiff profile, profile 6 at a low seismicity site, Butte, Montana.  The results show that in this case the Boulanger and Idriss (2014) model (yellow) will generally predict lower $FS_L$ values than the Ku et. al. (2012) model (green) except for where the $FS_L$ is greater than about 1 to 1.5.  In general engineers are most concerned with values that represent $FS_L$ less than 1, so for critical values of $FS_L$, the Boulanger and Idriss (2014) model can generally be considered as more conservative than the Ku et. al. (2012) model.

It can be also noted how the $FS_L$ profiles shift left at higher return periods (from the 475 to 2475 year return period).  This can be attributed to the greater seismic loading expected at a larger return period.  With a greater seismic loading the CSR will rise, causing a decrease in the value of $FS_L$.  This increased seismic loading would be more likely to cause a condition of $FS_L$ less than 1, thus increasing the likelihood of liquefaction initiation.  Also, it can be noted that the difference between the two models appears to be greater at higher return periods than at lower return periods.  Although the study for this thesis did not find a reason for the difference between the models being greater at larger return periods, it would seem plausible that this is caused by the conservative nature of some of these models relative to one another.
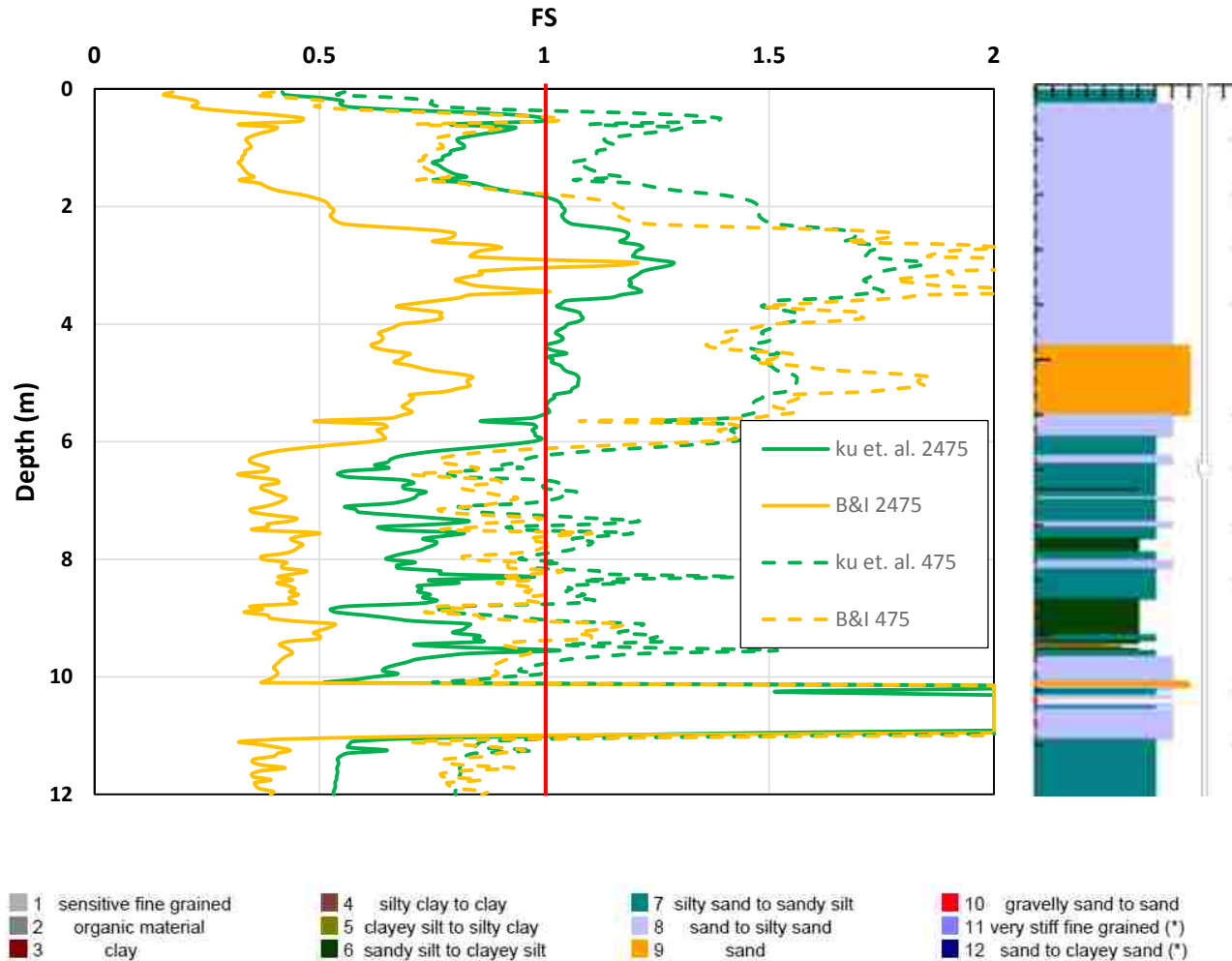
**Figure 7-3: Comparison of results from performance-based liquefaction analysis (Butte, MT., Profile 6, return periods of 475 and 2475 years).**

## 7.2 Outputs from Conventional Pseudo-Probabilistic Analysis

Unlike the performance-based analysis, a conventional liquefaction triggering analysis does not produce hazard curves. The results of this analysis simply provide a soil profile relating an engineering design parameter (generally $FS_L$) vs. depth. These profiles correlate with a certain return periods based on the input values that were chosen from the PSHA. In this study, the return periods of interest used were the same as used in the performance-based analysis (i.e.

475, 1039, 2475 years). Figure 7-4 is an example of an output profile from a conventional liquefaction triggering analysis using profile 2. As seen below, this profile is in a comparable format to the completed performance-based results discussed in 7.1.2. This conformity allows for a direct comparison between the results of the different methods.
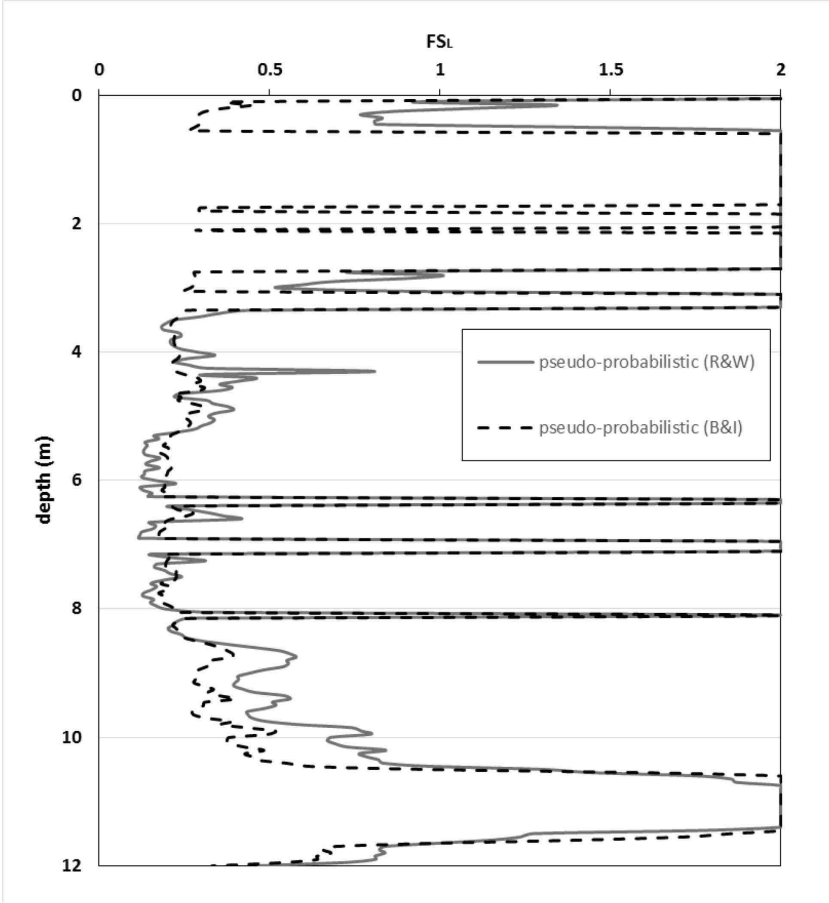


**Figure 7-4: Example results from conventional pseudo-probabilistic liquefaction triggering analysis.**

## 7.3    Comparison of Performance-Based Models

To compare the two models over a larger range of conditions, an analysis was completed comparing the results from all 20 profiles at the 10 different sites. Results are presented in

Figure 7-5. From the results, several observations can be made. First, the Ku et. al. (2012) model will almost always predict higher values for $FS_L$ if the computed $FS_L$ is less than one. For values of $FS_L$ greater than one, it becomes much more likely that the computed $FS_L$ from each model could be similar, or the Boulanger and Idriss (2014) model could predict larger values. Also, on this plot many points can be seen on the $FS_L = 2$ line; this is caused by a limit was placed at this value, at which value of $FS_L$ a soil is usually considered not liquefiable. Without the application of this limit the trends seen in this plot continue beyond the values shown.
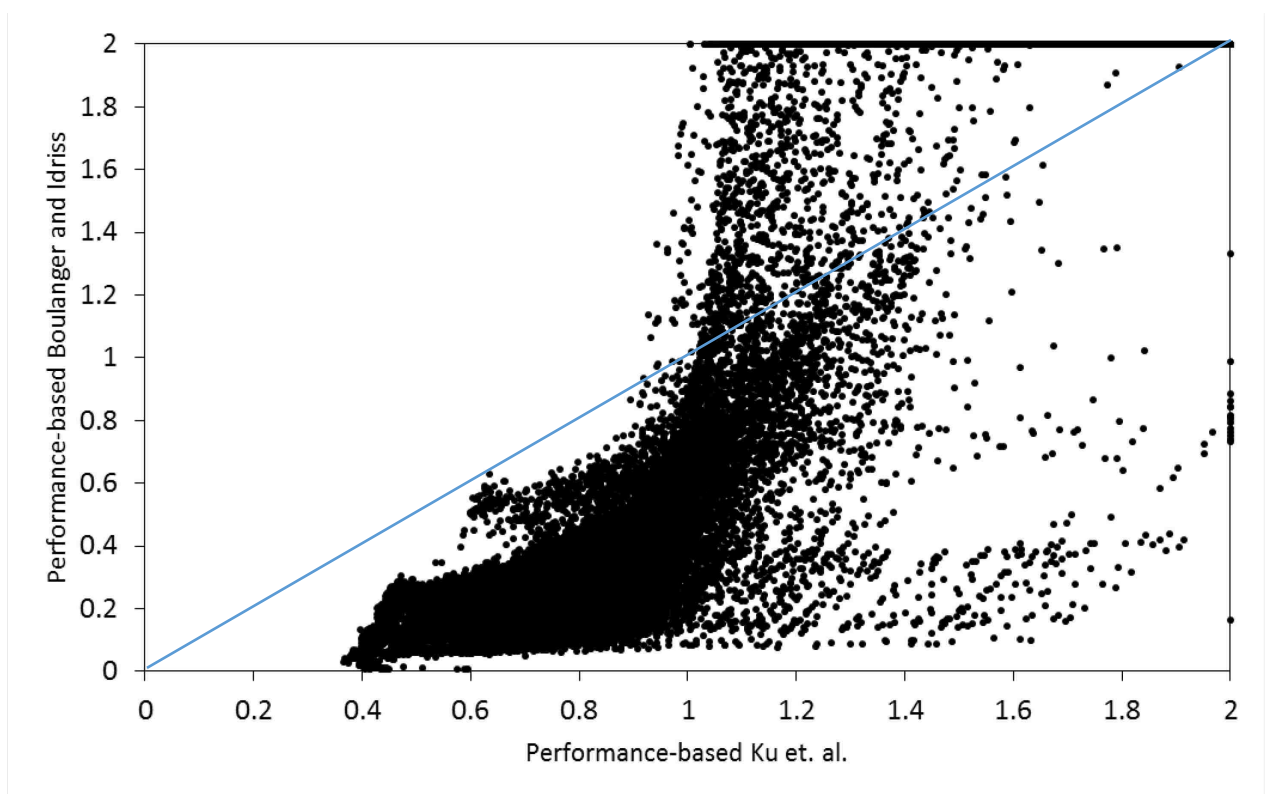


**Figure 7-5: Comparison of $FS_L$ for both performance-based models ($T_R = 1039$).**

### 7.3.1 Variation of Factor of Safety between Sites

To better see the effect of individual factors on the computed $FS_L$ values in each performance-based model, an analysis can be conducted using the results of one profile and all 10 sites. To obtain a wide range of $FS_L$ values to consider, a moderately liquefiable profile was chosen for this example. The results are presented below. The results from this analysis are that low seismicity sites such as Butte resulted in higher factors of safety for both models, and high seismicity sites such as Eureka had the lowest values for factor of safety for both models as well. Interestingly, the difference between the two models appear to be much greater at low values of $FS_L$. This is likely caused by the tendency of the Boulanger and Idriss (2014) model to predict significantly smaller factors of safety than the Ku et. al (2012) model for values less than $FS_L =$ 1. The results in Figure 7-7 and Figure 7-8 are for return periods of 1039 and 2475 years respectively. The data shifts notably downward as the return period increases. Also, data scatter appears to increase as the factor of safety increases.
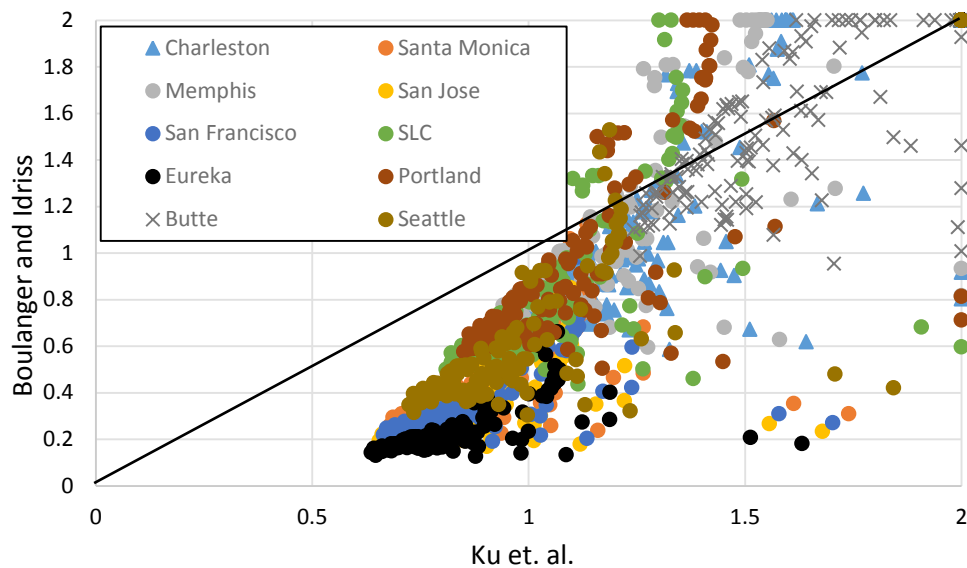


**Figure 7-6:** $FS_L$ **results for profile 14 at** $T_R = 475$ **years.**
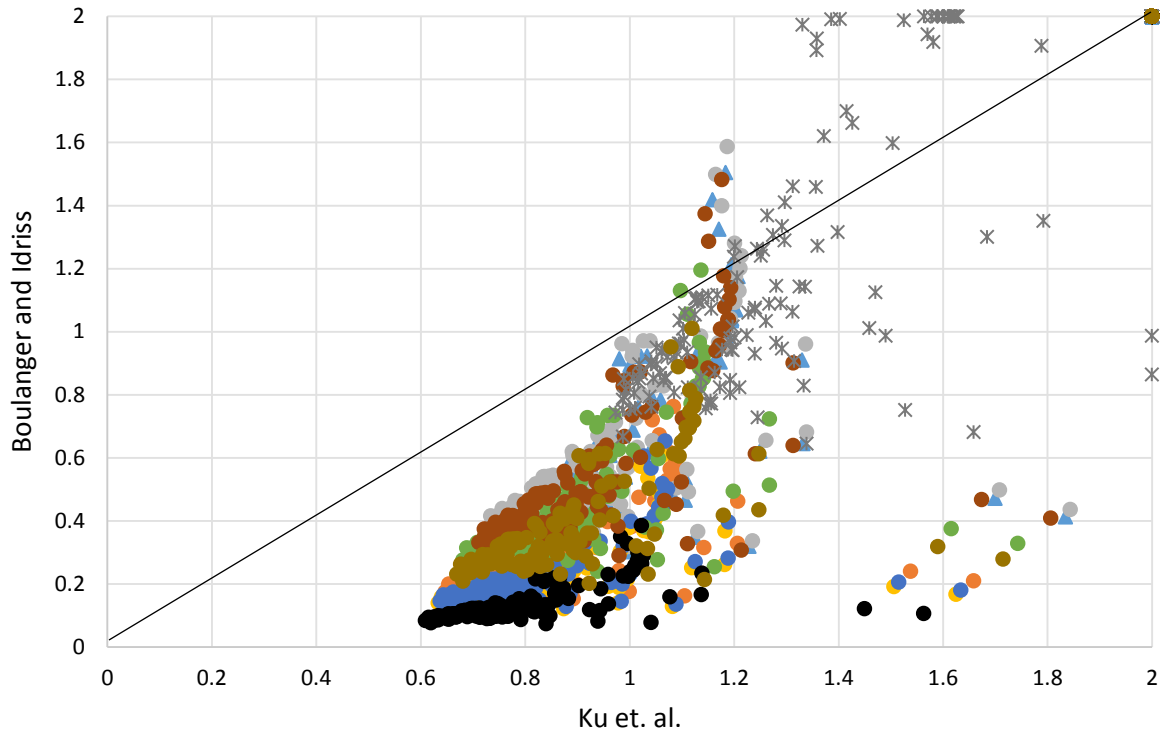
**Figure 7-7:** $FS_L$ results for profile 14 $T_R = 1039$ years.
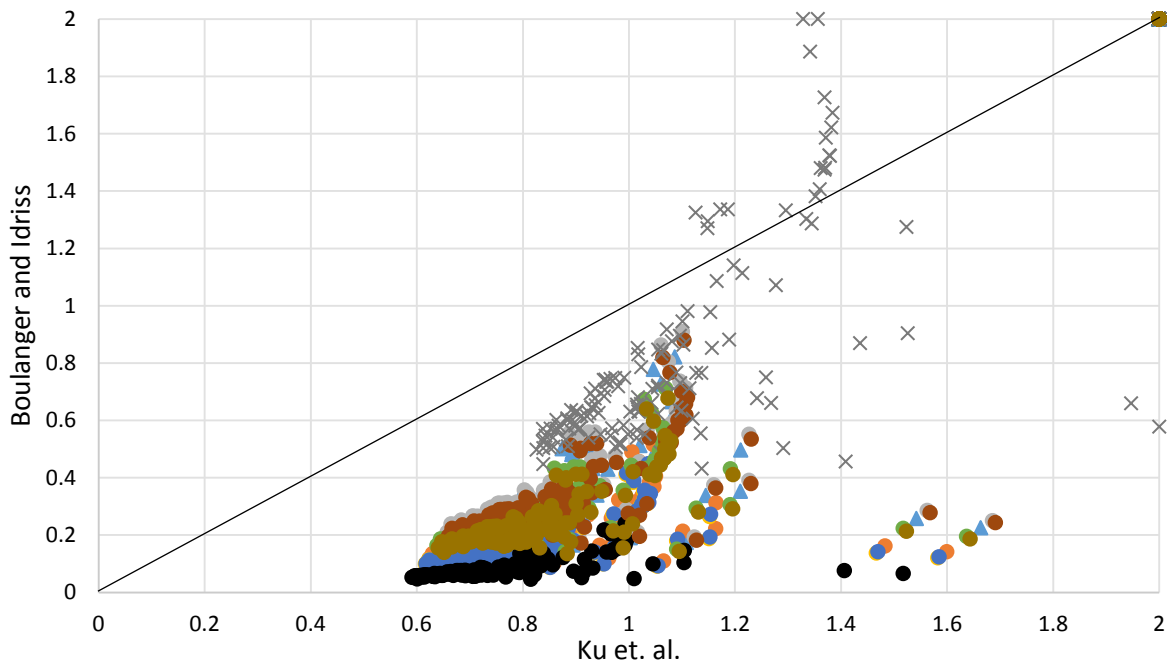


**Figure 7-8:** $FS_L$ results for profile 14 $T_R = 2475$ years.

**7.3.2 Variation of Factor of Safety for Different Return Periods**

As suggested previously, the effect of different return periods appears to have a measurable effect on the comparison of the two performance-based methods. To more clearly show this difference, a plot of one soil profile at a moderate seismicity site (Salt Lake City) is shown in Figure 7-9. As seen below, as the return period increases, the values drift farther from the 1:1 line, which represents where the two models would calculate identical results. This can be explained by the tendency of the Boulanger and Idriss (2014) model to predict significantly smaller values for $FS_L$ if $FS_L$ is less than 1, while predicting similar or even greater values if $FS_L$ is greater than 1.
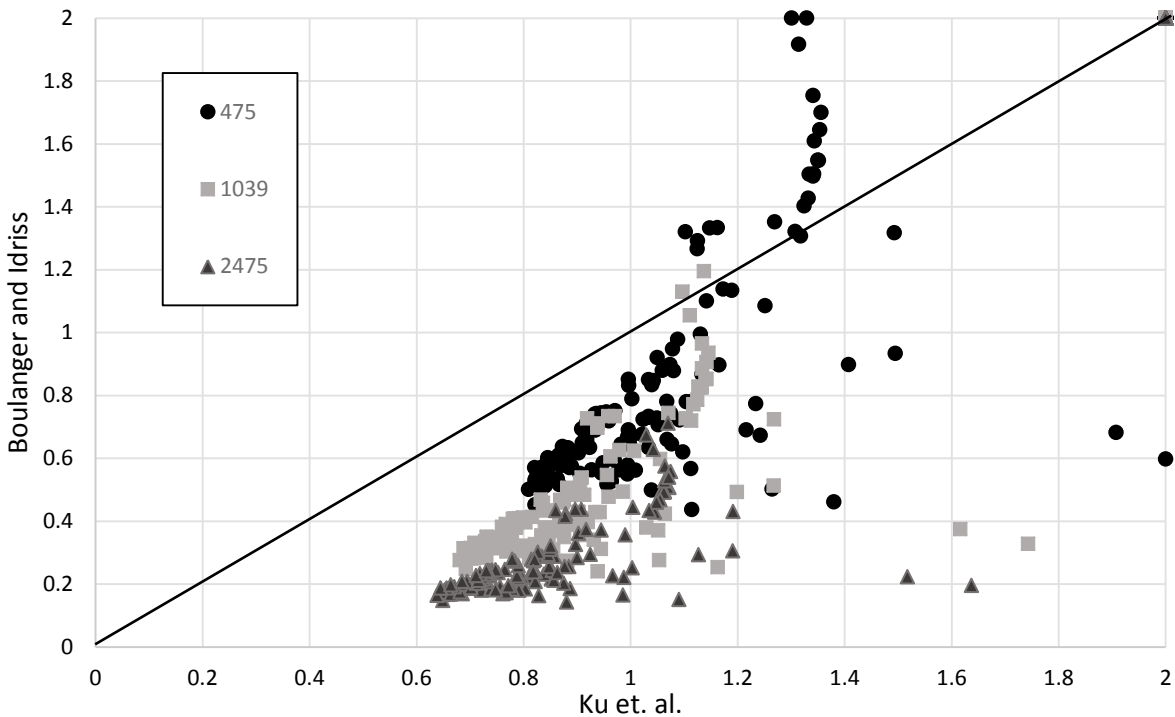


**Figure 7-9: Comparison of $FS_L$ for 3 different return periods (profile 14, Salt Lake City).**

**7.4    Comparison of Conventional Pseudo-Probabilistic and Performance-Based Methods**

A comparison of the conventional pseudo-probabilistic and performance-based results from this study is helpful in comparing the difference between engineering design values currently calculated by practicing engineers, and engineering design values calculated from a performance-based design method. The presentation of the results somewhat mirrors the process used by Wright (2013) in the analysis of SPT performance-based methods compared to conventional SPT liquefaction analysis methods. The pseudo-probabilistic results in this section were computed from a PSHA using either mean or modal values. All 20 CPT profiles and all 10 sites discussed previously were included in the body of the data to show trends from a wide range of conditions.

The following results are displayed in a scatter plot format with conventional values on the y-axis and performance-based values on the x-axis. If the two methods were to compute identical values, the data points would fall directly on the 1:1 line (blue) displayed in the following figures. Lines at the value which divide predicted liquefied and non-liquefied behavior ($FS_L = 1$) (red) are drawn from each axis on the plot to divide the plot into 4 quadrants (Figure 7-10). The four quadrants are defined as:

1.   Top Left- The performance-based method predicts liquefaction, the pseudo-probabilistic method does not

2.   Top Right- The performance-based method and pseudo-probabilistic method both predict no liquefaction.

3.   Bottom Left- The performance-based method and pseudo-probabilistic method both predict liquefaction.

4. Bottom Right- The performance-based method predicts no liquefaction, while the pseudo-probabilistic method predicts liquefaction.
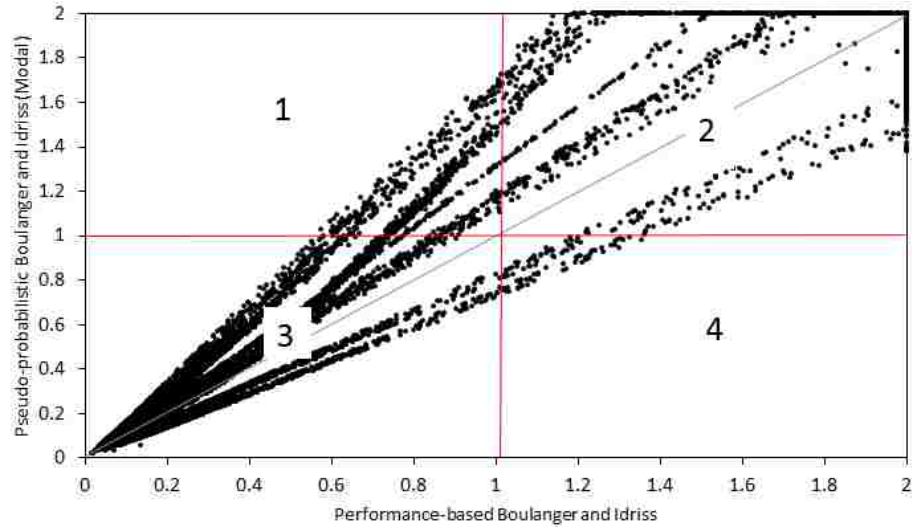


**Figure 7-10: Location of 4 quadrants on an example plot.**

### 7.4.1 Robertson and Wride (Conventional) vs. Ku et. al. (Performance-Based)

The results of the comparison between the Robertson and Wride pseudo-probabilistic and the Ku et. al. performance-based can be seen from Figure 7-11 to Figure 7-16. These figures illustrate that for $FS_L$ values less than 1, the conventional method generally predicts smaller values of $FS_L$ when compared to the performance-based method. However, it appears that most of the plotted points from the full comparison lie in quadrants 2 and 3, indicating a common prediction on whether liquefaction is expected to occur. The statistical distribution of the points will be discussed later in this chapter.

These plots also appear to show that for values of $FS_L$ greater than 1, the conventional method will generally give higher values for $FS_L$ than the performance-based method. This

121

could be significant if a different value of $FS_L$ is used as the boundary between liquefied and non-liquefied behavior (ex. $FS_L = 1.2$). In that case, the distribution of data in each quadrant would change. Differences between the mean and modal methods appears to be limited to small shifts of the trends to the left or right caused by values obtained from the PSHA (low seismicity shifts left for modal, high seismicity shift right for modal.) From observation of the figures, it also appears that the data tends to aggregate in bands based on the seismic loading at the different locations used in the analysis.
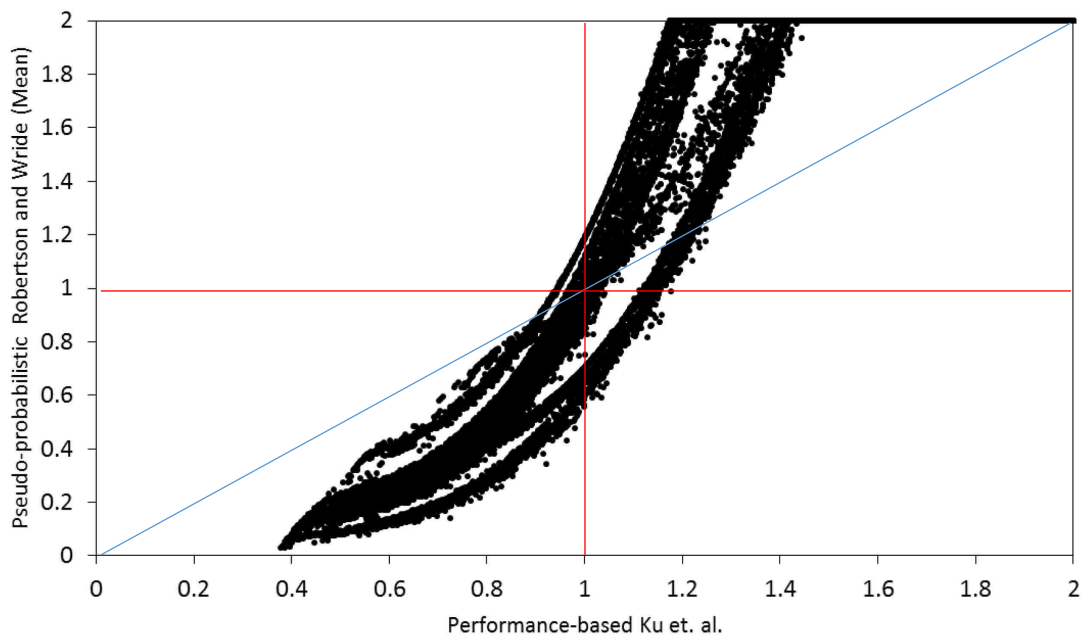


**Figure 7-11: Comparison of $FS_L$ from Robertson and Wride conventional (Mean) and Ku et. al. performance-based approaches, $T_R = 475$ years.**
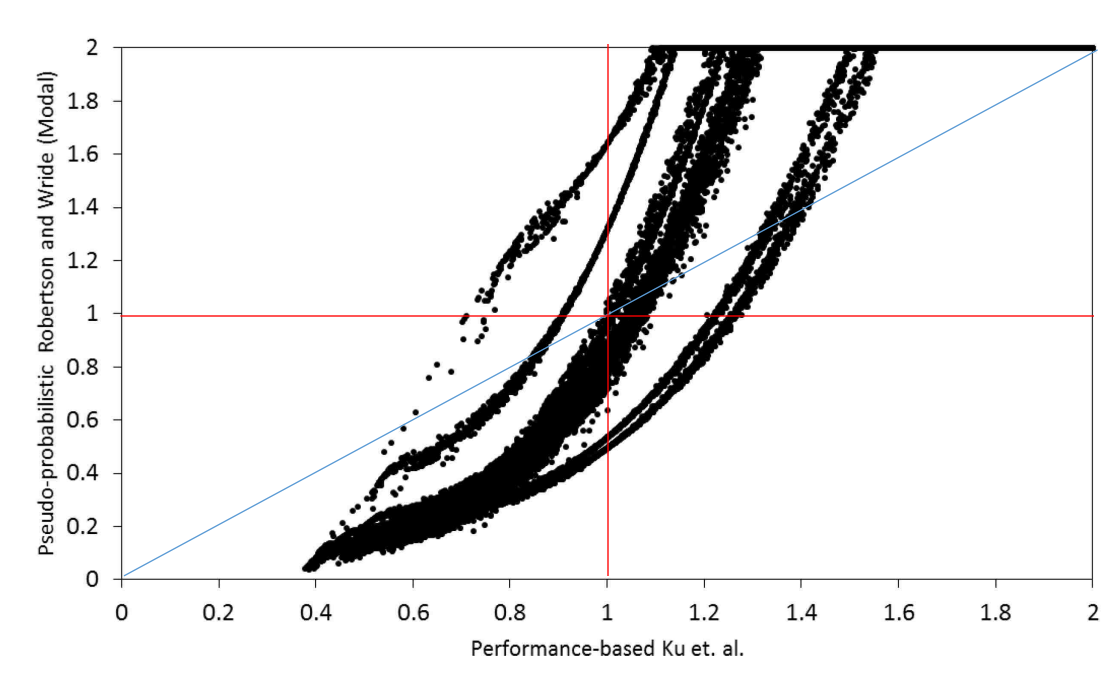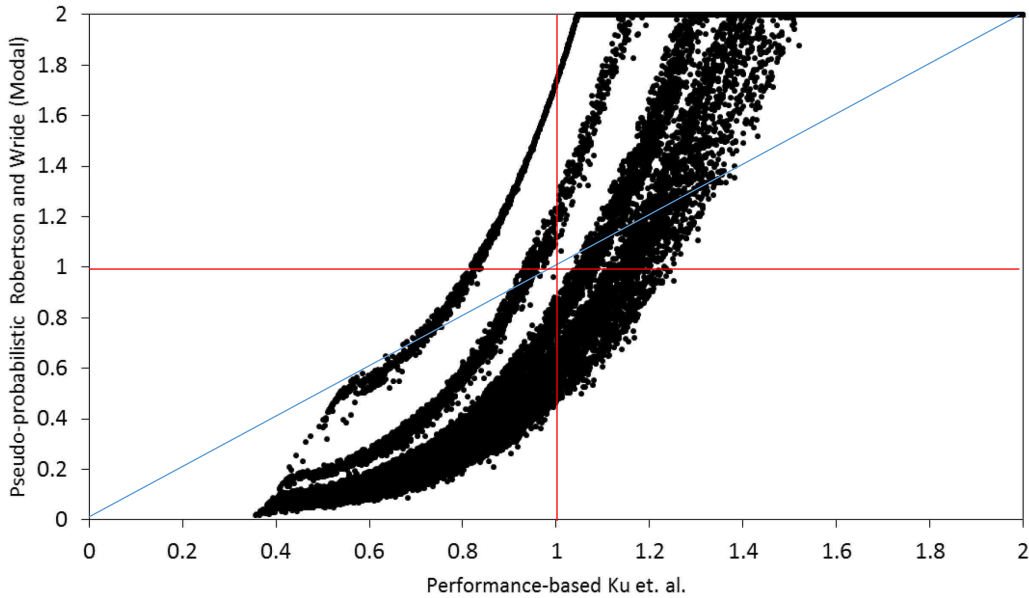
**Figure 7-12: Comparison of** $FS_L$ **from Robertson and Wride conventional (Modal) and Ku et. al. performance-based approaches,** $T_R$ **= 475 years.**
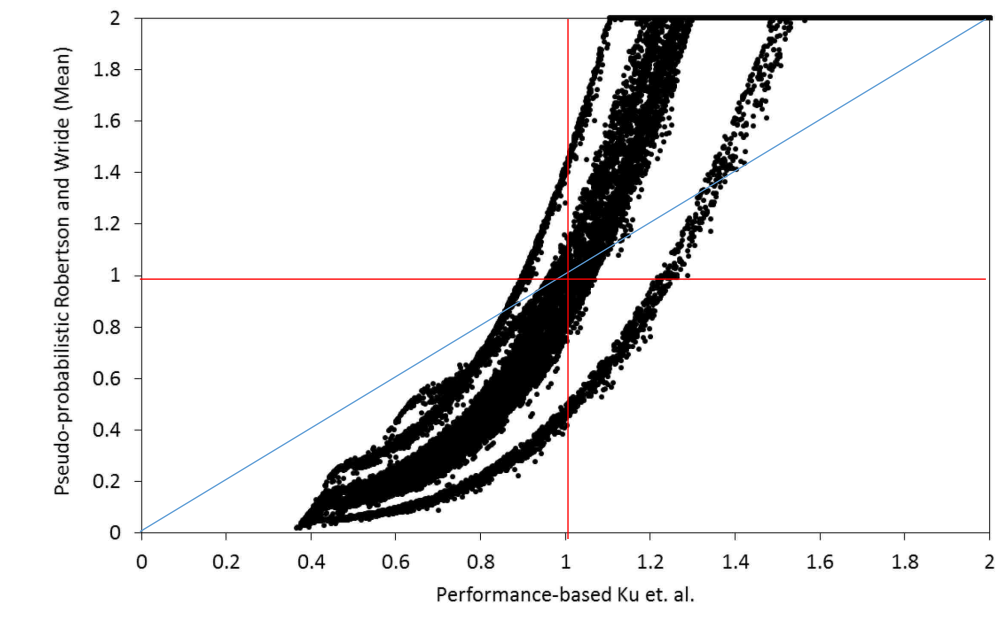


**Figure 7-13: Comparison of** $FS_L$ **from Robertson and Wride conventional (Mean) and Ku et. al. performance-based approaches,** $T_R$ **= 1039 years.**
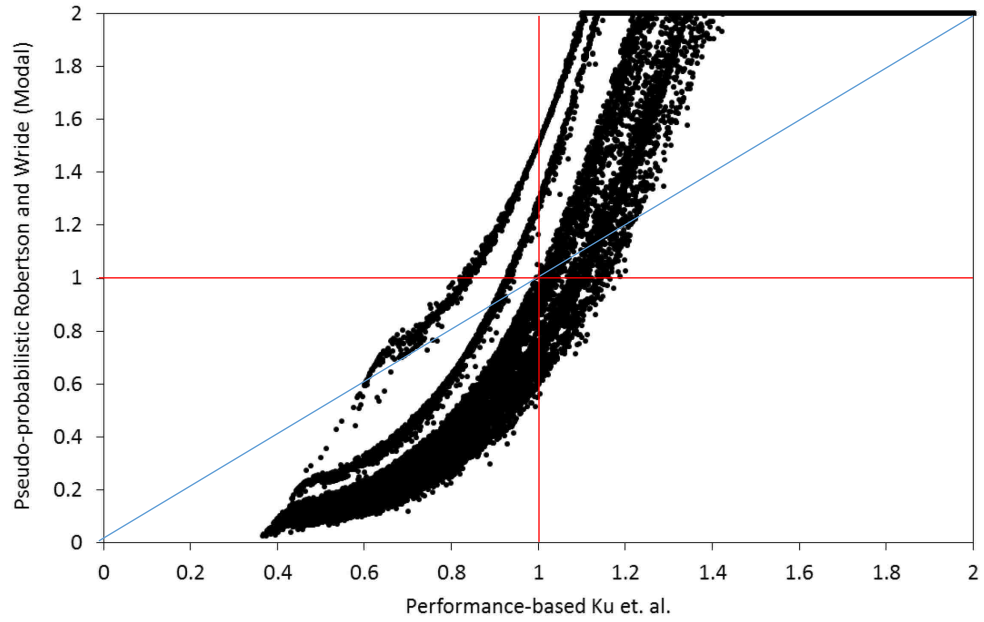
**Figure 7-14: Comparison of** $FS_L$ **from Robertson and Wride conventional (Modal) and Ku et. al. performance-based approaches,** $T_R$=1039 **years.**
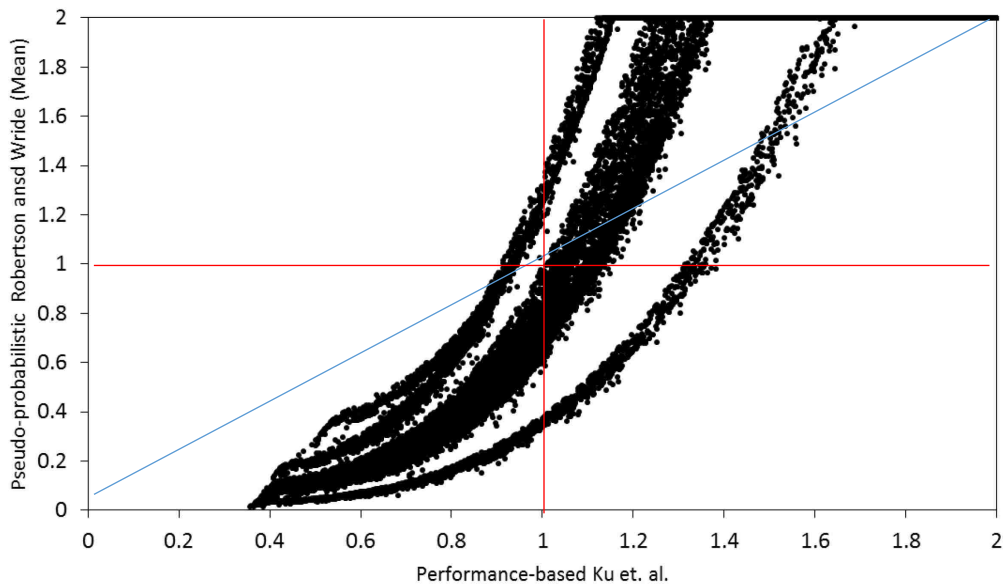


**Figure 7-15: Comparison of** $FS_L$ **from Robertson and Wride conventional (Mean) and Ku et. al. performance-based approaches,** $T_R$ = 2475 **years.**

**Figure 7-16: Comparison of** $FS_L$ **from Robertson and Wride conventional (Modal) and Ku et. al. performance-based approaches,** $T_R$ **= 2475 years.**

### 7.4.2 Boulanger and Idriss (Conventional) vs. Boulanger and Idriss (Performance-Based)

The trends noted in the comparison of the Boulanger and Idriss methods are somewhat different than those from the previous methods. While the previous comparisons showed a curved relationship, these results in Figure 7-17 to Figure 7-22 show a more linear relationship. Because of the generally linearity of the relationship, the results from the conventional analysis will generally either predict higher values for $FS_L$ for most all possible values of $FS_L$, or predict lower values of $FS_L$ for all possible values of $FS_L$. Although few of the predictions line up with the 1:1 line, relatively few data points seem to appear in quadrants 1 or 4, which represent a different prediction of liquefaction triggering between the methods. A statistical representation of this will be presented in the next section.

Similarly to the previous comparison, the results are seen to be separated into bands relating to the location of each analysis. Another interesting observation from this comparison is that data scatter seems to increase when using modal values instead of mean values for the pseudo-probabilistic analysis. Uniquely, this comparison showed divergent behavior, in that the comparison between the conventional and performance-based methods are very close at very low values of $FS_L$ but the predictions are farther apart at larger at values of higher $FS_L$. Of particular interest are values close to $FS_L = 1$. It is at $FS_L = 1$ that the conventional and performance-based methods would disagree in this particular analysis. It can be seen that at $FS_L = 1$ there is a significant difference between the methods, unlike at $FS_L = 0.2$ where the methods are in almost total agreement, but where liquefaction is essentially assured. Based on these results, it would be expected that during a statistical analysis there would be some degree of disagreement between the methods on the prediction of liquefaction initiation.
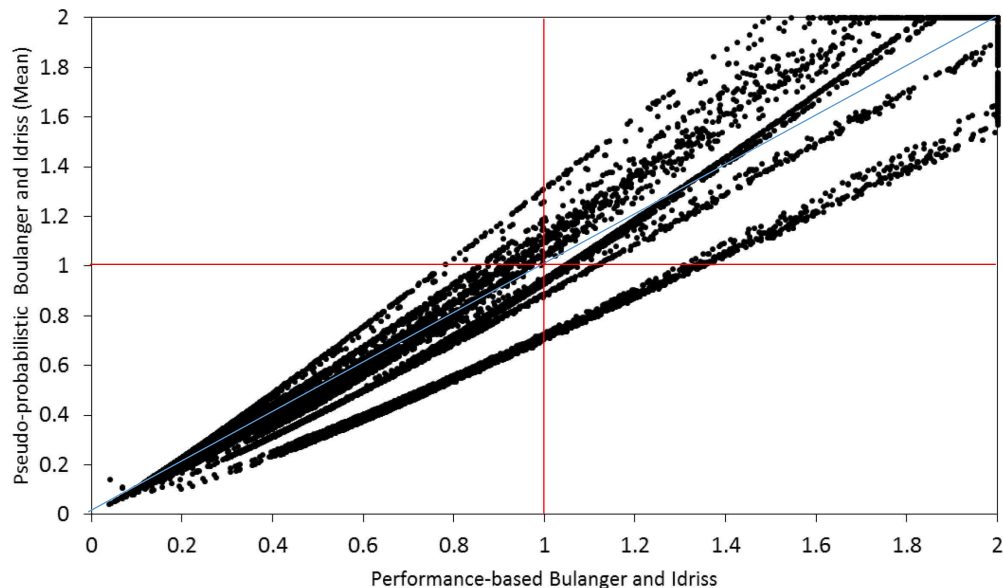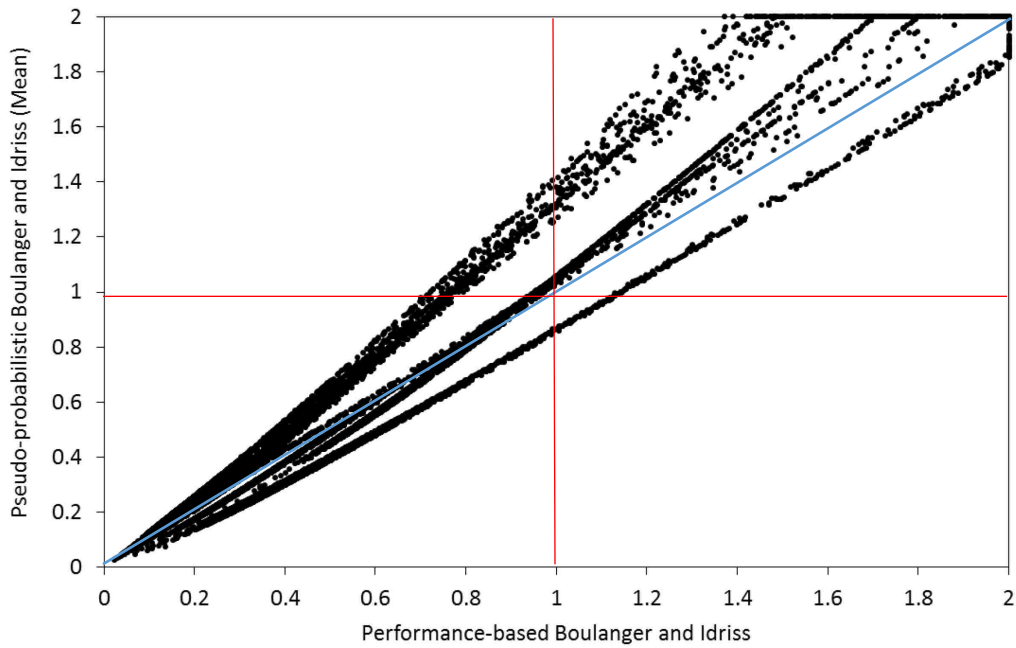


**Figure 7-17: Comparison of $FS_L$ for Boulanger and Idriss conventional (Mean) and performance-based approaches, $T_R = 475$ years.**
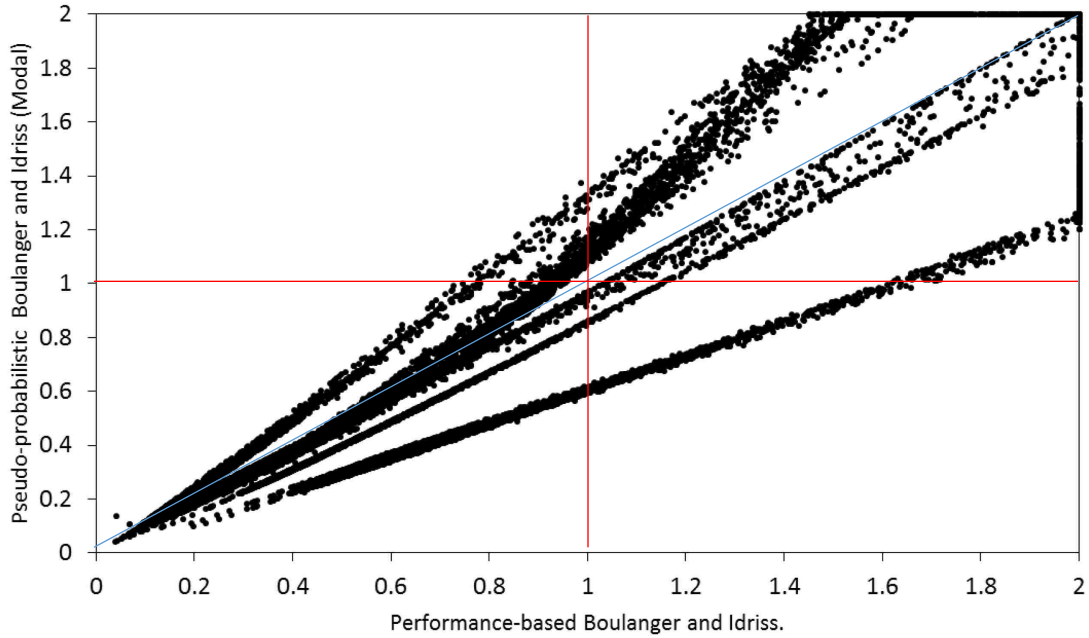
**Figure 7-18: Comparison of** $FS_L$ **for Boulanger and Idriss conventional (Modal) and performance-based approaches,** $T_R = $ **475 years.**
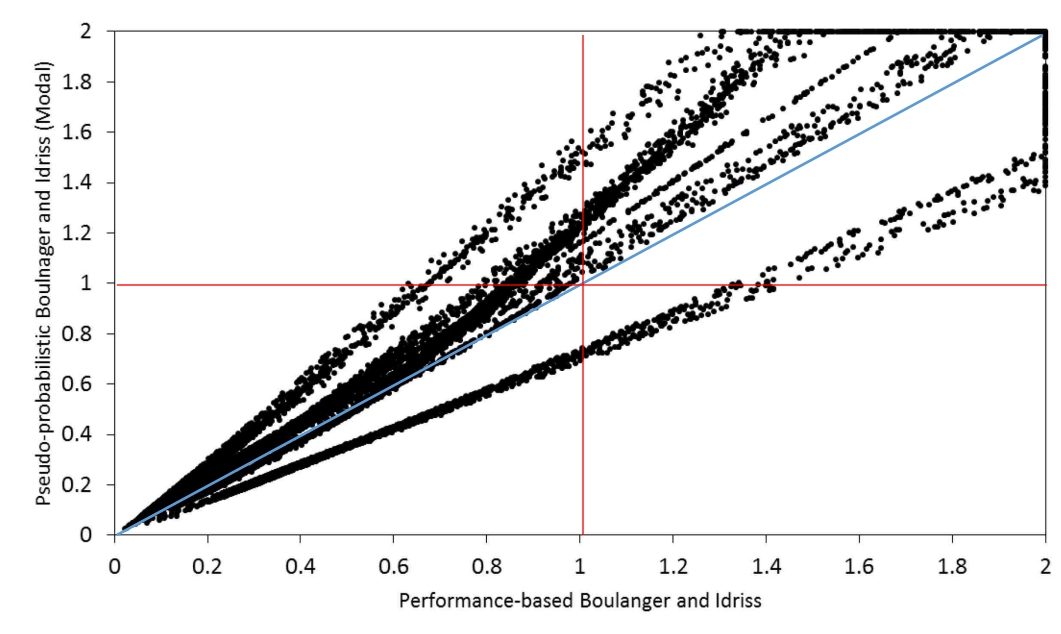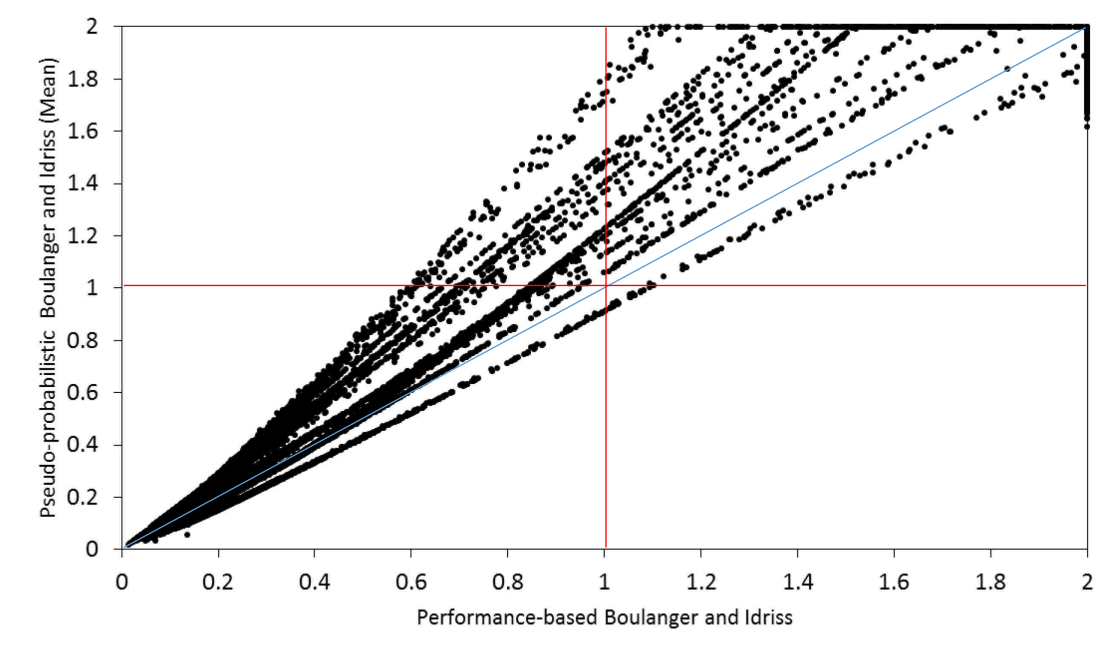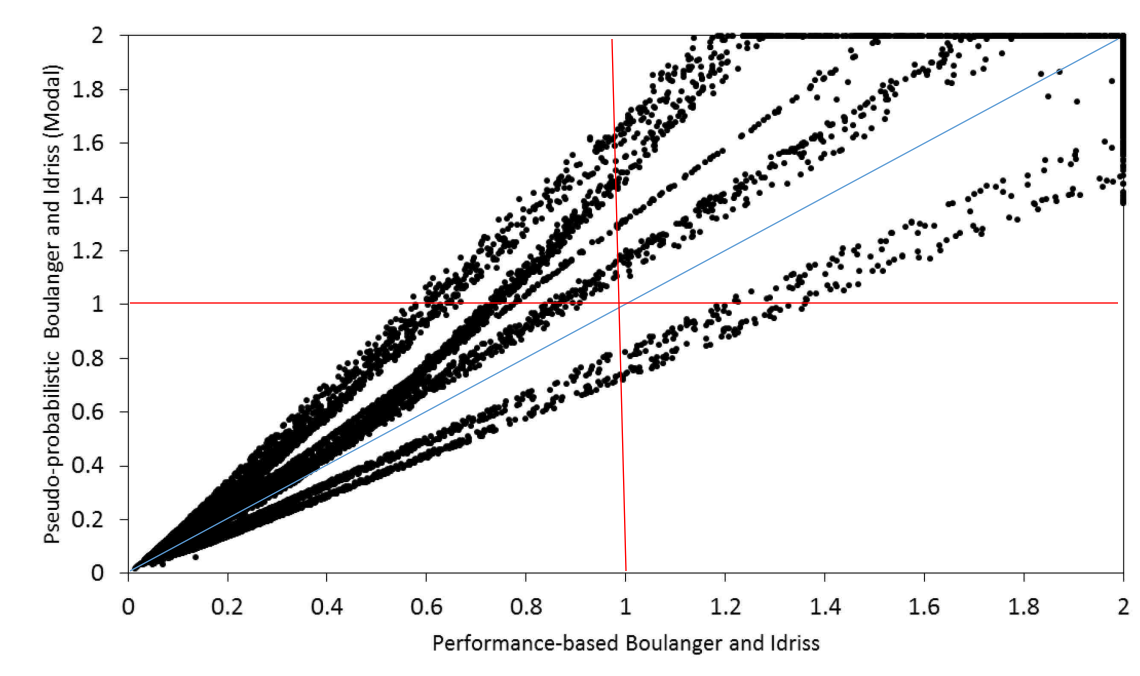


**Figure 7-19: Comparison of** $FS_L$ **for Boulanger and Idriss conventional (Mean) and performance-based approaches,** $T_R = $ **1039 years.**

**Figure 7-20: Comparison of** $FS_L$ **for Boulanger and Idriss conventional (Modal) and performance-based approaches,** $T_R = 1039.$



**Figure 7-21: Comparison of** $FS_L$ **for Boulanger and Idriss conventional (Mean) and performance-based approaches,** $T_R = 2475.$

**Figure 7-22: Comparison of $FS_L$ for Boulanger and Idriss conventional (Modal) and performance-based approaches, $T_R$ = 2475.**

## 7.5 Summary of Comparisons of Methods

A brief statistical analysis of the distribution of the liquefaction triggering data in each of the four defined quadrants was conducted. A total of 45,590 different liquefaction triggering predictions were analyzed from each of the plots in the previous sections. The results of this analysis can be viewed in tables 7-1 through 7-6.

These results suggest that the performance-based and conventional liquefaction triggering analysis methods agree on the prediction of liquefaction triggering around 95% to 99% of the time. The comparison of the Robertson and Wride pseudo-probabilistic vs. the Ku et. al. performance-based method showed that about 2 to 4 % of the time the performance-based method predicted the non-occurrence of liquefaction, while the pseudo-probabilistic predicted liquefaction to occur. Conversely, generally less than 1% of the cases represented predictions of

non-liquefaction by the pseudo-probabilistic method and liquefaction by the performance-based method. These values were fairly constant across the different return periods analyzed as well as when mean or modal values were used in the pseudo-probabilistic analysis.

The Boulanger and Idriss comparison values had a smaller percentage of points in quadrants 1 and 4 (different liquefaction triggering predictions). At low return periods, the performance-based method predicted non-liquefaction while the conventional method predicted liquefaction about 1.5 percent of the time. This value drops to well below 1 percent for higher return periods. Trends for the opposite prediction (pseudo-probabilistic predicts non-liquefaction and performance-based predicting liquefaction), followed a similar trend but in the opposite direction (percentage increase from low to high return periods).

**Table 7-1: Percentage data in each quadrant Robertson and Wride vs. Ku et. al. $T_R = 475$ years.**

| Robertson and Wride vs. Ku et. al. | | | |
|---|---|---|---|
| 475 | | | |
| Mean | | Modal | |
| 0.54% | 71.08% | 1.02% | 69.52% |
| 26.02% | 2.36% | 25.54% | 3.92% |

**Table 7-2: Percentage data in each quadrant Robertson and Wride vs. Ku et. al. $T_R = 1039$ years.**

| Robertson and Wride vs. Ku et. al. | | | |
|---|---|---|---|
| 1039 | | | |
| Mean | | Modal | |
| 0.92% | 63.88% | 1.21% | 63.25% |
| 33.17% | 2.03% | 32.88% | 2.65% |

**Table 7-3: Percentage data in each quadrant Robertson and Wride vs. Ku et. al.** $T_R = 2475$ **years.**

| Robertson and Wride vs. Ku et. al. | | | |
|---|---|---|---|
| 2475 | | | |
| Mean | | Modal | |
| 0.79% | 59.17% | 1.33% | 58.61% |
| 36.67% | 3.37% | 36.13% | 3.93% |

**Table 7-4: Percentage data in each quadrant Boulanger and Idriss (conventional) vs. Boulanger and Idriss (performance-based)** $T_R = 475$ **years.**

| B&I pseudo vs. B&I performance-based | | | |
|---|---|---|---|
| 475 | | | |
| Mean | | Modal | |
| 0.35% | 63.16% | 0.79% | 62.99% |
| 35.12% | 1.38% | 34.68% | 1.55% |

**Table 7-5: Percentage data in each quadrant Boulanger and Idriss (conventional) vs. Boulanger and Idriss (performance-based)** $T_R = 1039$ **years.**

| B&I pseudo vs. B&I performance-based | | | |
|---|---|---|---|
| 1039 | | | |
| Mean | | Modal | |
| 0.83% | 59.57% | 1.04% | 59.37% |
| 39.42% | 0.18% | 39.21% | 0.38% |

**Table 7-6: Percentage data in each quadrant Boulanger and Idriss (conventional) vs. Boulanger and Idriss (performance-based) $T_R = $ 2475 years.**

| B&I pseudo vs. B&I performance-based | | | |
|---|---|---|---|
| 2475 | | | |
| Mean | | Modal | |
| 1.03% | 57.39% | 1.28% | 57.22% |
| 41.52% | 0.05% | 41.28% | 0.22% |

The significance of these results is that when setting a boundary for liquefied and non-liquefied behavior at $FS_L = 1$, on average less than 5 percent of cases will result in a different prediction of liquefaction triggering between both methods.  Although this would make it appear that in 95 percent or greater of cases that the prediction of liquefaction hazard would be the same with both the pseudo-probabilistic and performance-based methods, this is not necessarily the case.   To explain how both methods do not necessarily compute equivalent values for liquefaction hazard even when both methods predict $FS_L < 1$, a brief example is provided.

Consider the hypothetical case of a prediction of $FS_L = $ 0.9 from the performance-based method, and a prediction of $FS_L = $ 0.3 from the pseudo-probabilistic method.  In this case, both predictions would indicate liquefaction, and would thus plot in quadrant 4.  Engineers tend to treat such a situation with a binary prediction of either liquefaction or no liquefaction.  Although these values would both represent a prediction that liquefaction will be initiated, they do **not** represent the same liquefaction initiation hazard.  The binary categorization of liquefaction initiation based on $FS_L$ does not adequately provide a full interpretation of these results.  In order to compare the liquefaction triggering hazard in a more precise manner, a simple

conversion to the probability of liquefaction ($P_L$) can be made. This conversion can be done using either the Ku et. al. or Boulanger and Idriss methods by using equations (4-34), and (4-36) respectively. By using these equations, the results of the value $FS_L$ = 0.9 gives: $P_L$ = 50.4% and $P_L$ = 58.2%, while the value $FS_L$ = 0.3 gives: $P_L$ = 99.9% and $P_L$ = 99.1%. From these $P_L$ values, the actual liquefaction initiation hazard can more accurately be analyzed, as the $FS_L$ = 0.9 prediction indicates that the soil will be about as likely to liquefy as to not liquefy, while the $FS_L$ = 0.3 prediction indicates that liquefaction is almost guaranteed to occur. This example represents how the actual liquefaction hazard has potential to vary significantly between the performance-based and pseudo-probabilistic methods even when both methods appear to make an similar prediction based on $FS_L$.

To see the full effect of the conversion to the realm of $P_L$, Figure 7-23 and Figure 7-24 show examples of the comparison of $P_L$ at a return period of 475 years. In the Ku et. al. comparison, out of the 45,590 predictions, 42 percent of the performance-based values predicted a lower liquefaction hazard compared to the conventional method, while 26% percent predicted a lower hazard from the conventional method. The remainder of the values computed an equivalent hazard with both methods (usually $P_L$ = 0% or $P_L$ =100%). For the Boulanger and Idriss methods, the performance-based method predicted a lower liquefaction hazard 23 percent of the time compared to the conventional method which predicted a lower liquefaction hazard 18 percent of the time. The remainder of predictions gave equivalent values for the predicted liquefaction hazard regardless of the method used. This paints a significantly different picture than the $FS_L$ comparisons, as a much larger percentage of the analysis could potentially calculate a reduced liquefaction hazard with use of the performance-based method.
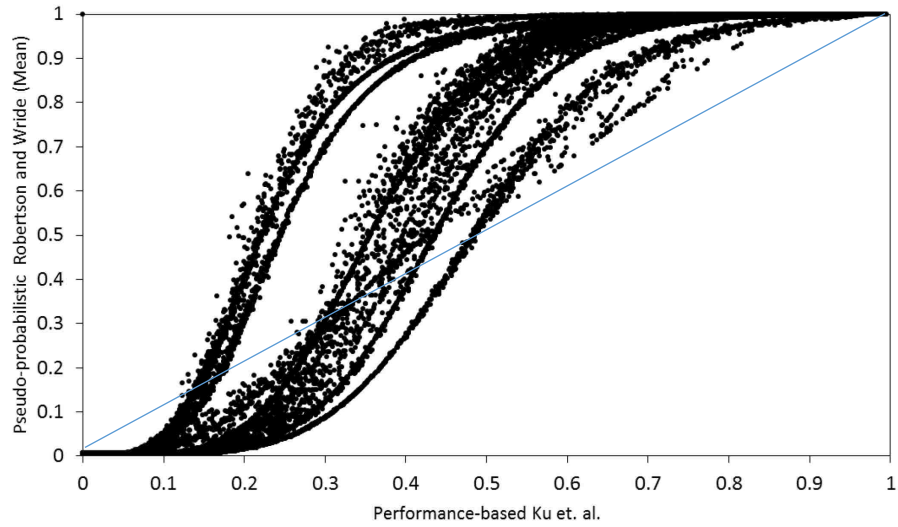
**Figure 7-23: Probability of liquefaction values from study (using Ku et. al. equation)** $T_R = 475$.
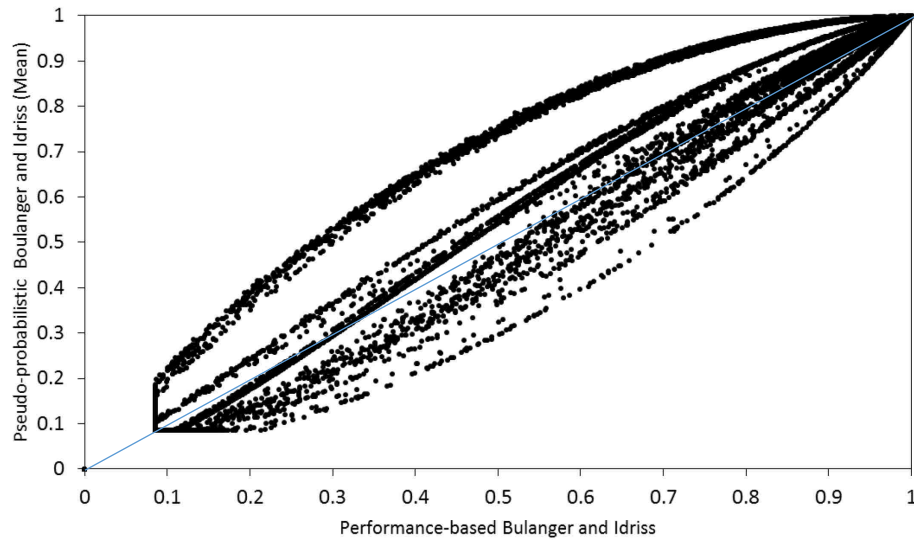


**Figure 7-24: Probability of liquefaction values from study (using Boulanger and Idriss equation)** $T_R = 475$.

Even though only a relatively small percentage of cases disagree in the prediction of liquefaction when considering $FS_L$, by looking at the $P_L$, as facilitated by a probabilistic framework, the conventional analysis on average will predict a slightly greater liquefaction hazard. This means that in many cases the conventional analysis would require a larger amount of ground improvement to bring the soil to a satisfactory state to resist liquefaction and related hazards. This also signifies the possibility that the use of a performance-based method could provide cost savings in a potential design.

# 8    CONCLUSIONS

Earthquake liquefaction is a serious hazard that is known to cause damage to buildings and infrastructure. This thesis has proposed a new performance-based liquefaction triggering procedure, and applied it to pre-existing probabilistic liquefaction triggering models for the CPT. Using numerous actual CPT soundings and cities across the U.S., comparisons were made between the results of the proposed performance-based procedure, and the pseudo-probabilistic liquefaction triggering procedure. The performance-based procedure developed herein was based on the liquefaction calculations from Ku et. al. (2012) and Boulanger and Idriss (2014) probabilistic models. Using the framework developed by Kramer and Mayfield (2007), each of the CPT-based probabilistic models were modified to be used in a performance-based manner. Uncertainty values were computed for both model and total (parameter and model) uncertainty relating to each method.

A computation tool called CPTLiquefY was developed to facilitate the calculation of the performance-based results, and to develop a comparison of conventional liquefaction analyses with the performance-based method. Due to the complexity of the calculations required for a performance-based analysis, an efficient and sophisticated free-standing computation tool was required. CPTLiquefY has the potential to be used by researchers in large comparative studies, mapping projects, and site-specific liquefaction analyses. Other useful applications of this

program include the prediction of liquefaction related hazards, such as seismically induced settlements, and lateral spreads.

The observed results from the comparison of conventional pseudo-probabilistic and performance-based liquefaction triggering procedures include:

1) The Ku et. al. performance-based model is generally less conservative (yields a higher factor of safety) than the conventional Robertson and Wride approach when considering values of $FS_L$ near or below $FS_L = 1$. Conversely, the Boulanger and Idriss model gives similar results for both the performance-based and conventional approaches at low values of $FS_L$, but for higher values ($FS_L > 1$), in many cases the Boulanger and Idriss performance-based model actually produces lower factor of safety against liquefaction values than the conventional approach.

2) For both the Ku et. al. and Boulanger and Idriss performance-based models, sites with high seismicity tended to predict lower liquefaction hazard than the conventional method. The opposite can be true as well, as in many cases the lower seismicity sites predicted higher liquefaction hazards compared to the performance-based method. At high return periods, the Ku et. al. model predicts lower liquefaction hazard than the conventional approach when compared to low return periods. The opposite of this was true with the Boulanger and Idriss which predicted lower liquefaction hazards than the conventional approach at low return periods, but greater hazard in general at higher return periods. Mean and Modal values from the PSHA were observed to have a relatively minimal effect on the comparison between the performance-based and conventional methods.

3) The Ku et. al model presents a curved relationship between the conventional and performance-based approaches, while the Boulanger and Idriss model provides a more linear relationship when considering $FS_L$ between the two methods.

4) For both the Ku et. al. and Boulanger and Idriss performance-based models, only a small percentage (1 to 4%) of liquefaction triggering predictions using $FS_L$ varied between the conventional and performance-based approaches. However, when computing the liquefaction hazard using the probability of liquefaction ($P_L$), a much larger percentage of cases (about 20 to 50 %) predicted a smaller liquefaction hazard from the performance-based method vs. the conventional method.

Overall, although most of the time the performance-based and conventional methods will make the same prediction about liquefaction initiation, the performance-based approach appears to on average predict smaller liquefaction hazards than the conventional method. If these results were considered in a liquefaction analysis, they could potentially produce substantial cost savings, as the price for liquefaction mitigation is often very high. Also, the performance-based method is useful, in that it can be adjusted to explicitly consider various form of uncertainty. If used correctly, the findings of this study and the new CPT performance-based method can help produce a more complete analysis of the potential of liquefaction initiation.

**REFERENCES**

Abrahamson, N., and Silva, W. (2008). Summary of the Abrahamson & Silva NGA ground-motion relations. *Earthquake Spectra*, 24(1), 67-97.

Ambraseys, N. N. (1988). "Engineering Seismology" *Earthquake Engineering & Structural Dynamics,* Vol. 17, 1-105.

Bannister, S., & Gledhill, K. (2012). "Evolution of the 2010–2012 Canterbury earthquake sequence." *New Zealand Journal of Geology and Geophysics*, 55(3), 295-304.

Been, K., and Jefferies, M. G. (1985). "A state parameter for sands." *Géotechnique*, 35(2), 99–112.

Bertero, R. D., and Bertero, V. V. (2002). Performance-based seismic engineering: the need for a reliable conceptual comprehensive approach. *Earthquake Engineering & Structural Dynamics*, 31(3), 627-652.

Boulanger, R. W., and Idriss, I. M. (2006). "Liquefaction Susceptibility Criteria for Silts and Clays." *Journal of Geotechnical and Geoenvironmental Engineering*, 132(11), 1413–1426.

Boulanger, R. W., & Idriss, I. M. (2007). "Evaluation of cyclic softening in silts and clays." *Journal of Geotechnical and Geoenvironmental Engineering*, 133(6), 641-652.

Boulanger, R. W., and Idriss, I. M. (2012). Probabilistic standard penetration test–based liquefaction–triggering procedure. *Journal of Geotechnical and Geoenvironmental Engineering*, 138(10), 1185-1195.

Boulanger, R. W., and Idriss, I. M. (2014). "CPT and SPT based liquefaction triggering procedures" Rep. UCD/CGM-14/01, Dept. of Civil and Environmental Engineering, Univ. of California-Davis, Davis, CA.

Bray, J. D., and Sancio, R. B. (2006). "Assessment of the Liquefaction Susceptibility of Fine-Grained Soils." *Journal of Geotechnical and Geoenvironmental Engineering*, 132(9), 1165–1177.

Castro, G. and Poulos, S.J. (1977). "Factors affecting liquefaction and cyclic mobility," *Journal of the Geotechnical Engineering Division*, ASCE, Vol. 106, No. GT6, pp. 501-506

Cornell, C. A. (1968). "Engineering seismic risk analysis." *Bulletin of the Seismological Society of America*, 58(5), 1583-1606.

Cornell, C.A., and Krawinkler, H. (2000). "Progress and challenges in seismic performance assessment." *PEER News*, April, 1-3

Deierlein, G.G., Krawinkler, H., and Cornell, C.A (2003). "A framework for performance-based earthquake engineering." *Proc., 2003 Pacific Conference on Earthquake Engineering.* Wellington, New Zealand. Paper No. 140.

ESRI (2011). ArcGIS Desktop: Release 10. Redlands, CA: Environmental Systems Research Institute.

Ferritto, J. M. (1992). *Ground motion amplification and seismic liquefaction: A study of Treasure Island and the Loma Prieta earthquake* (No. NCEL-TN-1844). NAVAL CIVIL ENGINEERING LAB PORT HUENEME CA.

Franke, K. W. (2005). "Development of a performance-based model for prediction of lateral spreading displacements." *M.S. Thesis*, 2005, University of Washington, Seattle, WA.

Franke, K., Mayfield, R., & Wright, A. (2014). Simplified uniform hazard liquefaction analysis for bridges. Transportation Research Record: Journal of the Transportation Research Board, (2407), 47-55.

Franke, K. W., Wright, A. D., and Hatch, C. K. (2014). "PBLiquefY: A new analysis tool for the performance-based evaluation of liquefaction triggering." *In Proceedings, 10th National Conference on Earthquake Engineering*, Paper (No. 87), EERI, Oakland, CA.

GEER (2015). "Geotechnical Field Reconnaissance: Gorkha (Nepal) Earthquake of April 25 2015 and Related Shaking Sequence," Report No. GEER-040, Version 1.1

Golesorkhi, R. (1989). *Factors Influencing the Computational Determination of Earthquake-Induced Shear Stress in Sandy Soils*, Ph.D. thesis, University of California at Berkeley, 395 pp.

Gutenberg, B., and Richter, C. F. (1944). "Frequency of earthquakes in California." *Bulletin of the Seismological Society of America*, 34(4), 185-188

Hayati, H., & Andrus, R. D. (2009). "Updated liquefaction resistance correction factors for aged sands." *Journal of geotechnical and geoenvironmental engineering*, 135(11), 1683-1692.

Idriss, I. M., & Boulanger, R. W. (2008). *Soil liquefaction during earthquakes*.

Juang, C. H., Chen, C. J., Jiang, T., & Andrus, R. D. (2000). "Risk-based liquefaction potential evaluation using standard penetration tests." *Canadian Geotechnical Journal*, 37(6), 1195-1208

Kramer, S. L. (1996). *Geotechnical Earthquake Engineering*, Prentice Hall, Upper Saddle River, New Jersey.

Kramer, S. L., and Mayfield, R. T. (2007). Return period of soil liquefaction. *Journal of Geotechnical and Geoenvironmental Engineering*, 133(7), 802-813.

Krawinkler, H. (2002). "A general approach to seismic performance assessment." *Proc., Int. Conf. on Advance in New Challenges in Earthquake Engineering Research*, ICANCEER, Hong Kong.

Ku, C.-S., Juang, C. H., Chang, C.-W., and Ching, J. (2012). "Probabilistic version of the Robertson and Wride method for liquefaction evaluation: development and application." *Canadian Geotechnical Journal*, 49(1), 27–44.

Kulhawy, F. H., & Mayne, P. W. (1990). Manual on estimating soil properties for foundation design (No. EPRI-EL-6800). Electric Power Research Inst., Palo Alto, CA (USA); Cornell Univ., Ithaca, NY (USA). Geotechnical Engineering Group.

Mayfield, R. T., Kramer, S. L., & Huang, Y. M. (2009). "Simplified approximation procedure for performance-based evaluation of liquefaction potential." *Journal of geotechnical and geoenvironmental engineering*, 136(1), 140-150.

Marcuson, W. F. (1978). "Definition of terms related to liquefaction." *Journal of the Geotechnical Engineering Division*, 104(9), 1197-1200.

Mitchell, J. K., and Tseng, D. J. (1990). "Assessment of liquefaction potential by cone penetration resistance." *In Proc., HB Seed Memorial Symposium* (Vol. 2, pp. 335-350).

Moss, R. E., Seed, R. B., Kayen, R. E., Stewart, J. P., Der Kiureghian, A., & Cetin, K. O. (2006). "CPT-based probabilistic and deterministic assessment of in situ seismic soil liquefaction potential." *Journal of Geotechnical and Geoenvironmental Engineering*, 132(8), 1032-1051.

NOAA/NGDC, University of Colorado at Boulder. "Sand Boil Produced by Liquefaction, El Centro, California" https://www.ngdc.noaa.gov/hazardimages/picture/show/39#data (accessed April 14, 2017)

Petersen, M. D., Frankel, A. D., Harmsen, S. C., Mueller, C. S., Haller, K. M., Wheeler, R. L., ... & Luco, N. (2008). Documentation for the 2008 update of the United States national seismic hazard maps (No. 2008-1128). Geological Survey (US).

Petersen, M. D., Moschetti, M. P., Powers, P. M., Mueller, C. S., Haller, K. M., Frankel, A. D., ... & Field, N. (2015). "The 2014 United States national seismic hazard model." *Earthquake Spectra*, 31(S1), S1-S30.

Robertson, P. K., and Campanella, R. G. (1985). "Liquefaction potential of sands using the CPT." *Journal of Geotechnical Engineering*, 111(3), 384-403.

Robertson, P., and Wride, C. F. (1998). "Evaluating cyclic liquefaction potential using the cone penetration test." *Canadian Geotechnical Journal*, 35(3), 442–459.

Robertson, P. K. (2009). "Interpretation of cone penetration tests — a unified approach." *Canadian Geotechnical Journal*, 46(11), 1337–1355.

Seed, H. B. (1983). "Earthquake resistant design of earth dams." *Proc.,Symp. on Seismic Design of Embankments and Caverns*, Pennsylvania, ASCE, New York, 41–64.

Seed, H. B. and Idriss, I. M. (1971). "Simplified procedure for evaluating soil liquefaction potential," Journal of the Soil Mechanics and Foundations Division, 97(SM9), p. 1249-1273.

Seed, B. (1979). "Soil liquefaction and cyclic mobility evaluation for level ground during earthquakes." *Journal of Geotechnical and Geoenvironmental Engineering,* 105(ASCE 14380).

Seed, H. B., and De Alba, P. (1986). "Use of SPT and CPT tests for evaluating the liquefaction resistance of sands." *In Use of In Situ Tests in Geotechnical Engineering*: (pp. 281-302). ASCE.

Shibata, T., and Teparaksa, W. (1988). "Evaluation of liquefaction potentials of soils using cone penetration tests." *Soils and Foundations*, 28(2), 49-60.

Slemmons, D. B. (1982, June). "Determination of design earthquake magnitudes for microzonation." *In Proceedings of the third international earthquake microzonation conference.*

Spudich, P., Hellweg, M., and Lee, W. H. K. (1996). "Directional topographic site response at Tarzana observed in aftershocks of the 1994 Northridge, California, earthquake: implications for mainshock motions." *Bulletin of the Seismological Society of America*, 86(1B), S193-S208.

Stewart, J. P., Liu, A.H., and Choi, Y. (2003). "Amplification factors for spectral acceleration in tectonically active regions." *Bulletin of the Seismological Society of America*, 93(1), 332–352.

Suzuki, Y., Tokimatsu, K., and Koyamada, K. (2003). "Correlation between soil liquefaction during earthquakes and CPT data." *Journal of Structural and Construction Engineering*, 571, 95-102.

Wright, A.D. (2013). "Comparison of performance-based liquefaction initiation analyses between multiple probabilistic liquefaction models using the standard penetration test." *M.S. Thesis*, 2013, Brigham Young University, Provo, UT.

Ulmer, K. J. (2015). "Development of a Simplified Performance-Based Procedure for Assessment of Liquefaction Triggering Using Liquefaction Loading Maps." *M.S. Thesis*, 2015, Brigham Young University, Provo, UT.

Ulmer, K. J., Franke, K. W., & Peterson, B. D. (2015). "Seismic hazard curves for the probability of liquefaction." *IFCEE 2015* (pp. 1308-1317).

Unno, T., Kazama, M., Uzuoka, R., & Sento, N. (2008). "Liquefaction of unsaturated sand considering the pore air pressure and volume compressibility of the soil particle skeleton." *Soils and Foundations*, 48(1), 87-99.

USGS, U. S. G. S. (2017). Seismic CPT Database. https://earthquake.usgs.gov/research/cpt/data/, United States Geologic Survey.

Vaid, Y. P., and Chern, J. C. (1985). "Cyclic and monotonic undrained response of saturated sands." *In Advances in the Art of Testing Soils Under Cyclic Conditions,* ASCE, pp. 120-147.

Youd, T. L., and Hoose, S. N. (1977). "Liquefaction susceptibility and geologic setting." *In Proc., 6th World Conf. on Earthquake Engineering,* Roorkee, India, Indian Society of Earthquake Technology. Vol. 6, pp. 37-42.

Youd, T. L., and Wieczorek, G. F. (1984). Liquefaction during the 1981 and previous earthquakes near Westmorland, California. USGS Numbered Series, rep., U.S. Geological Survey.

Youd, T. L., and Bartlett, S. F. (1995). "Empirical prediction of liquefaction-induced lateral spread." *Journal of Geotechnical and Geoenvironmental Engineering*, 121(4), 316–331.

Youd, T. L., Idriss, I. M., Andrus, R. D., Arango, I., Castro, G., Christian, J. T., ... & Ishihara, K. (2001). "Liquefaction resistance of soils: summary report from the 1996 NCEER and 1998 NCEER/NSF workshops on evaluation of liquefaction resistance of soils." *Journal of geotechnical and geoenvironmental engineering*, 127(10), 817-833.

Youd, T. L., Hansen, C. M., and Bartlett, S. F. (2002). "Revised Multilinear Regression Equations for Prediction of Lateral Spread Displacement." *Journal of Geotechnical and Geoenvironmental Engineering*, 128(12), 1007–1017.

Youngs, R. R., and Coppersmith, K. J. (1985). Implications of fault slip rates and earthquake recurrence models to probabilistic seismic hazard estimates. Bulletin of the Seismological society of America, 75(4), 939-964.

Wang, W. (1979). *Some Findings in Soil Liquefaction*. Water Conservancy and Hydroelectric Power Scientific Research Institute, Beijing, China.

Wells, D. L., and Coppersmith, K. J. (1994). "New empirical relationships among magnitude, rupture length, rupture width, rupture area, and surface displacement." *Bulletin of the seismological Society of America*, 84(4), 974-1002.

Wood, H. O. (1912). "The elastic-rebound theory of Earthquakes by HF Reid", *Bulletin of the Seismological Society of America*, 2(1), 98-100.

# APPENDIX A.

## ANALYSIS DETAILS – DEVELOPMENT OF THE CPT PERFOMANCE-BASED LIQUEFACTION ANALYSIS TOOL *CPTLIQUEFY*

CPTLiquefY has been developed as a research tool for the evaluation of earthquake liquefaction and associated hazards. To provide these capabilities, CPTLiquefY has the ability to read standard CPT soil profiles, apply desired data corrections, and perform both conventional and performance-based liquefaction hazard analyses. Data from CPTLiquefY can be easily exported to an excel format where various plots for liquefaction hazards can be created. This appendix will discuss in detail the functionality and purpose of the program.

## 8.1 Running the Program

CPTLiquefY has been designed to be a free standing executable program. Currently the program must be launched on a system with Visual Studio, but eventually the program will be executable. Currently, some setup is required before running the code. Most of the setup involves setting up the USGS NSHMP tool which obtains earthquake deaggreagation data for the running of pseudo-probabilistic and performance-based analyses. When the program is launched the following screen will appear (Figure 0-1).
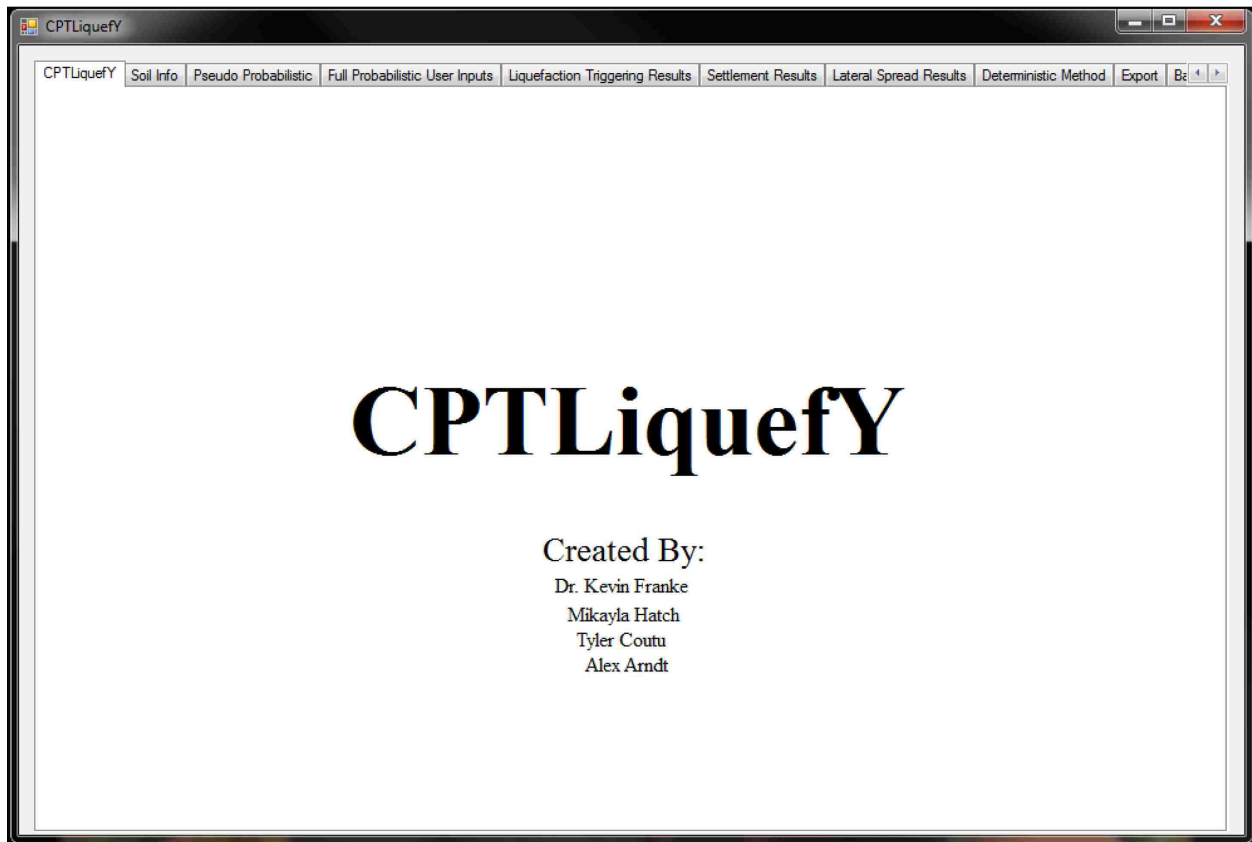


**Figure 0-1: Opening page of program.**

**8.1.1 Soil Info Tab**

To begin running the program the "Soil Info" tab must be clicked. Once this tab is selected, a new the soils tab will launch allowing the user to upload a CPT file. To load a CPT profile, the data must be converted into a .csv format with data in four simple columns. This can easily be done by copying and pasting data from any other format into an excel spreadsheet, and then saving the spreadsheet as a .csv file. The first column should contain the depth of the measurements taken by the cone. Column two should contain the tip resistance data in units of tsf, MPa, or KPa. Similarly, column three should contain sleeve friction data in similar units. Column four should contain the pore water pressure behind the cone, if no such data is available this column should be filled with zeros. An example of this data format can be seen in Figure 0-3. Once the CPT file is in an acceptable format it can be read by the program by selecting the "Browse for CPT File" button. This button will launch a window to allow the user to navigate to desired the file path.
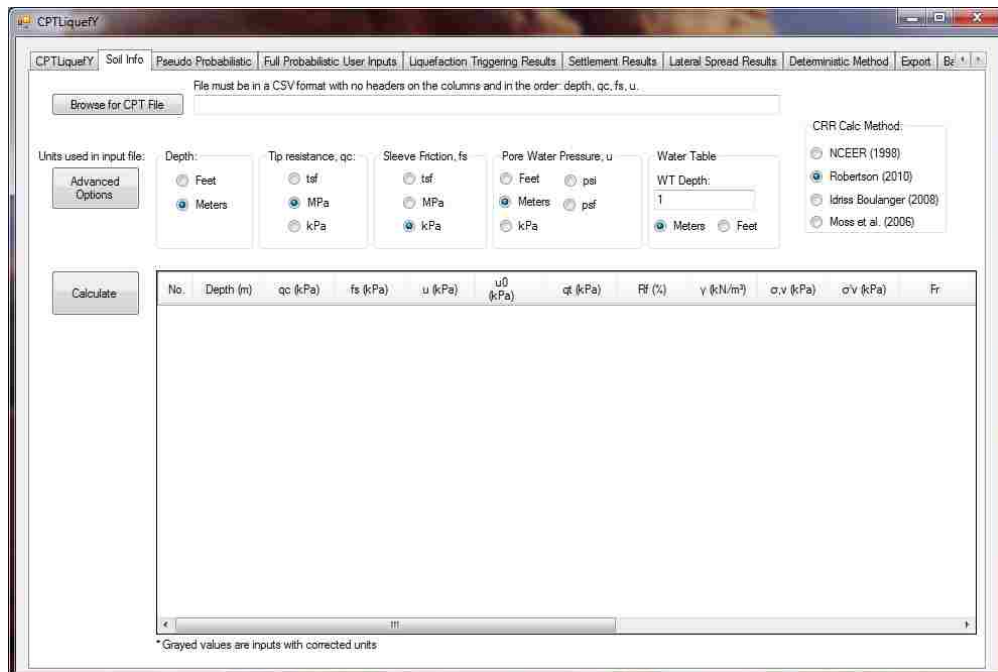
**Figure 0-2: Soil Info tab.**
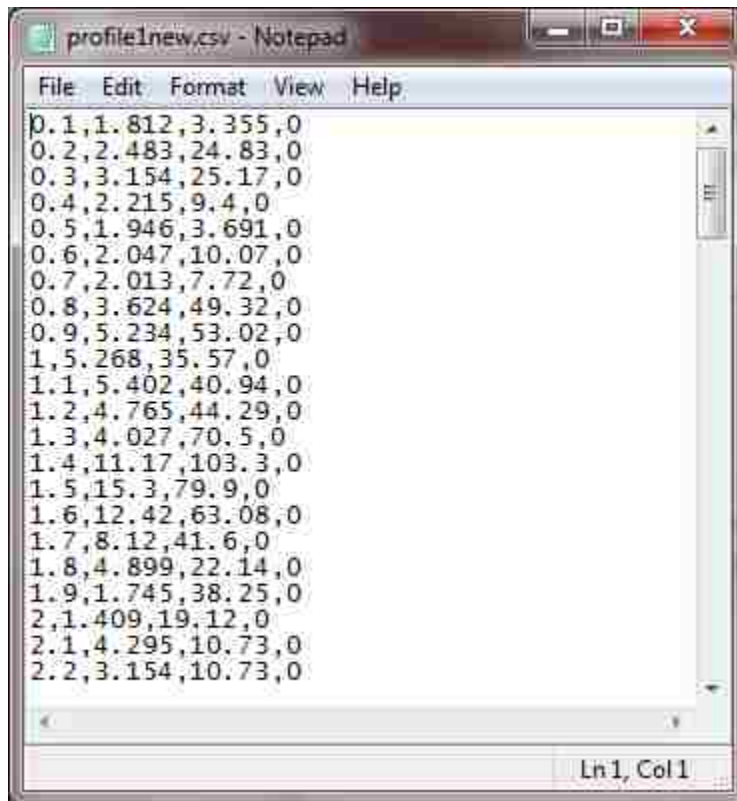


**Figure 0-3: Example CPT input file in .csv format.**

The next step will be to select the desired correction factors. Depending on the units of the given CPT file, the correct unit corrections must be selected before the "Calculate" button is clicked. CPTLiquefY has the ability to correct units of measure, and if the correct units from the input file are selected then the program will take care of all unit conversions. Next, an appropriate water table depth should be selected in either feet or meters (units of the input should be selected).

Before moving on, CPTLiquefY also has options to further fine-tune the CPT analysis. By pressing the "Advanced Options" button, a new window will launch allowing the user to modify these options. Default values are given before the program is loaded, so it is not required

to modify any of these values.  If the user desires, modifications such as the application of a $K_\alpha$ factor, thin layer correction, depth correction, lateral spread correction, or dilative/contractive behavior correction can be made.  Also, values for fines correction ($I_c$ susceptibility cutoff) and depth correction ($C_N$) cap can be adjusted in the advance options window.  After the desired adjustments are made, the user should press "OK" to return to the soils tab.
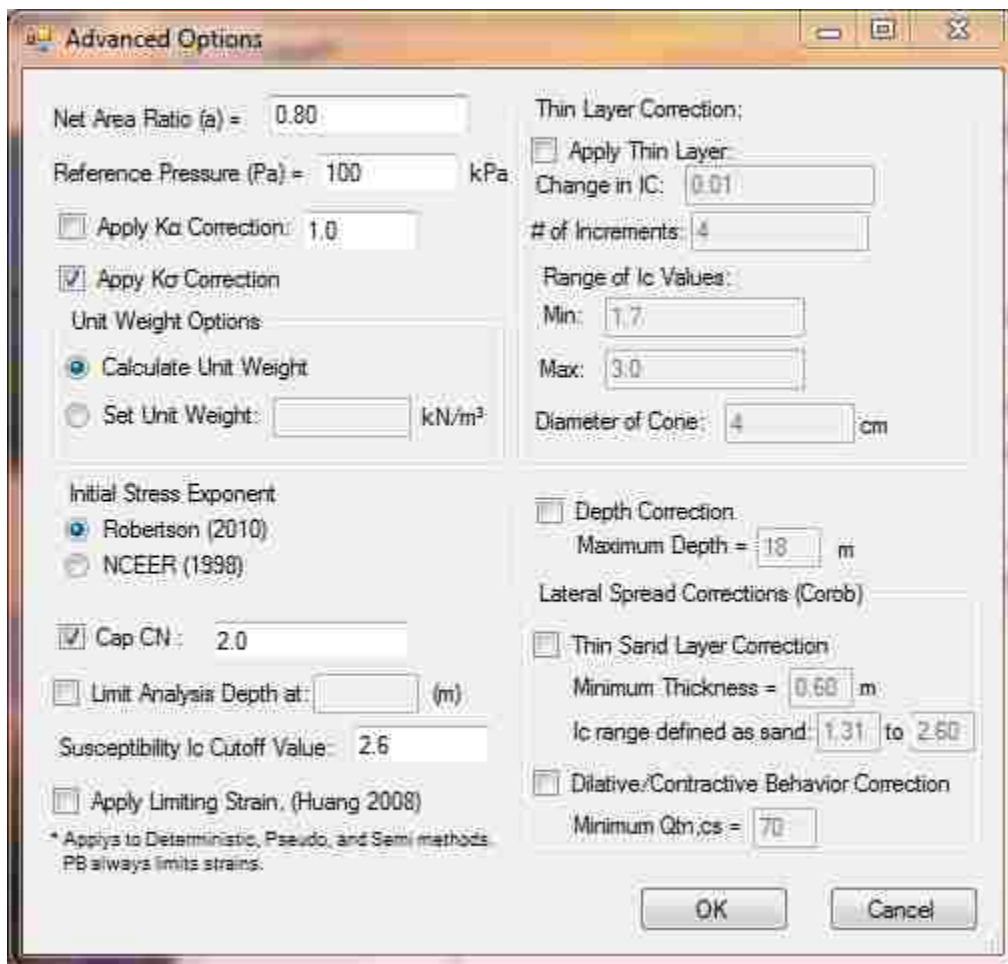


**Figure 0-4: Advanced options tab.**

The user is now ready to begin the upload of the CPT file. By pressing the "Calculate" button the CPT data will be uploaded and some preliminary liquefaction hazard calculations will be completed. An example of this is seen in Figure 0-5. Once the CPT data is sucessfully loaded, the liqufaction analysis can begin.
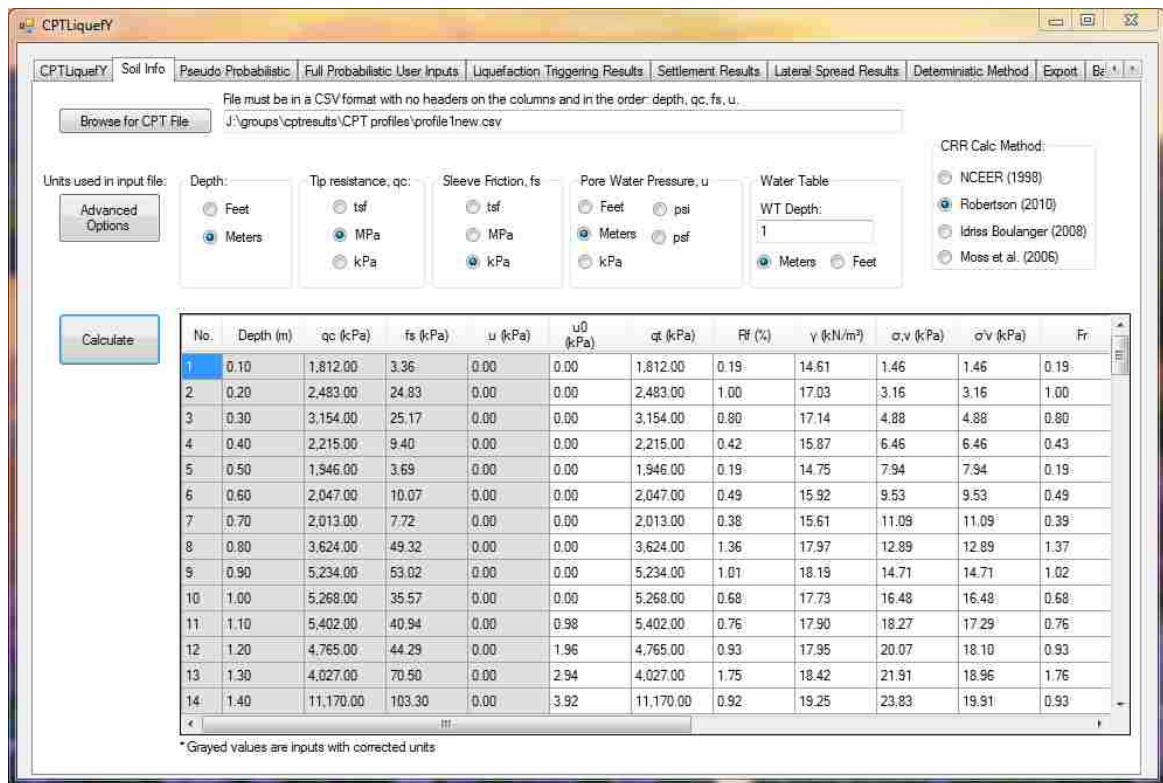


**Figure 0-5: Example of loaded CPT profile and completed preliminary liquefaction hazard calculations.**

### 8.1.2 Pseudo-Probabilistic Tab

Clicking on the "Pseudo Probabilistic" tab will present new options to the user. This tab will allow the user to run a conventional deterministic liquefaction analysis with probabilistic earthquake magnitude and acceleration data from a PSHA (hence pseudo-probabilistic). When selecting ground motion parameters from the PSHA, the user can choose either mean or modal

values. Before beginning these calculations, a site must be selected (latitude, and longitude), as well as an exceedance probability and a number of years to consider. These options are entered near the top left part of the window. Other options that must be selected are: USGS deaggregation year, and USGS model to use (West, or East). These values are required to run a deaggregation through NSHMP-haz, which was discussed earlier. Optional selections include: selection of deterministic liquefaction model, selection of lateral spread geometry, percentile of interest for settlement/lateral spread, and inclusion of site amplification factors.
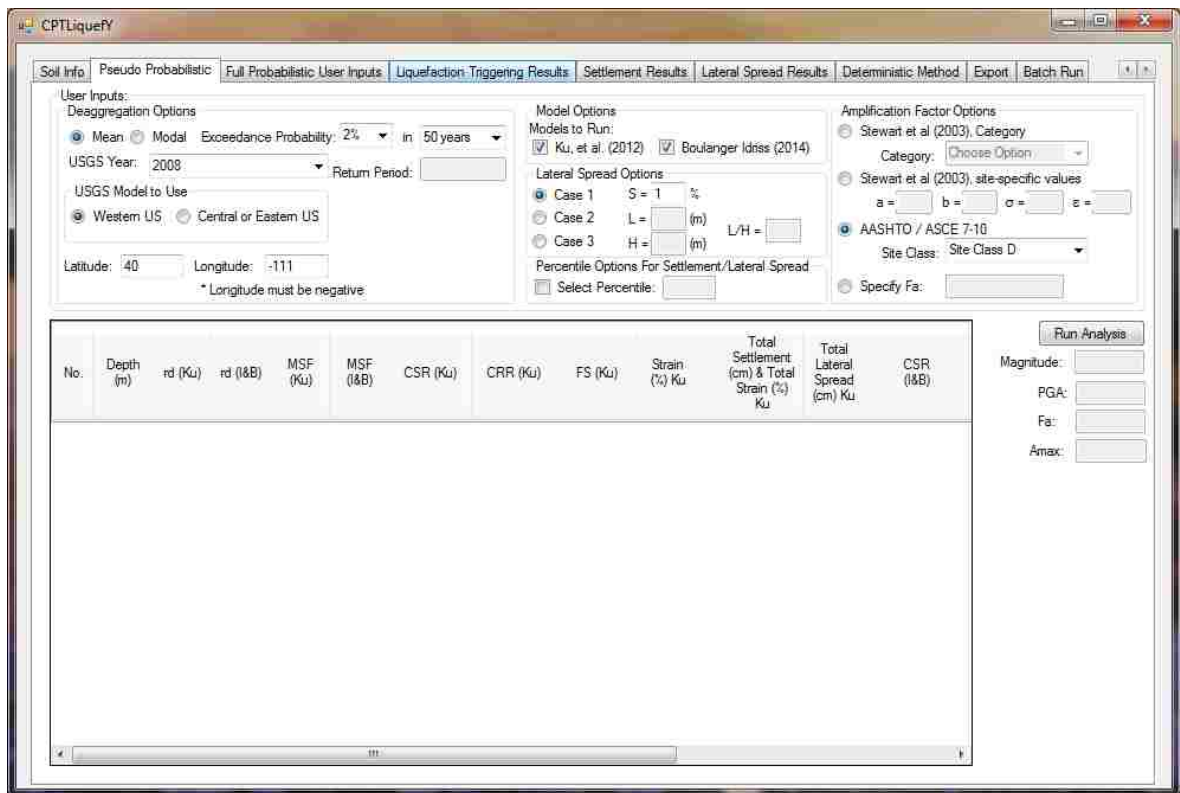


**Figure 0-6: Pseudo-probabilistic calculations tab.**

Once the desired options are selected the user should click "Run Analysis". When "Run Analysis" is pressed a new window displaying a command prompt will temporarily appear. This window is the NSHMP-haz tool running a PSHA for the desired location and exceedance

probability (return period). This code will generally run for a few seconds before concluding and passing on all required values to the CPTLiquefY program. Once the PSHA is compete CPTLiquefY will automatically update and present the loaded ground motion data in the text frames below the "Run Analysis" button, and the data grid view will fill with the completed calculations from the pseudo-probabilistic liquefaction hazard analysis. A completed example can be seen below. The program will present the liquefaction triggering, total settlement, and total lateral spread values calculated for the soil profile. This data is easily copy and pasted into excel for plotting purposes.
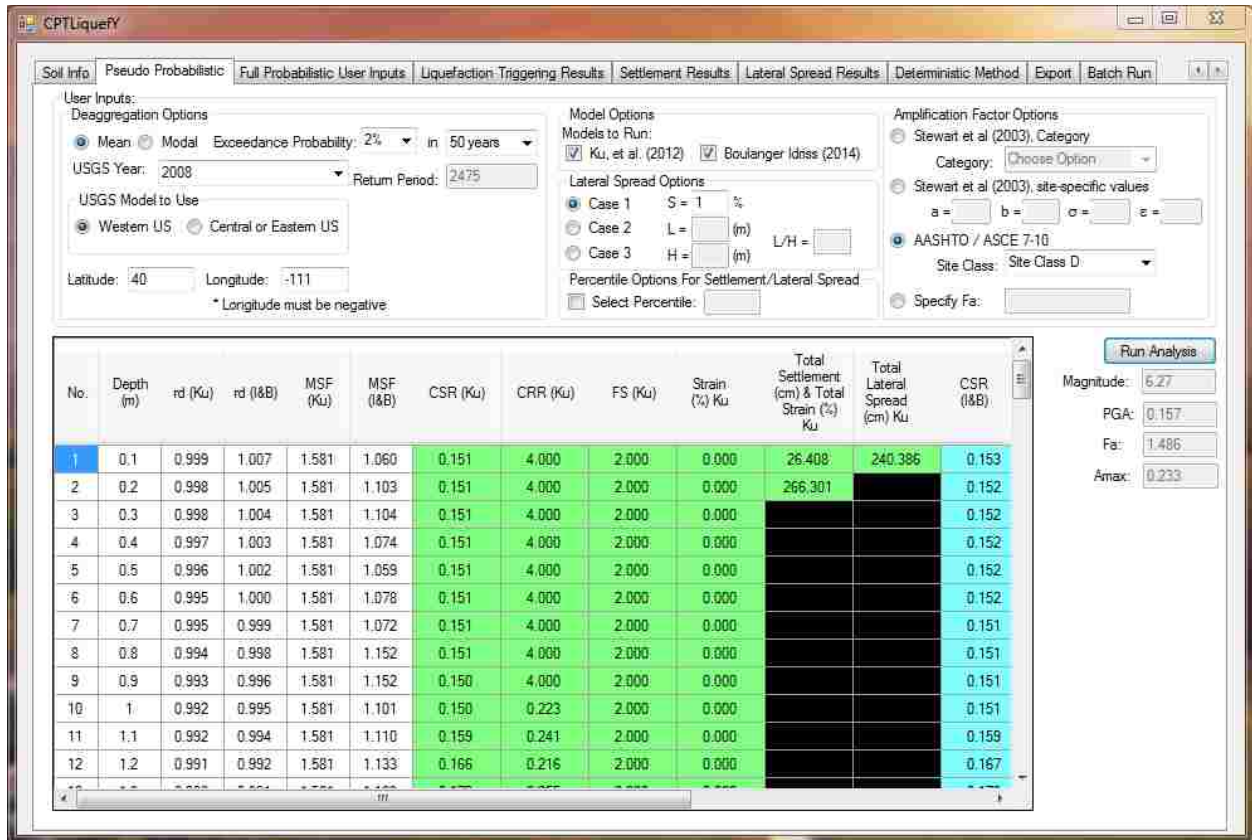


**Figure 0-7: Example of completed pseudo-probabilistic calculations**

### 8.1.3  Full Probabilistic User Inputs Tab (Performance-Based Tab)

To begin performance-based calculations in CPTLiquefY, the user must move to the "Full Probabilistic User Inputs" tab. This tab guides the user through the complete performance-based liquefaction hazard analysis process. First, the user must make some initial selections. The user has the choice to calculate the site amplification ($a_{max}$) using a probabilistic process, or by using the code or other amplification factor options like those used in the pseudo probabilistic tab. If the probabilistic process is chosen (consider uncertainty in Amax calcs), then a value for the uncertainty in these calculations must be selected.

In conversation with other researchers, it has been decided that a good default value is $\sigma = 0.3$ (Stewart et. al.), but for a site-specific analysis any value could be considered. The user also has the option to adjust the settlement and lateral spread inputs. Default values are selected if these other options are not needed for the current analysis. Before beginning calculations by pressing "Run Analysis", the uncertainty level for each of the performance-based liquefaction models must be selected. Generally, total uncertainty (model and parameter) should be used unless the uncertainty from the measurement of the CPT data can be minimized. For more info on these values see chapter 6.

In order to commence the performance-based calculations, ground motion data from all potential seismic sources must be obtained. This is done by pressing the "Load Seismic Data" button. Pressing this button activates the NSHMP-haz PSHA just as in the previous tab, but this time the code will run PSHAs for a wide range of return periods, rather than just one. Because of this, the loading of this data can take several minutes. Once NSHMP-haz completes all the calculations, the seismic data is loaded into the data grid view as seen below. After this data is

loaded, site amplification values are calculated and can be viewed in the sub-tab "Amax Curves Calculated Data".
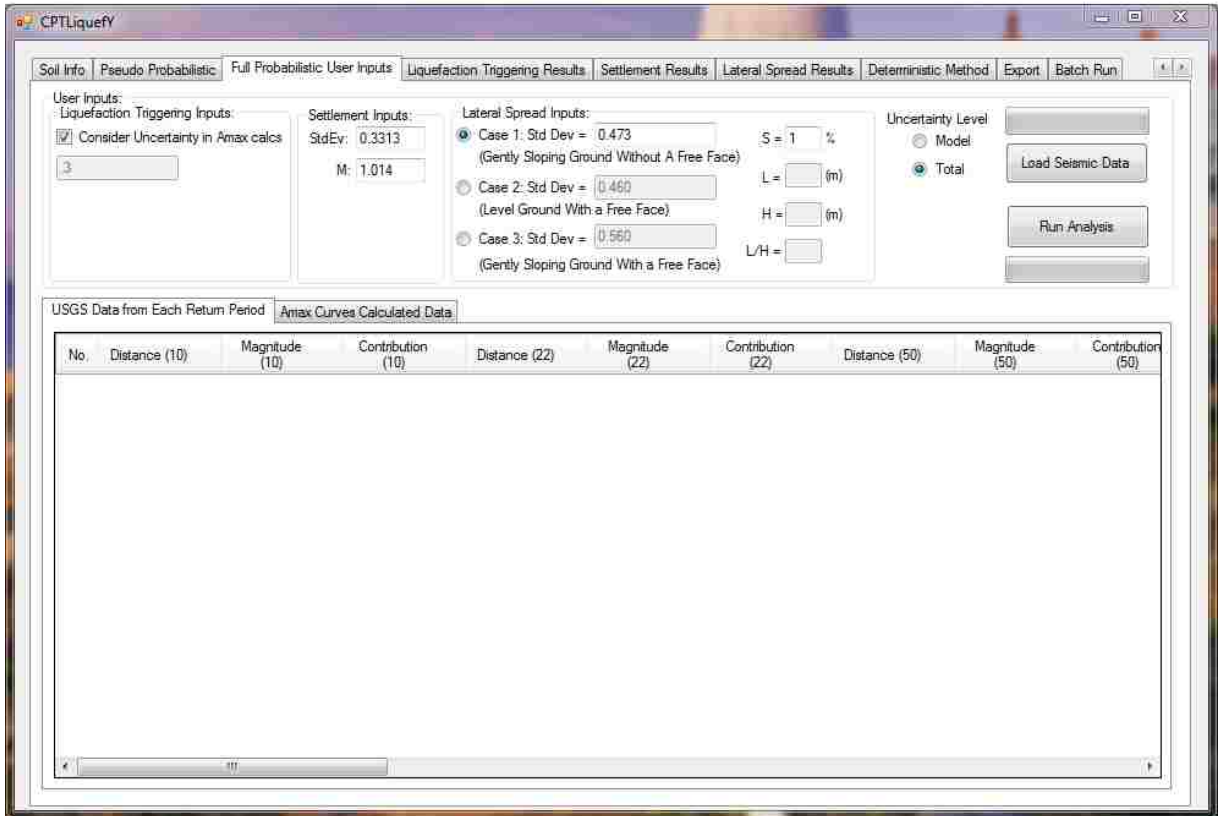


**Figure 0-8: Full Probabilistic User Inputs tab (performance-based analysis tab).**
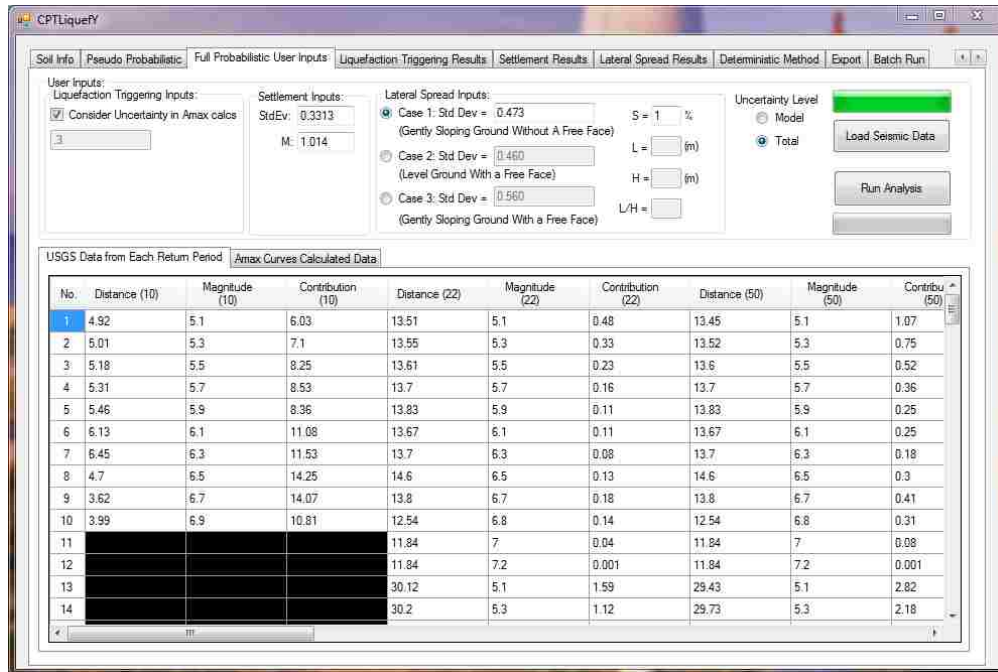
**Figure 0-9: Example of USGS data loaded in CPTLiquefY.**

These data are not critical for engineering design, but are helpful for researchers to see inside the

"black box" and have a better idea of what the program is computing.  These values were also

used widely for debugging purposes, and provide a helpful accuracy check for future users.
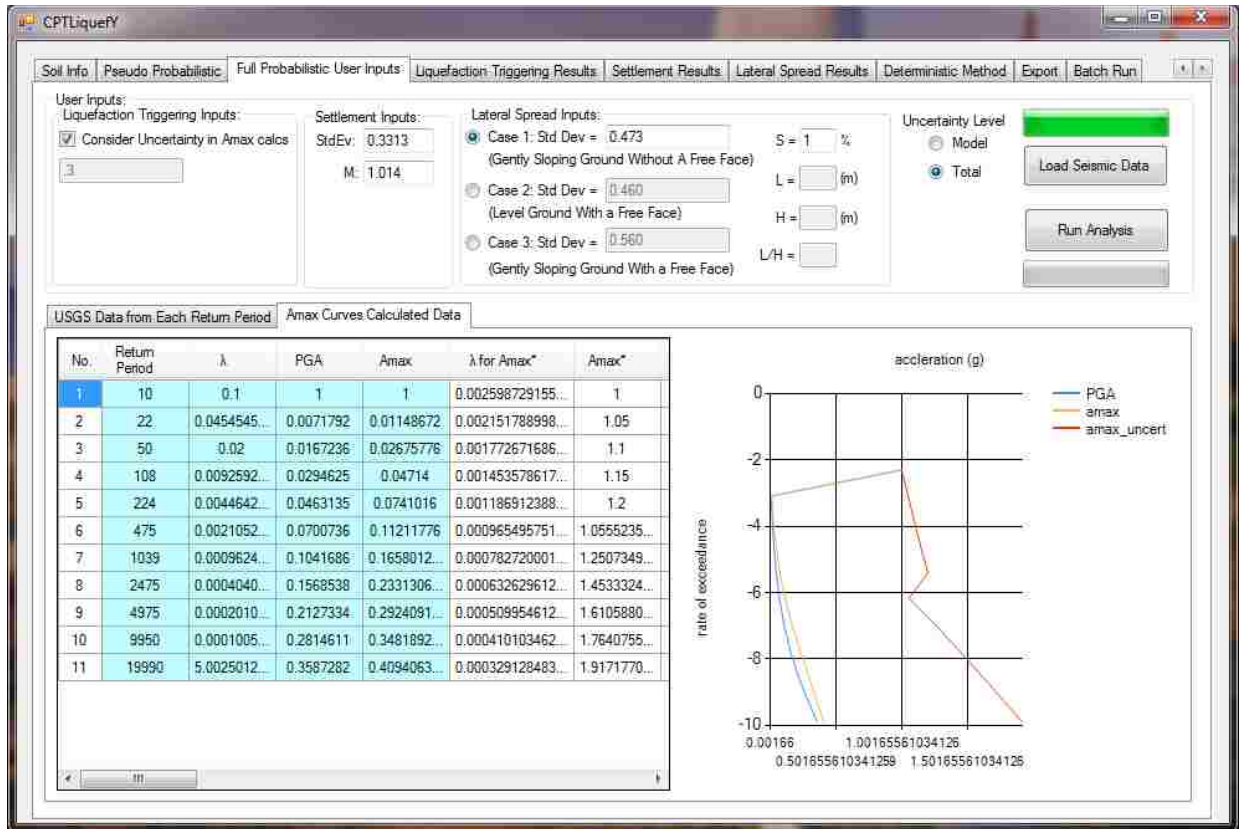
**Figure 0-10: Example of calculated site amplification data for performance-based liquefaction analysis**

Once the seismic data is loaded from NSHMP-haz, the performance-based calculations are ready to commence. By pressing the "Run Analysis" button the user will prompt the program to begin the millions of iterations required to compute the performance-based liquefaction hazards. This process can take several minutes, as all of the calculations must be complete for each depth increment in the soil profile. Once these calculations are completed, the lower green loading bar will fill, and the user will be allowed to progress through the program.

### 8.1.4   Liquefaction Results Tabs

Once the performance-based calculations are complete, the user should click on either the "Liquefaction Triggering Results", "Settlement Results", or "Lateral Spread Results" tab in order to view the desired results. In the liquefaction triggering tab the results are presented in a data grid view related to a single soil layer. To view the liquefaction triggering values for a desired layer, simply type the layer number into the "Enter Layer Number:" text box. Values will automatically update once a layer is chosen. Values for each liquefaction triggering model can be seen by selecting either the Robertson or Idriss and Boulanger sub-tabs. An example of these results is shown below. These results can be copy and pasted into excel in order to produce liquefaction triggering hazard curves for a soil layer of interest.



**Figure 0-11: Example liquefaction triggering results.**
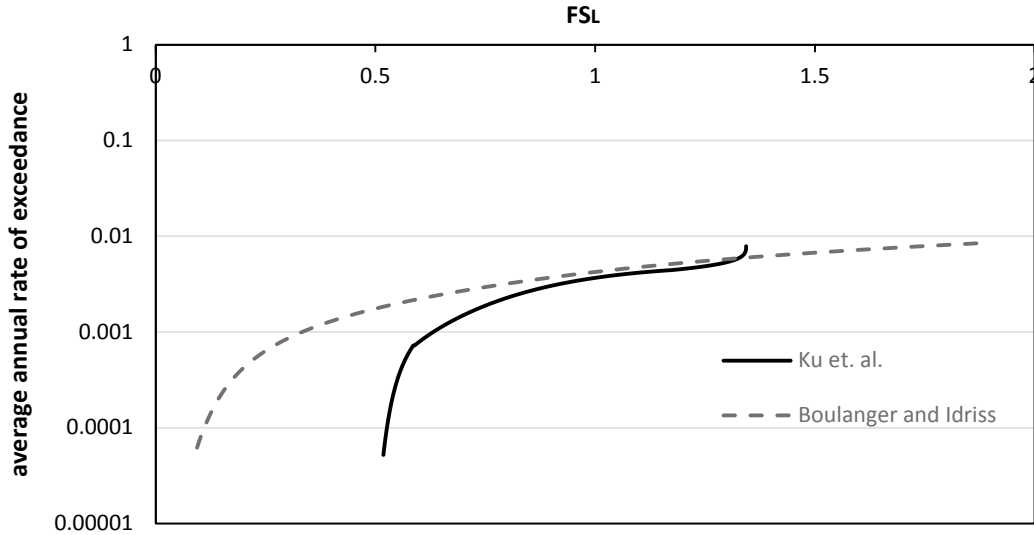
**Figure 0-12: Example of previous liquefaction hazard data in graphical format.**

Results from the settlement and lateral spread are in a similar format, and allow for the plotting

of hazard curves. The main difference on these tabs is that the resulting hazard curves relate to

the complete soil profile, rather than one single layer.



**Figure 0-13: Example performance-based liquefaction-induced settlement data.**

**Figure 0-14: Example of performance-based liquefaction induced lateral spread data.**

### 8.1.5   Deterministic Tab

For other site-specific conventional analysis, the deterministic calculations tab can be used.  This tab is nearly identical to the pseudo-probabilistic tab, but does not obtain ground motion values from the NSHMP-haz PSHA.  For this method, the site-specific values must be input manually into the "magnitude", and "acceleration (PGA)" text boxes respectively.  Once pressing the "Run Deterministic" button is pressed, the deterministic calculations will be run and the results will appear in the data view grid.
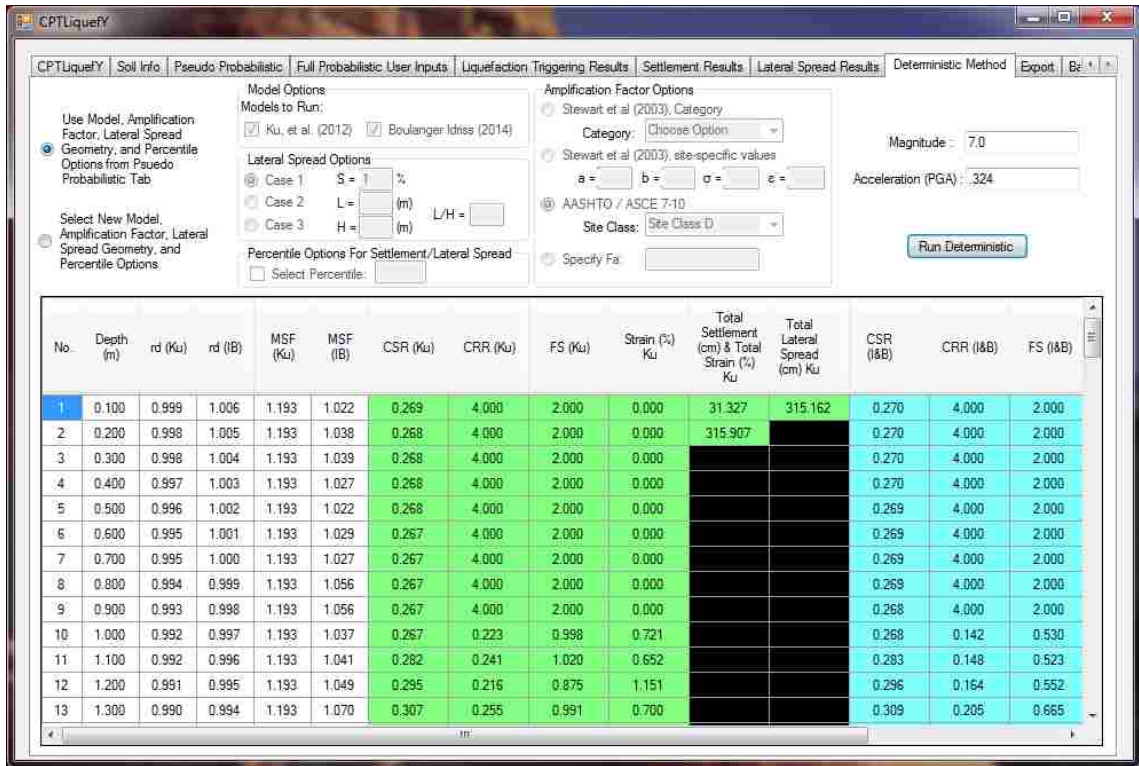
**Figure 0-15: Example of completed deterministic liquefaction hazard analysis.**

### 8.1.6   Export Tab

Once all desired calculations are completed, the completed liquefaction analysis data can be exported to an .xlsx format by use of the export tab. When the export tab is opened, the user should select which of the datasets the user would like to export to excel. Next, the user must choose a location to save their file by clicking the "Save Location" button. This will launch a new window that allows the user to navigate to the desired file location. In order to export the data, the "Export to Excel" button should be clicked. It will take several seconds for the data to be exported, but eventually a message will display notifying the user of the completion of the export process.
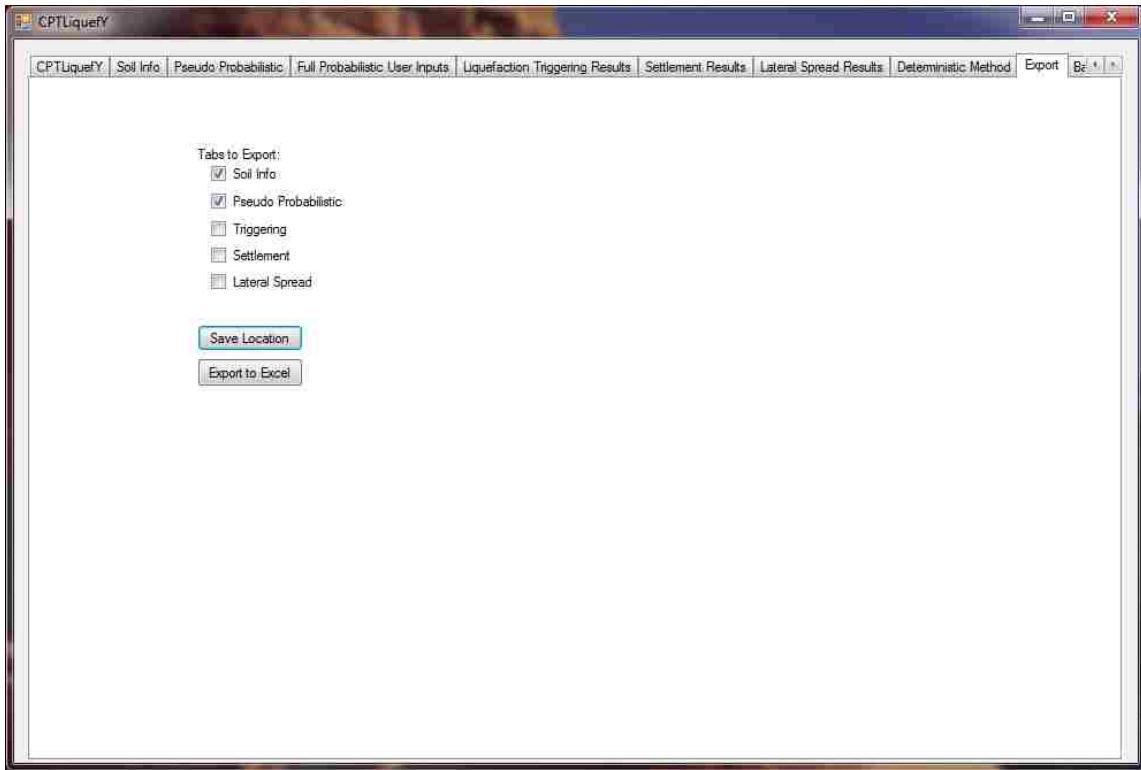
159

**Figure 0-16: Export tab of CPTLiquefY.**

### 8.1.7 Batch Run Tab

To complete comparative studies, such as was presented in this thesis, liquefaction hazard analyses must be completed for many different profiles and locations. To facilitate the process of running many performance-based analyses in a large batch, the batch run tab has been developed. This tab has many different options such as: analyzing one CPT file at multiple locations, analyzing many CPT files at one location, or analyzing multiple CPTs at multiple locations. Other options on this page are identical to those found on the pseudo-probabilistic, and full probabilistic user inputs, and export tabs. In order to run a large batch of analyses, the user can navigate directly to the batch run tab and select all required input without having to do anything on other tabs. This saves significant time, and allows the computer to do the heavy computational tasks while the system is not in use (i.e. overnight, weekends).
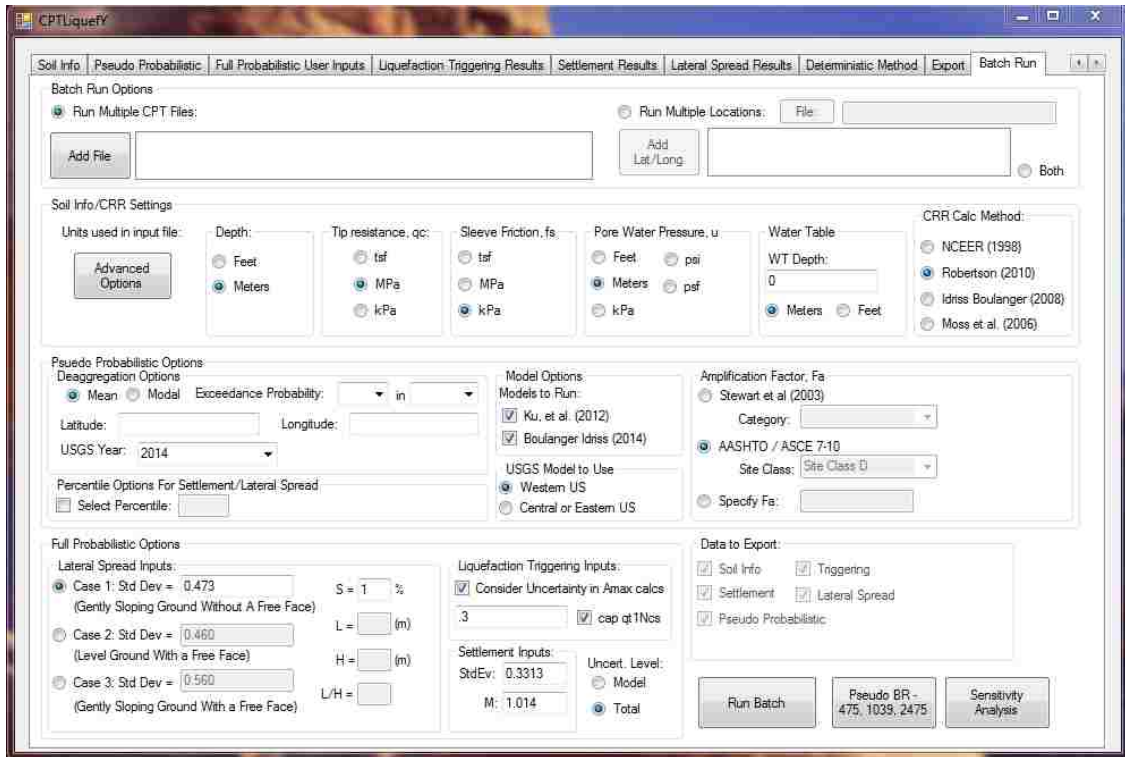
**Figure 0-17: Export tab of CPTLiquefY.**